Current and future evolution of the GLOF-hazard in the Bhilangna Valley, Indian Himalaya

GEO 511 Master's Thesis

Author

Anna Holzbecher

10-433-613

Supervised by

Dr. Simon Allen, University of Zurich

Dr. Christian Huggel, University of Zurich

Dr. Suraj Mal, University of Delhi[1]

Faculty Representative

Prof. Dr. Andreas Vieli

April 2017

Department of Geography, University of Zurich

[1]Shaheed Bhagat Singh College, University of Delhi, Delhi, India

Abstract

Current rapid climate change has profound impacts on the glacial and periglacial environment. Glaciers are retreating all over the world and in response numerous glacial lakes have formed in depressions of the exposed bed during the last century. These water reservoirs represent a serious hazard as they are located in potentially unstable terrain and in case an outburst flood is triggered severe damage can occur even far downstream. Past studies focused on the assessment of hazard posed by current lakes. Yet, glacial lakes are still growing and new lakes are expected to form as a consequence of deglaciation. Therefore, scientific attention is now shifting towards the anticipation of future hazards. This thesis analysed the future evolution of the glaciated area and the emerging outburst flood hazards related to the formation of new lakes in the Bhilangna Valley, Indian Himalaya. A medium (RCP4.5) and a worst-case (RCP8.5) warming scenario were considered. Based on past glacier outlines, glaciers in the Bhilangna Valley seem to have thinned by 5-37m between 1968-2015. The temperature change during this period was around 1.45°C for this region according to gridded CMIP5 model data. The GlabTop model was used to calculate current glacier ice thicknesses and potential sites of new lakes. Projecting past thinning rates into future, changes in ice thickness and glacier extent could be evaluated based on an adapted version of the thickness change parametrisation model proposed by Linsbauer et al. (2013). For the medium warming scenario, little change in glacier extent was observed with an overall area decrease of around 16% within the next eight decades. By comparison, the same area change of 16% is already seen after only 4 decades under the worst-case scenario, and within 80 years, 70% of the glacier area mapped for the year 2015 might disappear. Up to 35 new lakes could emerge in the next eight decades if a worst-case warming scenario is assumed, 27 of them having an area larger than 1ha. Particularly between 60 and 80 years in future a large number of new lakes appear. Their hazard was assessed based on the modelled lake volume and the probability of mass movement impacts, which was approximated by using the concept of topographic potential. For several lakes, an increase in the hazard level could be observed within the future decades. However, according to downstream flow modelling results, no debris flows originating from future lakes seem to affect infrastructure or human settlements in the Bhilangna Valley due to the remoteness of this region. In contrast, potential floods with minimal sediment entrainment propagate far downstream and could therefore cause damage to several hydropower stations. The approach proposed in this thesis is a first step to combine different methods and models to assess emerging outburst flood hazards of glacier lakes in data scarce mountain regions.

Acknowledgement

This work would not have been possible without the support of various people. First of all, I would like to thank Dr. Simon Allen. His input on methodological approaches and the joint discussions were always very valuable. He was taking a lot of time for meetings, which I greatly appreciate. I also like to remember the common field work in the Indian Himalayas where I could gain completely new experiences. I am also grateful to Simon for his numerous feedbacks on the content and text of this master thesis.

I would also like to thank Dr. Christian Huggel. He contributed significantly to the structure of this master thesis. Without his ideas on the subject this work would probably not have come about.

Dr. Suraj Mal provided me his glacier outline data as well as local temperature data. I would particularly like to thank him for the organization of the field work. This enabled a personal relation to the study area, which I felt was not only very valuable in the evaluation of my model results. At this point, I would also like to express my gratitude to all the porters who accompanied us during the field work and were responsible for our physical well-being.

Further persons contributed to the success of this work. These include Dr. Andreas Linsbauer, who helped me with the application of the GlabTop model, Franz Goerlich, who gave me information on Corona data and Dr. Philipp Rastner, who provided me his data on the Findelengletscher.

Big thanks go to my family and friends. Without the help and psychological support of my mother and my boyfriend Pascal Leimer, I would never have made it so far. I would also like to thank my proofreaders Jan Holzbecher, Jiri Holzbecher and Angela Hunziker. Finally, I am grateful to Fabiola Kälin, who borrowed me her computer.

Contents

1 Introduction

The Himalayas are as other mountainous regions in the world of major importance for human activities. Estimates show that almost 10% of the global population is directly dependent on mountains for its livelihood and another 40% are expected to rely indirectly on mountain ecosystems for forest products, fresh water and river valley projects for industry, agriculture or domestic purposes (Schild, 2008; Viviroli et al., 2007). Irrigation in the Himalayas as well as hydropower generation are strongly dependent on the water discharge from glaciers upstream, especially during the dry season (Bhambri et al., 2011). But exactly mountain regions seem to be exposed to rapidly changing climatic conditions with faster rising temperatures than in nearby low land areas (Rangwala and Miller, 2012). For the period 1971-2007, Kothawale and Rupa Kumar (2005) reported a decadal warming rate which was more than twofold higher for the western Indian Himalayas than the mean rate for whole India. As the glacial and periglacial environment is very sensitive to atmospheric warming due to intensifying ice melt with rising temperatures, new hazards might be the consequence. A destabilisation of rock and debris slopes is likely to occur related to permafrost degradation or glacier retreat leading to an increase in potential source zones for rock fall respectively debris flows. Moreover, a change of the thermal regime and geometry of glaciers can be caused by rising temperatures and therefore a change in frequency of ice avalanches is expected (Allen et al., 2016b). However, the hazard which is reported to have the highest impact on downstream living population is the glacier lake outburst flood (GLOF) (Richardson and Reynolds, 2000). After glacier retreat, lakes may form in the exposed depressions of the former glacier bed and represent water reservoirs which can be released suddenly. It is due to this sudden onset, potentially high-magnitude discharge and long runout distance which makes GLOFs such a serious threat for people living in proximity to river channels (Carrivick, 2010; Cui et al., 2013). Yet, not every glacier lake poses the same hazard and even lakes with an unstable dam require a trigger event to initiate partial or complete dam failure and subsequent drainage (Worni et al., 2014). It is probable that future lakes will mainly be dammed by bedrock instead of loose moraine material (Allen et al., 2016b). However, overtopping from displacement waves after the entering of a debris flow, rock or ice avalanche into the lake can still occur. Many of the currently and future growing lakes will be situated beneath hanging glaciers and seracs or below potentially unstable rock slopes (Haeberli et al., 2010). Therefore, the probability of mass movements triggering a GLOF will likely rise (Allen et al., 2016).

The fact that GLOFs represent a particularly dangerous glacial hazard was already demonstrated by several events in the past. A very severe example is the one of Kedarnath, Indian Himalaya, where hundreds of buildings were destroyed, thousands of people lost their life and roads and paths were disrupted (Bhambri et al., 2016). The total

economic damage was estimated to range around 1.1 Mio USD (Swiss Re, 2014). This event was such a disaster not least because of the ongoing pilgrim season and the high importance of Kedarnath as a pilgrimage site.

GLOF impacts on society always depend to a certain extent on population pressure and land use (Carrivick and Tweed, 2016). During the last decades, human settlements and activities have been observed to increase considerably in high mountain regions (Huggel, 2004). Residential, tourism and hydropower infrastructure expands now to higher altitudes and therefore conflicts with the natural environment will likely increase (Allen et al., 2016b). In India, energy consumption experienced a steep rise by 51% between 2000-2010. If rapid economic growth is sustained in future energy demands are expected to increase by another 75% by 2035. Currently, only a small fraction of the hydropower potential of the Himalayas is tapped, for example, Vaidya (2012) estimate that less than 20% of the $\sim$ 500GW available is used by the Himalayan countries. In consequence, there are numerous hydropower projects across the Indian Himalayas. In Uttarakhand, the Indian state where the study area is located, more than 450 hydroelectric power schemes are proposed or already in the development phase (Buechler et al., 2016). Currently, a push of hydropower projects into headwaters occurs adding uncertainty to expected GLOF peak discharges and impacts (Schwanghart et al., 2016). Peak discharges further downstream can be predicted more precisely as GLOF waves attenuate rapidly (Schwanghart et al., 2016).

In future, the land area which could be affected by a GLOF will likely increase due to growth and formation of new lakes. Across the Indian state of Himachal Pradesh, a neighbouring Himalayan state of Uttarakhand, a minimum $2 - 3$ fold increase is expected in several districts (Allen et al., 2016b). Assessment of current glacial hazards by magnitude and probability of occurrence is already in practice. However, as anticipating hazards is better than only reacting to problems after they appear, this thesis investigated the temporal evolution of emerging GLOF hazards in the Bhilangna Valley, Indian Himalaya.

Frey et al. (2010) state that predicting the time of occurrence of a future glacier lake needs to be coupled with simple but transient models which simulate the glacier retreat over large regions. In order to achieve time-dependent changes, glacier-evolution models must be linked to a climate scenario (Linsbauer et al., 2013). Schneider (2011) recommend to consider worst-case scenarios because climate is changing rapidly and therefore building simply on the basis of local empirical data of past events is problematic.

Linsbauer et al. (2013) proposed a simple glacier-evolution model which is based on ice thickness changes. The model was developed for the Swiss Alps where good historical data on thinning is available. However, in most mountain regions such as the Himalayas data are scarce. Therefore, this thesis focused on implementing an approach using commonly available simple input data such as glacier outlines to de-

rive the amount of thinning for glaciers in the Bhilangna Valley. Past ice thickness changes are then linked with past temperature change and thinning is projected into future. Thereby, two warming scenarios are considered which are based on the gridded temperature projections of the CMIP5 models for the two radiative forcing scenarios RCP4.5 (medium forcing) and RCP8.5 (worst-case forcing) for this region (IPCC, 2013). As future precipitation evolution is very uncertain it was excluded from analysis. The proposed model is strictly empirical and has no physical basis.

Mass movement impacts into glacier lakes are reported as common GLOF triggers (Allen et al., 2016b; Worni et al., 2014; Schneider et al., 2014). It depends on the topographic setting, i.e. steep rock faces or glaciers in proximity, whether a lake is prone to generate a GLOF. This aspect was operationalised using the topographic potential concept described by Allen et al. (2016b). In combination with the lake volume an assessment of future GLOF hazards posed by lakes could be performed. Of course, the likelihood of a GLOF is also conditioned by other factors such as dam stability. But as no information exists on future dams, although it can be expected that they will be composed of bedrock (Allen et al., 2016b), dam stability was not considered in the modelling part of this thesis.
To evaluate the exposure of current and planned hydropower stations in the Bhilangna Valley, paths of potential GLOFs were modelled with the modified single flow model (MSF) (Huggel et al., 2003) and intersected with station locations. Results were examined in a Boolean manner whether a site is or is not affected by a modelled flood path. An overlay of all modelled paths yielded a first order assessment of site exposures to potential GLOFs.

This thesis is affiliated to the scientific project "Flood Risk in Uttarakhand, India: Learning from the 2013 Disaster and Anticipating Emerging Threats" which examines the physical, social and institutional factors that played a crucial role in the Uttarakhand flood disaster 2013. An overall aim is to incorporate the findings in disaster risk reduction and climate adaptation measures. The thesis is linked to the work package "emerging threats".

1.1 Research questions

The thesis aims to provide a first order assessment of the spatiotemporal evolution of GLOF hazards in the Bhilangna catchment. The relative exposure of current and planned hydropower stations located along the Bhilangna River shall be estimated. To achieve this goal a sequential approach was adapted which seeks to answer the following questions:

1. What is the amount and pattern of glacier surface elevation change observed in the Bhilangna catchment between 1968 and 2015?

2. What was the temperature change during the last 50 years for the Garhwal Himalayan region?

3. Considering past rates of thinning, and projected warming scenarios for the future, when will new lakes in the Bhilangna catchment emerge from beneath the retreating glaciers?

4. How will the hazard in terms of water volume and mass movement impact probability evolve for current and future lakes in the future?

5. Are current and planned hydropower stations located in the Bhilangna Valley affected by potential GLOF paths and how will the exposure of these assets evolve in the future?

1.2 Structure

The thesis is divided into a first part describing the scientific background and a second practical part. The first chapter gives an overview about the Himalayan mountain range in general, its extent, topographic and climatic characteristics. A description of the study area situated in the Indian state Uttarakhand follows afterwards, mentioning topographic, glacial, geological and socioeconomic aspects of this region. In a next step, past climatic evolution in the Indian Himalayan region is reviewed and future projections are discussed. It follows an overview of past glacier changes in India. The section about future glacier modelling presents a selection of approaches to model ice thickness, future lake positions and glacier-evolution. The impact of climate warming on the evolution of natural hazards in the glacial and periglacial area is discussed in a next step. Afterwards a section on GLOFs describes general characteristics, i.e. dam failure, flow transformations, and the procedure to model potential GLOFs and process chains. A description of the flood disaster 2013 in the Mandakini Valley is included at the end of the GLOF-section. In the last section of the scientific background part an overview on hazard assessment is given. The practical part is divided into four sections each of these sections having a method and a results part. The following topics are treated in this sequence: past glacier changes, future glacier evolution, emerging GLOF hazards and the evolution of the downstream hazard. The discussion summarises the most important results of the practical part and compares them with results from other studies where possible. The conclusion proposes what could be investigated in future studies.

2 Scientific Background

2.1 Geographical setting

2.1.1 The Himalayas - an overview

The arc of the Himalayan mountain range extends from northwest to southeast roughly between 29-37°N and 72-96°E on a length of around 2500km (Seyfferth, 2006). Five countries have at least parts of their area located in the Himalaya, namely Pakistan, China, India, Nepal and Bhutan. The great extent of the mountain range leads to a variety of topographic, geologic and climatic conditions and therefore regions show different characteristics. A discussion exists which of the outermost regions in the NW such as the Karakoram, the Hindu Kush and the Pamir or in the SE such as the Hengduan Shan shall be attributed to the Himalayas. Authors resolve these ambiguities by talking i.e. about the Hindu Kush-Karakoram-Himalayan region (HKH) or about the Pamir-Karakoram-Himalayan region (PKH) (Gardelle et al., 2013; Kaab et al., 2012; Bolch et al., 2012). In this thesis the term Himalayas is used in a broader sense referring to the Himalayan Karakoram region. The Himalayas represent a rather long and narrow mountain chain with a width of only 150km in most parts of the central and eastern Himalaya. The northwestern part including Karakoram shows larger widths of up to 300km (Seyfferth, 2006). Despite the narrow N-S respectively NE-SW extent large elevation differences can be found within short distance. From the low lands of India and Pakistan at several hundred meters above sea level the altitudes rise to over 8000m. The Himalayas are therefore the highest mountain range of the world. North of the mountain chain the Tibetan Plateau follows with altitudes of around 4000m (Seyfferth, 2006).

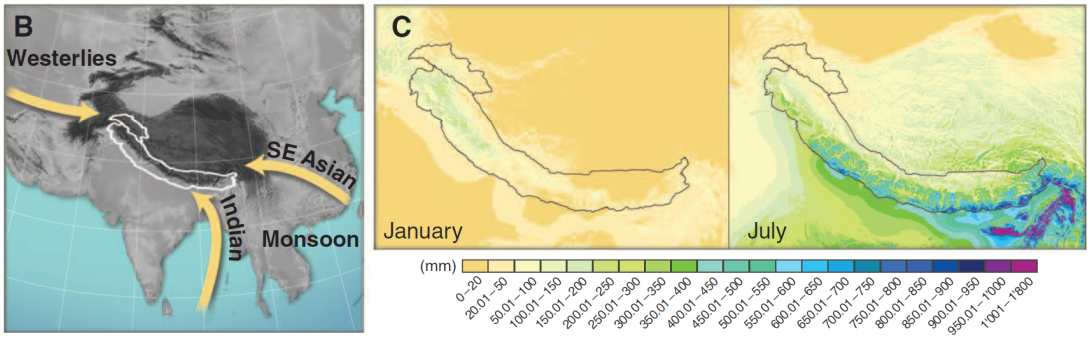

Figure 2.1: Main wind systems influencing the climate in the Himalayas (left) and mean precipitation in January and July (right). Figure reproduced from Bolch et al. (2012).

Climate and glaciers

Due to their high elevations, the Himalayas act as a barrier blocking transfer of moist air masses to the Tibetan Plateau (Bolch et al., 2012) and determine the regional climate in this way (Singh et al., 2016). Two major weather systems govern the timing and amount of precipitation in the Himalayas, one being the Indian monsoon which is replaced by the SE-Asian monsoon further in the east, the other being the mid-latitude westerlies (Bolch et al., 2012; Bookhagen and Burbank, 2010; Yang et al., 2008). Fig. 2.1 shows these major weather systems and the amount of winter and summer precipitation for the different regions. According to this, glaciers in the Karakoram and the western Himalaya receive most of their snow supply in winter whereas for glaciers in the central and eastern Himalaya the main accumulation period coincides with the summer ablation period (Bolch et al., 2012). Therefore glaciers in the northwest belong to winter accumulation type glaciers and those in the central and eastern part to the summer accumulation type (Benn and Evans, 2010; Bolch et al., 2012).
Closely linked to mass gain from snow accumulation and mass loss due to meltwater runoff and sublimation is the equilibrium line altitude (ELA). It indicates the elevation where accumulation equals ablation (Cuffey and Paterson, 2010). On temperate glaciers, it can be approximated from the position of the snow line at the end of the ablation period (Cuffey and Paterson, 2010) and therefore determined from remote sensing data. Bolch et al. (2012) state that the mean ELA for the whole Himalayan range is around $5360m$ with highest values in the central Himalaya ($\sim 5600m$) and lowest values in the western part ($\sim 5150m$) where more accumulation occurs.
But not only the altitude of the equilibrium line, also the glaciated area reflects different amounts of accumulation and ablation. The Himalayan region showing the largest glaciated area is the Karakoram in the northwest. Glaciers here extend to relatively low elevations (down to $\sim 2300m$ (Seyfferth, 2006)). Bolch et al. (2012) estimated a glacier coverage of $\sim 40800km^2$ for the whole Himalaya, the Karakoram contributing with $\sim 18000km^2$ almost 50% to this value. This is remarkable as the Karakoram covers less than 10% of the Himalayan mountain range. Frey et al. (2014) analysed the volume of glaciated area in different major regions, fig. 2.2 shows the hypsometry results. Areas were determined by remote sensing techniques and the volumes presented in the figure were calculated using the GlabTop2 model (more information on GlabTop2 is given in section 2.3.2). It can be seen that smallest areas and lowest volumes are found in the eastern Himalaya. Central and western Himalaya show similar glaciated areas and volumes but glaciers located in the central Himalaya seem to be situated at higher elevations. Largest glacier coverage and volume can be found in the Karakoram. However, in terms of number of glaciers the highest number was not determined for the Karakoram but for the western Himalaya (Frey et al., 2014).

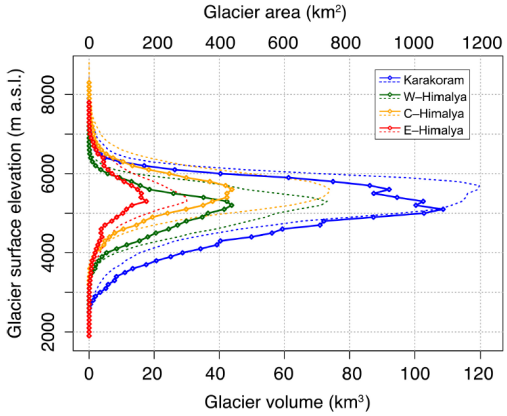

Figure 2.2: Areas (dashed line) and volumes (solid line) for different regions of the Himalayas as calculated with GlabTop2. Altitudes correspond to glacier surface elevations. Figure reproduced from Frey et al. (2014)

.

Indian Himalayan Region

The Indian Himalayan Region (IHR) covers an area of around 0.67 million km^2 (Singh et al., 2016) and can be subdivided in a western and an eastern part. The states Jammu-Kashmir, Himachal Pradesh and Uttarakhand belong to the western IHR (western and central Himalaya) and Sikkim and Anurachal Pradesh to the eastern IHR (central and eastern Himalaya). Therefore, intense summer precipitation is experienced in the eastern IHR as well as in the east of the western IHR in the form of rainfall at lower altitudes and snow at higher elevations (Singh et al., 2016). In the northwest of the IHR the dominance of mid-latitude westerlies leads to more than a third of the precipitations (37%) occurring from January to March (Singh et al., 2016). Another third (31%) of the yearly precipitations is registered during April to June and the last third (32%) during 6 months from July to December (Singh et al., 2016). Around 9600 glaciers are located in the Indian Himalayas (Bhambri et al., 2011).

2.1.2 Bhilangna Valley

The study area is situated in the Bhilangna Valley which is part of the Indian state Uttarakhand and belongs to the Garhwal Himalaya (fig. 2.3). Local population here lives from farming, fishing, livestock rearing and fodder collection (Buechler et al., 2016). The Bhilangna Valley is rather a remote region with small villages neither frequently visited by tourists nor by pilgrims which distinguishes it clearly from the highly visited neighbouring valleys of Mandakini with the pilgrimage site Kedarnath and from the Bhagirathi Valley with the holy place Gangotri at the source of Ganges. The Bhilangna

Valley extends approximately between 30.43°N and 30.88°N and 78.66°E and 79.03°E and shows a total length of $\sim 60km$. Its orientation is from NE to SW with highest elevations in the NE. Here, peaks attain altitudes of more than $6000m$ above sea level, the highest peak Thaley Sagar named also Phating Pithwara at the northeastern end of the valley raises up to $6904m$ (fig. 2.5). The southwestern boundary of the Bhilangna Valley is at Ghansali, a small village with a censed population of around 400 people (Census Organisation of India, 2011). The valley covers around $628km^2$ with the main study area situated at the glacierised northeastern end ($\sim 233km^2$).

Glaciers

Two main valley glaciers dominate the study area, the first being Khatling in the west covering about $31km^2$ and the second being Phating in the east with roughly $10km^2$ (fig. 2.4). In 2015, the tongue of Khatling Glacier terminated at $\sim 3975m$. It seems to be strongly covered by debris up to an elevation of around $4300m$ followed by a zone of either very thin debris or dust cover between $4300m$ and $4730m$. This zone shows transversal crevasses as the glacier passes over a topographic steepening. At $4800m$ the confluence of Sangli Glacier and Khatling Glacier is located from where a prominent middle moraine develops in downstream direction. Around and above the confluence zone the glacier is gently sloped with angles below 10°. And even the accumulation zone is characterised by gentle to moderate slope values rarely exceeding 20°. Vaster steep zones with slopes of more than 30°can be found only at the highest elevations between $5420m$ and $6100m$ on the northeastern and eastern flank of Jaonli (6632).
Phating Glacier is in several aspects different to Khatling Glacier. The exact position of its terminus is difficult to determine as it is heavily debris covered. However, it seems to be at around $3820m$ in 2015. But not only the terminus, the whole glacier tongue is under a rather thick debris cover which seems to continue up to the confluence of Bhartekhunta Glacier with Phating Glacier at an altitude of around $4320m$. According to satellite images the debris cover seems to be thinner on both glaciers above the confluence with ice showing through the debris. Clean ice can be found above $\sim 4420m$ on Phating and above $\sim 4450m$ on Bhartekhunta Glacier. Compared to Khatling Glacier, Phating Glacier shows an even flatter tongue. Over a distance of $4.8km$ the elevation difference is $580m$ which results in a mean slope of 7°. However, a major disparity between Khatling and Phating Glacier can be found in the accumulation zone. In contrast to Kathling, it is quite steep for Phating and Bhartekhunta Glacier with vast areas being steeper than 30°. Bhartekhunta Glacier extends to an altitude of $\sim 6330m$ and Phating to $\sim 6150m$.

Satellite imagery from the end of the hydrological year (Landsat 8, 8. Sept. 2015) suggest that the equilibrium line altitude (ELA) is located somewhere between $5000m$ and $5200m$ for the whole catchment. Assuming a value of $5100m$ allows to determine

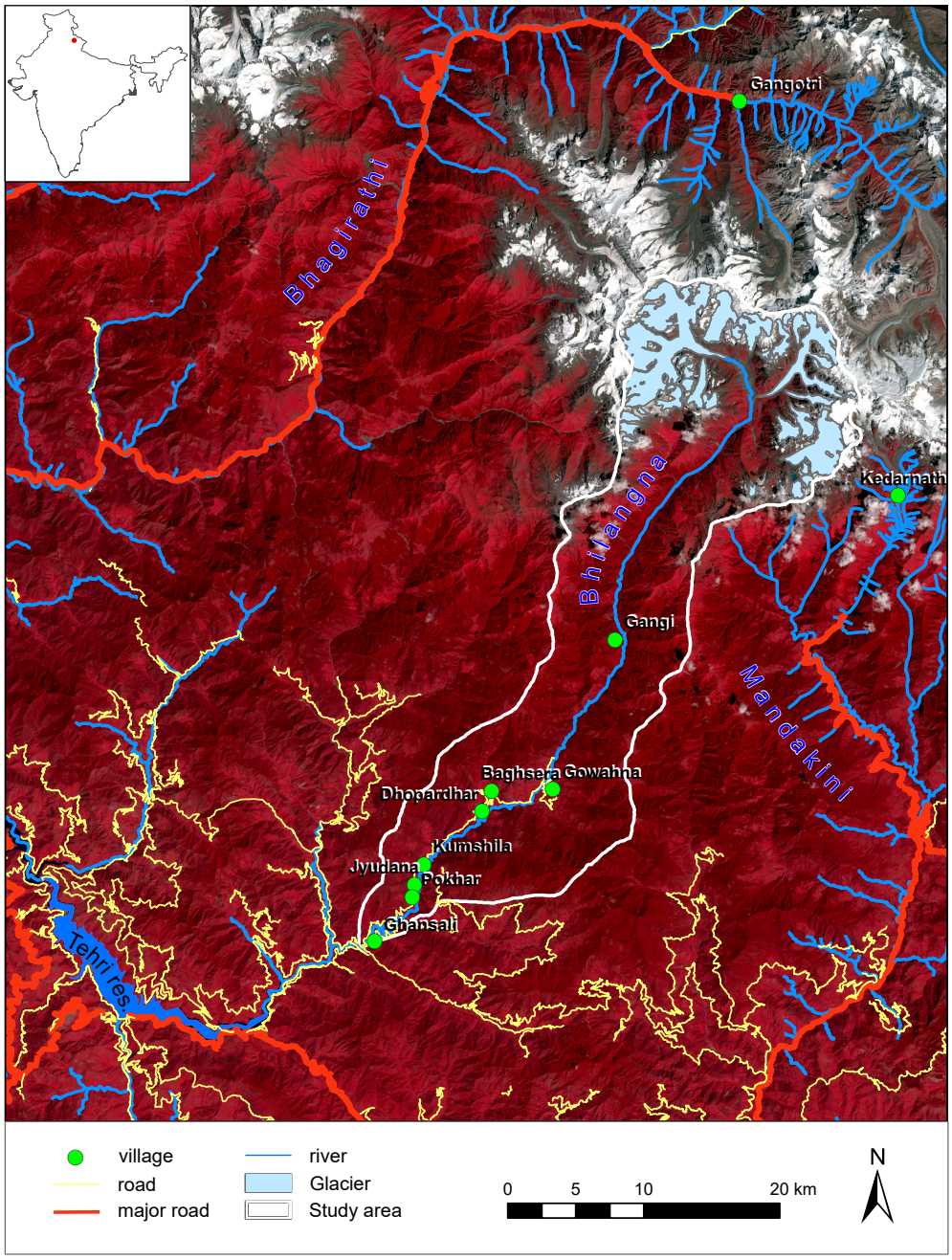

Figure 2.3: Overview of the study area (white frame), red dot in the small map (top left) is indicating the position within India. Villages (green dots) and glaciers (light blue) are shown within the Bhilangna Valley. Gangotri and Kedarnath are added for orientation purpose. A motorable road exists up to Gowahna, Gangi is the last village in the valley and only accessible by a trek path. Gangotri and Kedarnath are important Hindu pilgrimage sites and therefore major roads exist high up in the Bhagirathi and Mandakini Valley. The Tehri reservoir (bottom left) is the largest reservoir in India and a very important source for hydropower energy. Road, village and river data are taken from OpenStreetMap.

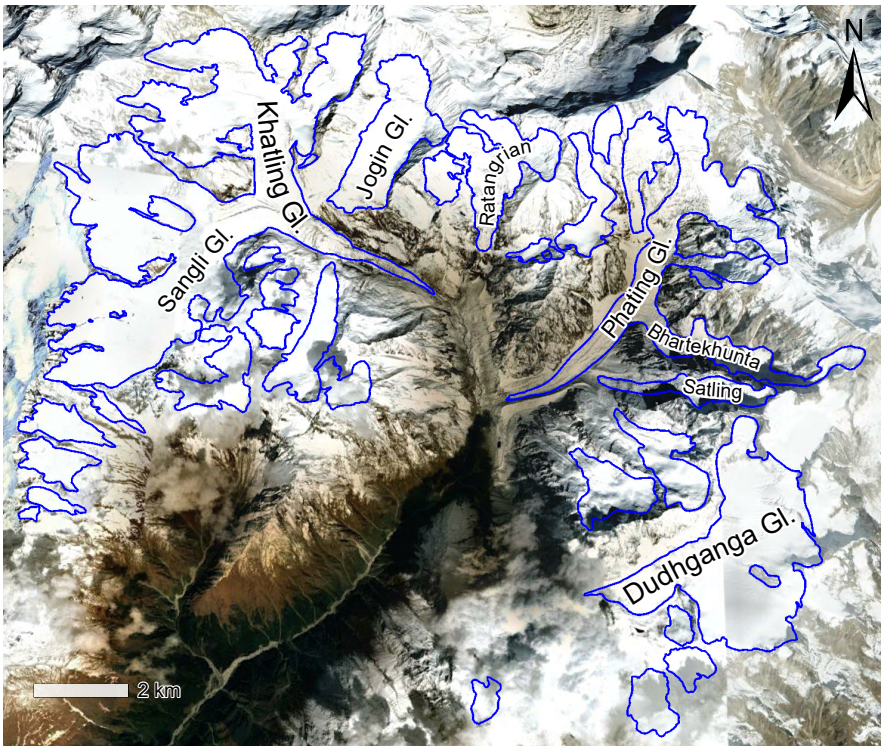

Figure 2.4: Glaciers located in the study area overlaid on Google Earth imagery (acquisition date: 16 October 2014).

the accumulation area ratio (AAR) of the glaciers. The accumulation zone of Khatling Glacier situated below Jaonli ($6632m$) and below Bhetiara ka Danda ($5748m$) where the contributing Sangli Glacier originates covers around $21km^2$ and though the AAR for Khatling is 0.69 or 2:1. This lies in the range of values which were calculated by Haeberli et al. (2003) for 63 alpine glaciers. They stated that for glaciers with a net mass balance of 0 the AAR can take values from 0.22 to 0.72 with a mean of 0.55. With this the Khatling Glacier has an AAR exceeding the mean value. The accumulation area of Phating Glacier (including Bhartekhunta Glacier) covers around $4.6km^2$ and the AAR takes a value of 0.46.

Further glaciers located in the catchment are Jogin Glacier, Ratangrian Glacier, both former contributors to Khatling Glacier, Satling Glacier a former contributor to Phating Glacier and the rather flat and vast Dudhganga Glacier.

Figure 2.5: Best available map of the study area (ca. 30 years old). Map section reproduced from Huber (1985).

Geology

Rao and Pati (1980) investigated the geology of the Bhilangna Valley. They stated that the valley comprises two tectonic units in the Central Himalayan Crystalline Group of rocks and a third Deoban/Garhwal tectonic unit. The Deoban/Garhwal unit is characterised by sedimentary rocks and is separated from the crystaline rocks of the Central Himalayan Crystalline Group by the Thayeli Thrust which is located less than $5km$ northeast of Ghansali. The Thayeli Thrust corresponds to the Main Central Thrust in this area. The Central Himalayan Crystalline Group located at north from the Deoban/Garhwal unit can be subdivided into the Bhilangana Formation and the Gangi-Kedarnath Formation. The study area lies in the Gangi-Kedarnath Formation which in general comprises various types of schists, phyllite, porphyroblastic gneiss, granulite, marble, quartzite, granite and amphibolite. More specifically, the main study region belongs to the Rambara member of the Gangi-Kedarnath Formation. Rao and Pati (1980) found a sequence of marble, quartzite, various types of schist and porphyroblastic gneiss, granulites, calc silicates and metabasites being characteristic for this area. As the glacierised area of Bhilangna Valley was at the margin or even outside of the area of investigation of the mentioned study, more details are not available for this uppermost valley part.
According to field observations in May 2016 especially crystalline rocks such as quartzite or gneiss seem to dominate this area even though other rocks such as schists were also observed. It is important to note, that no detailed analysis was carried out during the field work and consequently a confusion between similar rocks such as gneisses and granulites is possible. All observed rocks are crystalline, medium to high grade metamorphic rocks of high hardness (Softusvista Inc., 2017). This fact could explain why many steep mountain flanks can be found in the area. However, observations indicate that the rock is locally strongly fractured allowing for faster erosion. Debris is present everywhere in the proglacial area in large amounts accumulating especially in the flat proglacial area where stream power is too low to transport it down valley.

Landcover

From a landcover point of view, the percentage of cultivated land is diminuishing from Ghansali towards Gangi with a simultaneous increase of forested area. Upstream of Gangi, forest covers most of the area up to an elevation of approximately $3200m$. At higher elevations a sequence of shrubs follows which is replaced by grass above $3600m$. The proglacial area as well as flatter parts within the main study area are higly debris covered with little vegetation. However, the prominent lateral moraine of Phating Glacier shows vegetation cover on the outer southern and east oriented side.

Figure 2.6: Cultivated area around a small village situated upstream of Gowahna and downstream of Gangi (top left). Area vacated by the Khatling Glacier, its debris covered tongue is marked with a blue polygon; the arrow shows the former position of Ratangrian Glacier which joined Khatling Glacier in the past (top right). Exposed bedrock showing the crystalline rocks downstream of Dudhganga Glacier (bottom left). Proglacial area of Khatling and Phating Glacier, the middle moraine of these two glaciers is visible in the centre of the image; in the background Ratangrian Glacier and Thaley Sagar (6904m, snow-covered peak at right) can be observed (bottom right).

Socioeconomic situation

Numbers and derived statements presented in this section are based on statistical tables provided by the Office of the Registrar General & Census Commissioner India (2011) if not indicated differently.
The Bhilangna Valley is located in the Ghansali Tahsil which belongs to the district Tehri Garhwal. Ghansali Tahsils population grew slightly by 2.42% between 2001 and 2011 and counted 120775 inhabitants in 2011. Most inhabitants live in rather small villages populated by several hundreds of people. 100% of the population of Ghansali Tahsil lives in rural area. Literacy rates are rising, however, 40% of the population is still uneducated, two thirds being female (Villageprofile, 2017). 220 out of 260 villages have a primary school, 104 a middle school and 41 a secondary school. Medical facilities and post offices are rather scarce 201 villages having no medical facility and only 43 having a post office. All villages have access to drinking water and power is available in

every village with one exception. A large part of the villages is accessible either by bus or taxi. Agriculture is of major importance in the whole state of Uttarakhand. Around 31% of the gross domestic product of Uttarakhand comes from agriculture and more than 70% of the population depends on agriculture for their livelihood (Thadani et al., 2015). In Ghansali Tahsil more than 80% of the working population is engaged in the agricultural sector. The main food crops planted are wheat and paddy (rice), millet is cultivated in third place (Office of the Registrar General & Census Commissioner India, 2011). Most of the villages have rather a small proportion of their fields irrigated. 43.88% of the total area in Ghansali Tahsil is cultivable and 27.46% of this cultivable area is irrigated demonstrating the high dependency on natural water input.

Hydropower

The following information are drawn from the Census Handbook provided by the Directorate of Census Operations Uttarakhand (2011) The construction of the Tehri dam started in 1978 and it could be put into operation in June 2006. Tehri dam was built at the confluence of Bhagirathi and Bhilangna River at the former position of old Tehri town and is the largest hydropower dam in India with a height of $261m$. Bhilangna River is an important source of water for this reservoir which has the capacity to generate 2400 MW of power. Additionally, it stabilises irrigation for a vast area and supplies 270 million gallons (equivalent to 1.2 billion litres) of drinking water per year to industrialised cities in the states of Delhi, Uttar Pradesh and Uttarakhand. Along the Bhilangna River four smaller hydropower stations (H1-H4) were constructed between Ghansali and Gangi, their locations can be consulted in fig. 3.24. Another station (H5) is planned $\sim 2.5km$ downstream of Gangi.

2.2 Climate change

2.2.1 Past evolution

Climate is defined as the long-term average of weather conditions including temperature, precipitation, humidity, wind speed and direction (Singh et al., 2016). A time span of 30 years is often used to obtain climate parameters for a given site. Any long-term deviation of these averages which can be provoked by natural variability or human activities is regarded as climate change (IPCC, 2007). Climate is changing continually across the world with random fluctuations from one year to another superimposed on longer term trends (Cuffey and Paterson, 2010). As many energy exchange processes, such as longwave radiation flux or sensible heat flux, are governed by air temperature, temperature is considered to be a good indicator of climate change (Bhutiyani et al., 2007). Various authors stated a systematic increase in temperatures

all over the world. A rise of $0.85K$ was determined for the period 1885-2012 which leads to a global mean temperature increase of around $0.05K$ per decade (IPCC, 2013; Diaz and Bradley, 1997; Easterling et al., 1997; Folland et al., 2001). It is important to bear in mind that these numbers represent a global average and warming patterns of different global regions differ considerably. Particularly mountainous regions seem to be subject to increased warming rates. Different studies registered a significantly stronger increase in minimum temperatures for mountainous regions such as the Swiss Alps, the Colorado Rocky Mountains, the Tibetan Plateau and the Tropical Andes as compared to surrounding low lands (Rangwala and Miller, 2012).

Observed temperature changes in the Himalayas

The Himalayas show non-uniform evolution of temperatures across the mountain range. In contrast to other mountainous regions large parts of the Himalayas experienced a more prominent increase in maximum than in minimum temperatures (Bhutiyani et al., 2007; Kattel and Yao, 2013). However, the rather difficult accessibility of mountain areas and therefore the lack of long-term in situ observations leads to uncertainties and problems in quantifying the magnitude of climatic trends in complex topography such as the Himalayas (Kattel and Yao, 2013). Xu and Grumbine (2014) determined a warming rate that is more than twofold higher for the Himalayan region than for worldwide data. A sharp rise was registered in the last few decades (Singh et al., 2016).

Bhutiyani et al. (2007) analysed the long-term trends of annual maximum, minimum and mean temperatures in the north-western Himalayas for a total of 10 stations located in the Indian states of Jammu-Kashmir and Himachal Pradesh. They found a warming of $1.6K$ for the last century with particularly noteworthy temperature increase during the winter season. Also Bolch et al. (2012) write in their report that warming was more prominent in winter than in summer between 1959-2007 at Tingri weather station located at $4300m$ north of Mount Everest. The rise in mean annual air temperature was $\sim 0.03K$ per year for this period. Kothawale and Rupa Kumar (2005) estimated warming trends for different Indian regions. Their results show that the western Indian Himalayan region has warmed stronger compared to the Indian average ($0.2K$ per decade) during 1971-2003. Moreover, they could determine an accelerated rate of warming for the period 1971-2003 in comparison to 1901-2003. Bhutiyani et al. (2007) observed a clearly distinguishable onset of modest warming in the decade of 1961-1970 which continued until the end of the period analysed at all stations the only exception being the decade of 1981-1990. The end period 1991-2002 showed the highest rates of warming compared to the preceding decades.

Bhambri et al. (2011) describe an increasing trend in the annual maximum temperature but a decreasing trend in the annual minimum temperature for the Indian

Garhwal Himalaya and the study period 1968-2011. Their temperature data stem from Mukhim, Tehri and Bhojbasa station (Bhojbasa station is located at $\sim 3780m$ near the terminus of Gangotri Glacier). (Bhambri et al., 2011) investigated also the correlation of meteorological data between Mukhim and Bhojbasa station. But any correlation could be found which is possibly due to the short data overlapping period of only 5 years. Anyway, it seems that transferring measured station data to another location is problematic and climate in mountainous region is influenced more by local factors than the general synoptic situation (Bhambri et al., 2011). Therefore, it remains uncertain whether temperature trends measured far below the lower limit of glaciers are also valid for higher altitude sites (Bolch et al., 2012).

Effect of temperature change on precipitation across the Himalayas

Temperature affects the amount and type of precipitation. Particularly the minimum temperature is decisive whether rain or snow fall occurs (Snehmani et al., 2015). As an increasing temperature trend is observed in all regions of the Indian Himalayas the rain-snow-boundary is expected to shift to higher elevations. However, no spatiotemporal trend could be determined for precipitation yet (Singh et al., 2016). The Garhwal Himalaya which is located in the Indian state of Uttarakhand receives precipitation from the Indian monsoon in summer as well as from the Westerlies in winter. Its climatic regime corresponds to a transition regime between the climate found in the eastern and the Karakoram Himalaya (Bhambri et al., 2011). Guhathakurta and Rajeevan (2008) conducted a detailed study of precipitation pattern for entire India. Their results suggest that precipitation has decreased significantly during the winter season for the period 1901-2003. Annual precipitation in Uttarakhand shows a decreasing trend too but it is not significant in this case (Guhathakurta and Rajeevan, 2008).

Key observations

In summary, it can be said that different datasets and periods analysed make it challenging to compare warming values of different studies. In general, it can be stated that warming has accelerated during the last few decades and winter temperatures seem to have risen more than summer temperatures. For the Karakoram this leads to additional solid precipitation in winter (Shekhar et al., 2010; Fowler and Archer, 2006) as warmer air can contain more moisture. In contrast, for glaciers depending on summer snowfall increasing temperatures during the summer months lead to less accumulation.

2.2.2 Future projections

Climate change is not restricted to national boundaries and therefore transnational cooperation is needed. The Intergovernmental Panel on Climate Change (IPCC) has the

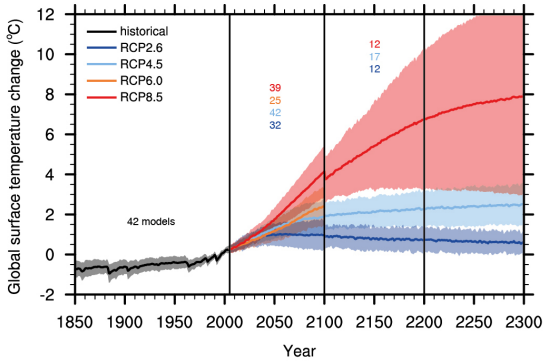

Figure 2.7: Global annual mean surface air temperature anomalies (relative to 1986-2005) from CMIP5 concentration-driven experiments. Solid lines represent the multi-model mean and the coloured area the 5 to 95% range across the distribution of individual models. Numbers in the figure represent the number of models used for the different time periods. Differing numbers of models between 2000-2100 and beyond 2100 are also the cause why discontinuities can be found at 2100. Only two models are available for RCP6.0 projections beyond 2100 therefore no ranges are figuring in the plot. Figure reproduced from the IPCC report (IPCC, 2013).

scope of informing about the current state of knowledge and the potential environmental and socio-economic impacts related to climate change (IPCC, 2017). To model future climate evolution, historic data as well as assumptions on future emissions and concentrations of greenhouse gases, aerosols and other forcing agents are required. Especially socioeconomic development and the related emissions are difficult to predict (IPCC, 2013). Therefore, the use of multiple scenarios has become a standard and allows to compare a wide range of potential climate evolutions (IPCC, 2013). In consequence, results do not represent probabilities but only a variety of possible outcomes.

Global temperature changes

The Representative Concentration Pathways (RCPs) were defined by scientists considering a large set of mitigation scenarios which distinguishes them from the previously used SRES scenarios (Special report on Emission Scenarios) (IPCC, 2013). Four scenarios exist which are defined by their approximate radiative forcing at the end of the 21th century compared to 1750. RCP2.6 represents a scenario with a very low forcing of only $2.6 W/m^2$ by 2100, RCP4.5 and RCP6.0 are two different stabilisation scenarios and RCP8.5 is a scenario with a very high forcing of $8.5 W/m^2$. RCP2.6 shows a peak and a decline of radiative forcing before 2100, RCP4.5 stabilises by then and no peak appears by 2100 for RCP6.0 and RCP8.5 (IPCC, 2013). Fig. 2.7 shows the resulting air temperatures if RCP scenarios are used to model temperature evolution.

Temperature changes are very similar for all RCP scenarios for the first two decades after 2005. The longer the time period investigated the more do the results of the RCP scenarios differ. Mean global warming is less than $2K$ until 2100 for RCP2.6 which demonstrates the capability of aggressive mitigation policies (IPCC, 2013). For all other RCP scenarios temperature increase exceeds this value by 2100, RCP8.5 even showing a mean temperature change higher than $4K$. A stronger temperature increase is modelled for land areas compared to ocean surfaces. For RCP8.5 air temperature is expected to increase by $4.8 \pm 0.9K$ over land for the period 2081-2100 which is more than $1K$ higher than the global mean of $3.7 \pm 0.7K$ (IPCC, 2013). In general, a higher radiative forcing leads to higher temperatures as well as to a wider spread of possible future values. In this way, a temperature rise of $0.3 - 1.7K$ was modelled for RCP2.6 by the end of the 21th century considering the 5 to 95% range of all CMIP5 models, $1.1 - 2.6K$ for RCP4.5, $1.4 - 3.1K$ for RCP6.0 and $2.6 - 4.8K$ for RCP8.5 (IPCC, 2013).

Temperature projections for India

Fig. 2.8 shows the temperature projections based on RCP4.5 and RCP8.5 for different time scales on a world regional level for South Asia. It can be observed that for the first period up to 2035 temperature increase appears similar for the two RCP scenarios. Between 2046-2065 temperature changes for RCP4.5 are lower than for RCP8.5 and an increase of $1 - 3K$ is expected. For RCP8.5 values range between $1.5 - 4K$. The projections for 2081-2100 appear similar as the for the previous period 2046-2065 for RCP4.5 with slightly increased temperature change values. However, a remarkable difference exists for the two states 2046-2065 and 2081-2100 of RCP8.5 with temperature changes ranging from $3 - 7K$ over land surface for the latter period.
In all images of fig. 2.8 a temperature gradient can be observed when proceeding inland. Therefore temperatures are likely to increase more for the Indian Himalayan region than for mid- or south-India. Here, a warming of $2 - 3K$ or $5 - 7K$ might occur until 2081-2100 considering RCP4.5, respectively RCP8.5.
If changes are analysed on a seasonal level shifts appear to be larger in winter than in summer (IPCC, 2013). The study of Mathison et al. (2013) support these findings. According to their model simulations for the Ganges and Brahmaputra catchment temperatures will increase the most for winter (December-February) and autumn (September-November) in future. Concerning future precipitation evolution, no clear trend could be detected based on the simulation results of the IPCC report (IPCC, 2013) or on the study of Mathison et al. (2013).

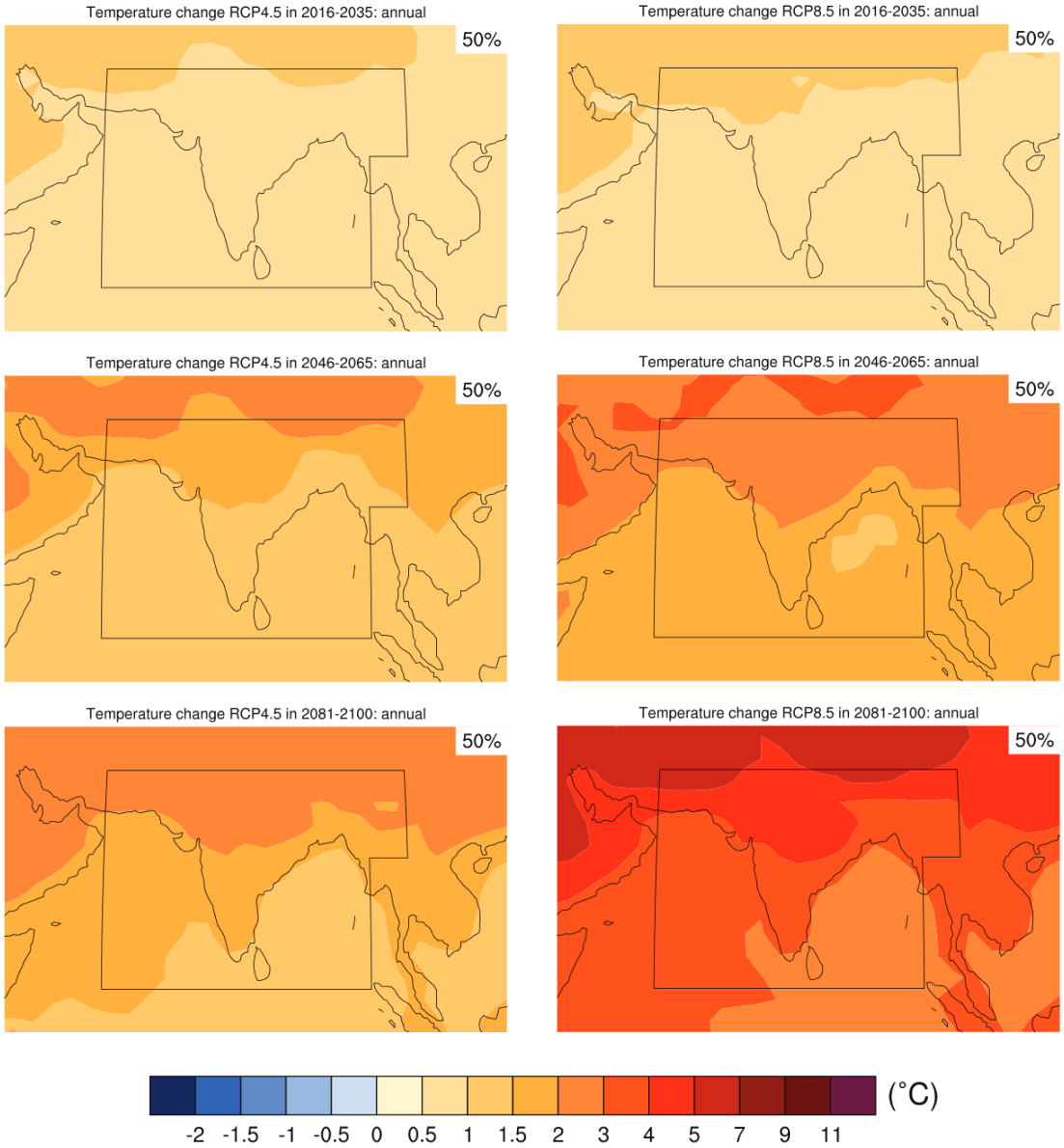

Figure 2.8: Temperature changes for RCP4.5 (left column) and RCP8.5 (right column) for 2016-2035, 2046-2065 and 2081-2100 (from top to bottom) relative to the reference period 1986-2005. Results are given for the median of all CMIP5 model runs. Figure reproduced from the IPCC report (IPCC, 2013).

2.3 Glacier changes

2.3.1 Past glacier evolution in the Indian Himalayas

Glacier changes are triggered by changes in accumulation and ablation and these in turn are strongly influenced by climate (Singh et al., 2016). On one hand, air temperature can be considered as a proxy for energy balance components and therefore as a driving factor for snow and ice melt (Ohmura, 2001). On the other hand the amount and form of precipitation governs the accumulation of glaciers (Singh et al., 2016). Across the Himalayan mountain range different glacier responses to climate change were recorded in the past. In the Karakoram even advances could be registered which can be attributed to surging or associated with the increasing precipitation trend in accumulation areas in recent past (Hewitt, 2005; Hewitt, 2007; Fowler and Archer, 2006). However, most glaciers in the Himalayas show a retreating behaviour (Cuffey and Paterson, 2010). In general, periods of rapid glacier retreat coincide with the episodes of rapidly rising global temperatures (Cuffey and Paterson, 2010). The observed variability for Himalayan glacier changes is founded on differing factors between individual glaciers and regions, i.e. monsoonal intensity, characteristics and thickness of supraglacial debris cover, altitudinal distribution of the glacier area as well as glacier size or the underlying and surrounding topography (Kargel et al., 2005; Bolch et al., 2008; Scherler et al., 2011; Kulkarni et al., 2007; Cuffey and Paterson, 2010).

Length changes

A very common way to evaluate glacier changes is to study length changes. Although the significance of length records concerning glacier changes is limited, measurements can be accomplished easily based on remote sensing data which explains the wide use of this method. Different variables were already estimated based on length change measurements, such as glacier mass balance, glacier contribution to sea-level rise, historical equilibrium line altitudes or glacier response times (Hoelzle et al., 2003; Luethi et al., 2010; Oerlemans, 2007; Leclercq et al., 2011; Klok and Oerlemans, 2003; Oerlemans et al., 2007; Pelto and Hedlund, 2001).
Singh et al. (2016) suggest an average retreat rate of around $18m$ per year for glaciers situated in the Indian Himalayan region and an observation period of four decades. Bhambri et al. (2012) investigated the length changes for Gangotri Glacier in the Garhwal Himalaya. They determined values based on changes along the central flow line and for the whole front. For the period 1965-2006 they report a total length change of $-818.9 \pm 14m$ and an average retreat of $-19.9 \pm 0.3m$ per year. This value is very close to the suggested $18m$ per year of Singh et al. (2016). If only the length along the central flow line is considered, values are higher; a total retreat of $-1085 \pm 14m$ was

determined by Bhambri et al. (2012). In general, averaging along the front should be preferred as this method is more robust and estimations based on a single point are more susceptible to outliers (Bhambri et al., 2012).

The Gangotri Glacier being the largest glacier in the Garhwal Himalaya is well studied. Other authors (Tangari et al., 2004; Bahuguna et al., 2007) suggest for a similar period as studied by Bhambri et al. (2012) higher recession values of the glacier front of about $1600m$ and $1510m$. This leads to approximately a twofold higher retreat rate per year ($\sim 40m$ per year). The reason for these discrepancies could be the mapping inaccuracies of the glacier tongue position. Mapping is hampered by debris-cover, shadow areas as well as seasonal snow on satellite images (Bhambri et al., 2011). Additionally, remote sensing products used in studies have different times of acquisition and therefore levels of accuracy for glacier mappings vary (Bhambri et al., 2011). The increase in debris-covered area, i.e. $11.8 \pm 3.0\%$ for the Bhagirathi basin containing Gangotri Glacier (Bhambri et al., 2011), can be considered leading to further delineation difficulties. Studies have shown that inaccuracies are also inherent in topographical maps produced by the Survey of India and consequently errors may propagate if these maps are used for length change measurements (Vohra, 1980; Bhambri and Bolch, 2009). For these reasons, the use of high resolution satellite data is recommended. Results based on these data are considered to be more reliable than those based on coarser resolution satellite data such as Landsat MSS and TM or topography maps (Bhambri et al., 2011; Tangari et al., 2004; Bahuguna et al., 2007).

Area changes

Besides length change, area change is widely investigated for glaciers as well. Overall, the glacierised area decreased for different parts of the Indian Himalayan region with an increased rate after the 1990s (Singh et al., 2016). Bhambri et al. (2011) focused on the glacier area loss in the Garhwal Himalaya and report a reduction by $4.6 \pm 2.8\%$ for the period 1968-2006 with an increased rate between 1990 and 2006. The annual recession rate in the Garhwal is comparable to the one determined for Khumbu Himalayan glaciers in Nepal both being $\sim 0.12\%$ per year (Bhambri et al., 2011; Bolch et al., 2008). The absolute area loss for the Gangotri Glacier front between 1968-2006 was $0.38 \pm 0.03 km^2$ and in the whole Bhagirathi basin the relative loss ranged from 2% to $\sim 28\%$ (Bhambri et al., 2011).
Bhambri et al. (2011) investigated also the effect of different factors on glacier area change in the Bhagirathi and the Saraswati/Alaknanda basin. Fig. 2.9 shows their results. According to that, glaciers with a larger elevation range and area show smaller relative area changes. However, if absolute area change is considered higher values can be found for larger glaciers. Bhambri et al. (2011) conclude that small glaciers are more sensitive to climate change than large glaciers probably due to their altitudinal

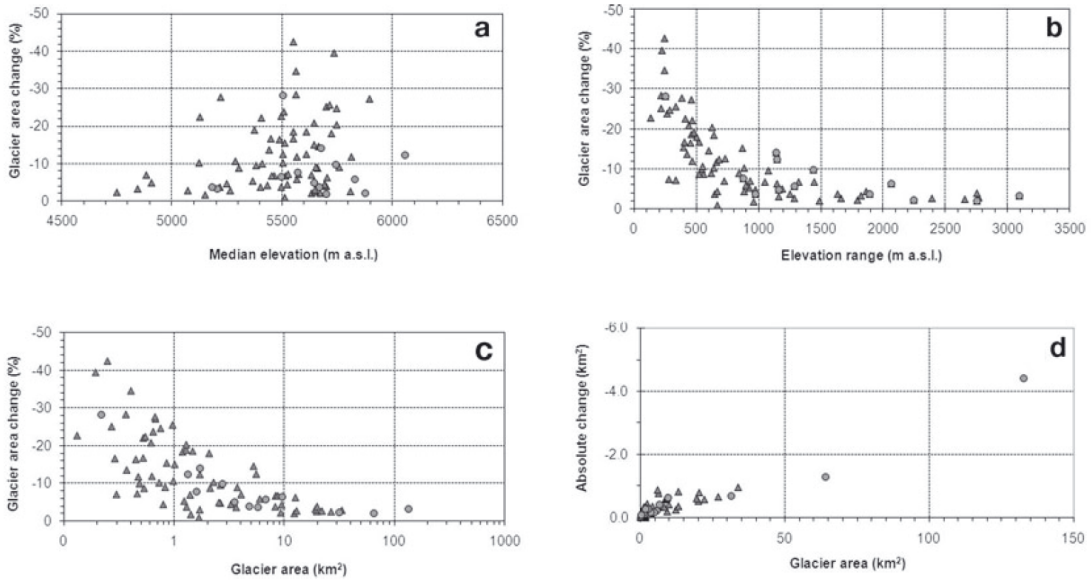

Figure 2.9: Scatter plots of (a) median elevation vs. glacier area change (%), (b) elevation range vs. glacier area change (%), (c) glacier area (km^2) vs. glacier area change (%) and (d) glacier area (km^2) vs. absolute glacier area change (km^2). Triangles correspond to glaciers in the Saraswati/Alaknanda basin and circles to those located in the Bhagirathi basin. Glacier area changes were derived from Corona (27 September 1968) and ASTER (11 October 2006) images. Figure reproduced from Bhambri et al. (2011).

distribution and the restricted or lacking accumulation zone. In contrast, the large glaciers studied receive ice contributions from tributary glaciers in accumulation zones and they often show a thick debris cover in their ablation zones reducing the ice melt below. Furthermore, Bhambri et al. (2011) found that north facing glaciers in the Bhagirathi and Saraswati/Alaknanda basin react more slowly than south facing glaciers by having lost only $\sim 4.7\%$ of their area compared to $\sim 19.4\%$ which is four times higher.

Mass balance changes

Neither glacier length nor area change capture the overall change in the amount of ice volume occurring for a glacier as they show only horizontal variation in extent. However, the process of downwasting[1] has been observed for many glaciers in the Himalayas especially for those with a vast debris cover (Benn et al., 2012). In addition, length and area changes can be also influenced by factors controlling the flow and dynamics of a glacier (i.e. bed topography, aspect, slope). Therefore, length

[1] vertical surface elevation change

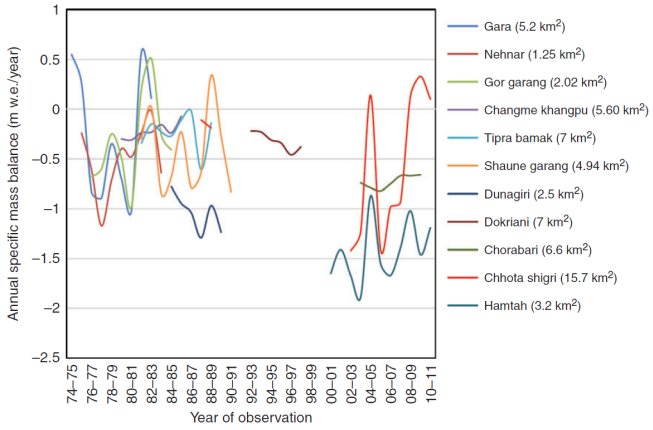

Figure 2.10: Mass balances for glaciers situated in the Indian Himalayan region with more than 5 years of observation. Numbers in the brackets correspond to glacier area. Figure reproduced from Singh et al. (2016).

and area changes cannot be considered as conclusive indicators of climate change (Singh et al., 2016). In contrast, glacier mass balance measurements are a more reliable and direct way to determine the response of a glacier to changing climate conditions (Singh et al., 2016). The term mass balance refers to the change in total mass of ice over a specified time period for a glacier (Cuffey and Paterson, 2010; Benn and Evans, 2010). Factors influencing mass balance are of climatic as well as non-climatic nature (Singh et al., 2016). Although mass balance reflects the unfiltered signal of climate change, measurements are more complex than for area and length changes. For the Indian Himalayan region a total of 15 glaciers with glaciological mass balance measurements exists and only 11 of them were monitored during a period longer than 5 years (Singh et al., 2016), the results are summarised in fig. 2.10. Negative mass balances can be observed for most of the glaciers with tendentially less negative values (ranging between -1 and $0m$ water equivalent (w.e.) per year) for glaciers monitored before 2000. Year to year variances in mass balance are well visible and glaciers within the same region show similar mass balance evolution behaviour (i.e. Gara, Gor garang and Shaune garang or Chhota shigri and Hamtah). Close to the study area only two glaciers exist with longer field based mass balance measurements, i.e. Dokriani and Chorabari Glacier (Bhambri et al., 2011).
Dobhal et al. (2008) measured mass balances for the Dokriani Glacier between 1992 and 2000. They found an annual average mass balance of 0.45 to $0.55m$ w.e. per year for the accumulation area during the study period. In the ablation area stakes were installed and analysed for each $100m$ elevation band. A value of -3.0 to $-4.0m$ w.e. was determined for the lower ablation zone between $3900m - 4300m$ and -2.0 to $-3.0m$

w.e. for the higher ablation zone (Dobhal et al., 2008).
Mass balances were investigated for Chorabari Glacier between 2003 and 2010 (Dobhal et al., 2013). Fig. 2.11 shows that mass balances ranged mostly between -2 and $-3m$ w.e. for altitudes $3900m - 4400m$. Above they decreased to $5070m$ where the ELA is situated. Mass gain ranged from 0.42 to $0.94m$ w.e. per year in the accumulation area (Dobhal et al., 2013). The altitude of the equilibrium line increased by $15m$ between 2003 and 2010 (Dobhal et al., 2013). Glaciers in the Garhwal Himalaya are fed by

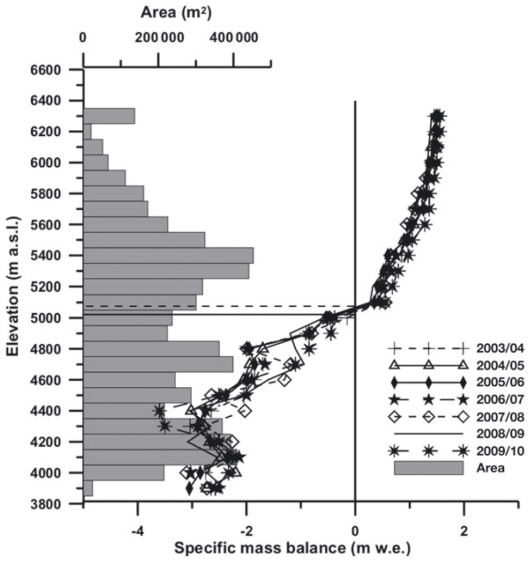

Figure 2.11: Specific mass balances derived by field measurements and the area distribution of Chorabari Glacier for the period 2003-2010. The increasing ablation gradient from $4200m$ to $4500m$ is most likely due to a decreasing debris cover thickness. Figure reproduced from Dobhal et al. (2013).

summer and winter accumulation and therefore knowledge about their response to climate change at different time scales remains limited (Bhambri et al., 2011). However, the studies of Fujita (2008) and Fujita and Ageta (2000) revealed that summer accumulation type glaciers are more vulnerable to warming than winter accumulation type glaciers. The reason is the combination of decreased accumulation together with the severe increase in ablation due to surface-albedo lowering if rainfall instead of snowfall occurs (Fujita and Ageta, 2000).

2.3.2 Modelling future glacier evolution

Cuffey and Paterson (2010) define three main reasons why temperature exerts a strong control on the altitudinal gradients of annual surface balances and therefore on glacier response to climate warming:

1. Precipitation changes from solid to liquid state when temperatures increase.
2. Melt rates increase strongly as soon as air temperatures exceed the melting point.
3. Ice surface remains at the melting point for longer time if the mean temperature increases.

However, in case of very cold climates (mean annual temperatures below $-15°C$) where almost no melt occurs and surface balance is mainly influenced by the amount of snowfall an inverse trend can be observed. Warmer air can have a higher moisture content and therefore rising temperatures tend to increase the rate of snowfall in these locations (Cuffey and Paterson, 2010).

Climate change affects glaciers by modifying the gain and loss of mass which take place through snowfall, melt and other processes (Cuffey and Paterson, 2010). However, glacier reaction to a changing climate is also closely related to the flow regime and ice flow in turn is related to climate[2] (Cuffey and Paterson, 2010). Further factors influencing glacier change are the distribution of surface area with altitude, glacier size, bed topography, debris cover, glacier exposition and surrounding terrain.
A process which should not be neglected when considering glacier reaction to climate change is the altitude-mass-balance feedback (Cuffey and Paterson, 2010). Thinning leads to a decline in surface altitude which in turn leads to an increase in ablation as the surface experiences warmer conditions. The opposite applies when a glacier is thickening.

As can be seen, glacier response to climate change is complex and influenced by a multitude of variables. Consequently, models of future glacier evolution include varying degrees of simplifications. In this thesis, future glacier states are modelled based on thickness evolution which requires initial ice thickness as input. Below, a brief overview of different methods to model ice thicknesses and future glacier change is given.

Ice thickness calculation

Frey et al. (2014) describe three distinct methods for calculating ice thickness estimates. The first is an area-related thickness estimation method which relies on empirically

[2] Mass loss or gain modifies the driving forces which are responsible for ice flow. Additionally, increased input of water towards the glacier bed related to melt on warm summer days or intense rainfalls can augment the water pressure at the bed reducing friction and changing the ice flow (Cuffey and Paterson, 2010).

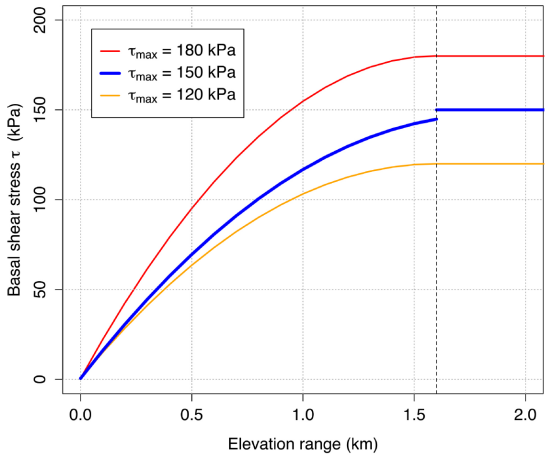

Figure 2.12: Glacier elevation extent vs. basal shear stress τ. The original parametrisation from Haeberli and Hoelzle (1995) is represented as a blue line, the modified parametrisations ($\tau_{\max} \pm 30kPa$) are depicted in red and orange. Figure reproduced from Frey et al. (2014).

determined scaling parameters. Furthermore, ice thickness can be approximated using digital elevation model (DEM) information. Glacier surface topography reflects the underlying bed in a smoothed way (Oerlemans, 2001) and as slope is a driving factor for ice flow it is used for determining ice thicknesses along the glacier (Allen et al., 2016b). An acceleration in ice flow as is the case for steeper topography leads to thinner ice thicknesses and a deceleration which can be found below ice falls and in overdeepened sections results in compressive flow and larger ice thicknesses. This is summarised in the widely used physical equation

$$h_f = \frac{\tau}{f \rho g \sin(\alpha)} \tag{2.1}$$

which calculates the ice thickness h_f based on the basal shear stress τ, the form factor f, the ice density ρ, the gravitational acceleration g and the slope α. Basal shear stress is parametrised by the elevation extent of a glacier, an illustration is shown in fig. 2.12. Slope is therefore used in slope-dependent thickness estimations as well as in ice-thickness distribution models (Frey et al., 2014). GlabTop (Glacier bed Topography model) (Paul and Linsbauer, 2012) is an ice thickness distribution model which works in a geographic information system (GIS) environment and calculates local ice thicknesses using the mean surface slope within $50m$ elevation bins (Linsbauer et al., 2012; Paul and Linsbauer, 2012; Allen et al., 2016b) (more information on GlabTop can be found in sec. 3.3 and in Paul and Linsbauer (2012)). Fig. 2.13 illustrates the model im-

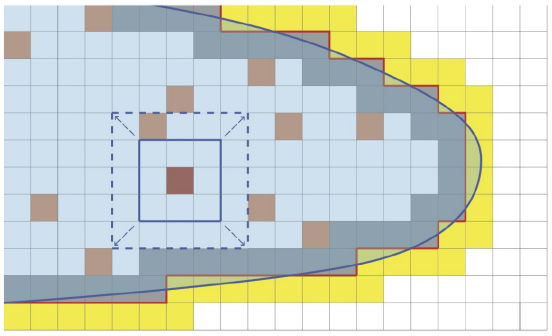

Figure 2.13: Illustration of GlabTop2 implementation: glacier polygons (blue curved line) are converted to a raster matching the DEM cells (red outline). Cells are classified as inner glacier cells (light blue), glacier marginal cells (powder-blue), glacier adjacent cells (yellow), and non-glacier cells (white). Auburn cells are randomly selected cells (r) for which local ice thickness is determined; the blue square symbolizes the buffer of variable size, which is enlarged (dashed blue square), until an elevation extent of h_{min} is reached within the buffer. Figure reproduced from Frey et al. (2014).

plementation. Another ice-distribution model used within the study of Frey et al. (2014) is the model proposed by Huss and Farinotti (2012). Here, local ice thickness is derived from surface topography by determining ice balance fluxes through glacier cross profiles based on Glens flow law (Glen, 1955).
Frey et al. (2014) found that the method selected affects ice thickness results significantly. It appears that calculated ice thicknesses from slope-dependent thickness models and ice thickness distribution model correspond well to local field measurements whereas the area-related scaling method yields too large values (note: for the area-related thickness estimation model only mean ice thickness for the whole glacier can be calculated). Major sources of uncertainty for all methods are uncertainties inherent in the DEM and the glacier outlines (Frey et al., 2014).

Glacier overdeepenings and future lakes

The subtraction of modelled ice thicknesses from a current DEM enables to determine overdeepenings in the glacier bed topography which will be exposed as glacier retreat proceeds. Within the GlabTop model overdeepenings are detected by applying the fill tool of the GIS and calculating the slope values for the filled DEM subsequently. Areas with a slope $< 1°$ situated within the glacier outlines are classified as overdeepenings. The difference between the filled DEM and the DEM of the glacier bed topography allows to quantify the area and volume of potential lakes forming in these overdeepenings (Allen et al., 2016b). However, not every overdeepening transforms into a lake. It can fill with water leading to lake formation (deep depression, rock beds) or with sediment

Figure 2.14: Depression filled by sediment (marked by red outline) downstream of Dudhganga Glacier. Image taken in May 2015.

which results in floodplains (shallow depressions, sediment beds) in the glacier forefield after glacier retreat (Linsbauer et al., 2012). Fig. 2.14 shows such a possibly filled depression within the study area located downstream of Dudhganga Glacier.
Frey et al. (2010) describe an alternative approach to detect the possible location of future lakes. They define a set of morphological criteria which can complement the results of the modelled overdeepenings/lakes when a more detailed evaluation on the most probable lake formation sites is required. Frey et al. (2010) state that lakes are likely to develop in overdeepenings where a distinct slope increase, reduction of glacier width or a crevasse-free part followed by a heavily crevassed part are found (fig. 2.15).

Glacier evolution models

A distinction should be made between regionally calibrated empirical models and process-oriented models, which rely on physical laws (Hoelzle et al., 2005). Linsbauer et al. (2013) compared three approaches to model future glacier evolution. The first was an empirically based ELA-shift model (Paul et al., 2007) which uses a balanced budget accumulation-area ratio of 60%. Rising temperatures are responsible for the shift of the ELA to higher elevations. A value of $150m/K$ was used which was estimated by Kuhn (1981). Once the ELA has shifted glacier area was recalculated based on the AAR value of 60% and the lowest part of the glacier was removed to adjust to the new glacier size (Paul et al., 2007; Linsbauer et al., 2013). This model delivers only the state after the adjustment and no information about when changes will occur. Therefore it was adjusted by assuming a mean response time of 50 years for all glaciers and then final area change could be divided into single time-steps (Linsbauer et al., 2013).

A more sophisticated model presented in the study of Linsbauer et al. (2013) was

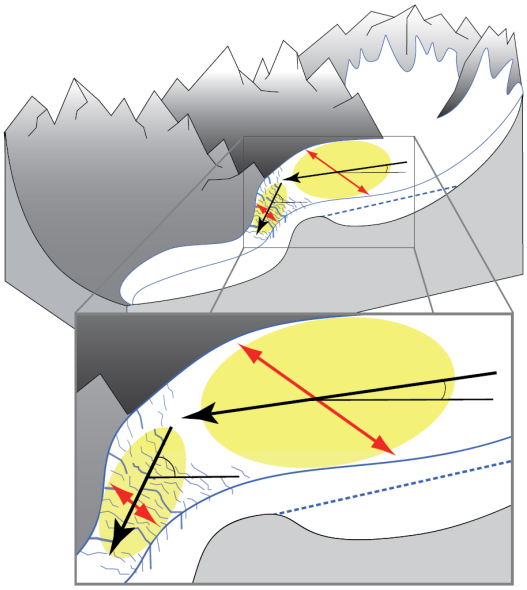

Figure 2.15: Sketch of morphological criteria which indicate the position of an overdeepening and a potential future lake after Frey et al. (2010). A prominent slope break is indicated by the black arrows (criterion I), narrowing of the glacier width by red arrows (criterion II) and a flat and crevasse-free area followed by a heavily crevassed area by yellow areas. The potential future lake level is illustrated by a dashed line. Figure reproduced from Frey et al. (2010).

based on thickness change parametrisation. Haeberli and Hoelzle (1995) state that small and steep mountain glaciers which have an average thickness of a few tens of metres are prevalent in the alpine environment. These static ice bodies appear to respond rather through vertical altitude changes than by horizontal advance or retreat (Haeberli and Hoelzle, 1995). But also large debris-covered glaciers in the Himalayas were observed to react mainly through downwasting instead of area change to warming climate (Benn et al., 2012). Therefore, a model based on thickness changes seems to be legitimate. Model implementation as described in Linsbauer et al. (2013) is based on current ice thickness and an empirically derived elevation-dependent thinning function which is related to a specific temperature change. Different time steps are assumed for $1K$ temperature increase which represent different warming scenarios. The surface is lowered in every iteration and once the cumulative thickness loss exceeds the initial ice thickness, the glacier disappears at this location (Linsbauer et al., 2013).

The third model type presented in the study of Linsbauer et al. (2013) constitutes a glacier mass-balance model which computes mass balances using a simplified energy-

balance model. Besides a DEM and glacier outlines, three meteorological parameters (air temperature, shortwave incoming radiation and precipitation) which are derived from a gridded regional climate model (RCM) are needed as input for the model. The model runs on a daily basis and glacier geometry is updated annually according to calculated elevation changes (Machguth et al., 2009). In this manner, it takes the altitude-mass-balance feedback into account. Glacier grid cells are converted to ice-free cells when their elevation is lower than the elevation of the glacier bed (Machguth et al., 2009; Linsbauer et al., 2013).

It appears that models based on thickness change parametrisation and mass balance distribution deliver better results in terms of glacier shrinkage patterns (inward shift of glacier boundaries) which seem to be closer to reality than for the ELA-shift model (Linsbauer et al., 2013). The ELA-shift and thickness change model are valid rather at a regional scale (i.e. the use of a single elevation-dependent thinning function for all glaciers results in area changes which might be strongly over- or underestimated for individual glaciers) (Linsbauer et al., 2013). The largest spread in modelled area loss was due to the choice of climate scenarios (40%) whereas uncertainty in ice thickness estimates caused around half this spread (Linsbauer et al., 2013).
Any of the models described above consider ice flow. However, a multitude of models exists which are based on mass balances including glacier flow behaviour. The studies of Rimac et al. (2017) or Zekollari et al. (2014) being only two examples.

In summary, a variety of glacier evolution models exist with different levels of complexity. Strongly simplified models can give only rough estimates of future glacier response. However, even for more sophisticated models large uncertainties persist due to the choice of variable values and processes in- or excluded. Also the relation of glacier shrinkage to future climate warming is not trivial and a source of uncertainty. Nevertheless, modelling future glacier evolution is important as it can indicate time frames when factors such as water availability or natural hazards may change.

2.4 Natural hazards

Many of the hazards which are expected to emerge in the glacial and periglacial environment in relation with climate warming can be attributed to ice melt. On the one hand, ice can act as stabiliser, i.e. in steep debris slopes or for hanging glaciers, and therefore melt of interstitial ice or presence of water at the glacier bed leads to a destabilisation at these sites. On the other hand, melt water can act as a lubricant in case of glacier sliding and in steep glacier sections ice avalanches can be the consequence due to reduced friction. Last but not least, if melt water gathers in depressions glacial lakes may form which influence their surroundings by accelerating glacier melt and exerting forces on the natural dam holding them. The following section aims to give

a rough overview of the impact rising temperatures have on the glacial and periglacial environment.

2.4.1 Impact of climate change

Warmer conditions affect without doubt the permafrost distribution (Huggel, 2004). A deepening of the active layer zone may occur and rockfall activity may increase or evolve at sites where no events were recorded previously (Harris et al., 2001). Matsuoka and Sakai (1999) found that rock fall frequency increased as the seasonal thawing front penetrated to greater depths for their study site in the Japanese Alps. Freeze-thaw penetration seemed to govern the maximum dimensions of detachable rock mass (Matsuoka and Sakai, 1999). Similarly, an unusually high number of rock falls occurred during the hot summer 2003 in the European Alps related to extensive thawing of the active layer of permafrost bodies (Gruber et al., 2004). But progressive deepening of active layer zones is not the single cause for increased rock fall frequencies. Lateral rock walls can be also destabilised by stress changes following glacier retreat (Haeberli et al., 1997; Kaab, 2000; O'Connor and Costa, 1993). Huggel et al. (2012) could detect an increase in rockfall activity in the European Alps over the past 100 years attributable to glacier retreat and thawing of permafrost.

As mentioned in the beginning of section 2.4, climate change can affect the stability of glaciers which is linked to topography and temperature (Haeberli et al., 1989). Cold glaciers which are frozen to their bed become unstable at steeper slope angles ($\sim 45°$) than warm glaciers which are in large parts separated by a thin water film from the bedrock (stable up to $\sim 25°$) (Allen et al., 2016b). Therefore, a change in frequency and spatial distribution of ice avalanches can be expected with proceeding climate warming and changing glacier geometry (Stoffel and Huggel, 2012). Although hazards related to ice avalanches are significant they might be more of a transient nature as glaciers continue to retreat (Schaub et al., 2015). In contrast, unstable rock slopes are likely to represent a hazard for a much longer time because effects of warming on subsurface bedrock are long-term (Harris et al., 2009; Noetzli and Gruber, 2009).

In relation to glacier retreat large and steep reservoirs of loose sediment can become exposed and constitute a potential source for debris flows (Huggel, 2004). These debris flows can be triggered by a high water input related to strong precipitation, intense snow or ice melt or also by the outburst of a glacial lake upstream (Rickenmann and Zimmermann, 1993; Huggel, 2004).

Glacial lakes are currently growing and emerging around the globe in alpine areas due to enhanced glacier melt which stands in relation with warming climate. The increasing number and larger size of lakes rises the opportunity for ice or rock avalanches to impact a lake, especially, as many of the lakes are situated close to potentially unstable rock slopes and glaciers (Allen et al., 2016b; Haeberli et al., 2010). Not only an increase in

potential source area for rock or ice avalanches reaching a lake can be expected with progressive growth of the water bodies but also the direction of impact may change as a consequence of lake expansion. Future impacts could possibly enter the lake from an angle where the full wave energy would be directed towards the lake outlet (Allen et al., 2016b).

Carrivick and Tweed (2016) analysed the past evolution of outburst floods around the world and they state that floods at some sites are occurring progressively earlier in the year. Since the mid-1990s all major world regions appear to have experienced a decrease in the number of floods. This is unlikely an issue of detection and one possible explanation could be that floods from ice-dammed lakes are becoming less frequent whereas no such trend exists for moraine-dammed lakes (Carrivick and Tweed, 2016).

In summary, climate warming can lead to the emergence of new hazards. Destabilisation of steep rock slopes, exposure and potential erosion of large debris reservoirs, formation of new glacial lakes, or change in glacier geometry and the related change in avalanche activity are possible outcomes (Huggel, 2004). Therefore a shift of hazard sources may be expected in relation to present climate change. The following section focuses on glacier lake outburst floods.

2.5 Glacier lake outburst floods

A glacier lake outburst flood (GLOF) is defined as the sudden discharge of a water reservoir which has formed either underneath, at the side, in front, within, or at the surface of a glacier (Richardson and Reynolds, 2000). It can be triggered by the collapse of the holding dam, an overtopping wave related to a mass movement impact or a combination of these two processes which is the most frequent case at presence.

Natural dams which assure the water retention can be composed of various materials such as ice, moraine or bedrock. The dam stability plays a crucial role in the process of GLOF generation, more information on dams is given in the following section 2.5.1. GLOFs show all characteristics of dam break floods (Carrivick and Tweed, 2016), a fast increase in discharge, a pronounced and high peak discharge and a rather fast decline in discharge after the peak. As floods attenuate downstream, these characteristics become less pronounced.

Once an outburst flood is triggered drag forces in the water flow can entrain sediment along the flood path and the flood may transform into a debris flow. GLOFs are known to be highly dynamic processes, erosion and sediment entrainment can provoke an increase in volume and peak discharge by a factor of three or more relative to initial values (Worni et al., 2014). Sediment to water ratio can even exceed 60% (Jakob and Hungr, 2005). It has already been observed that debris flows can transport blocks of several meters in diameter.

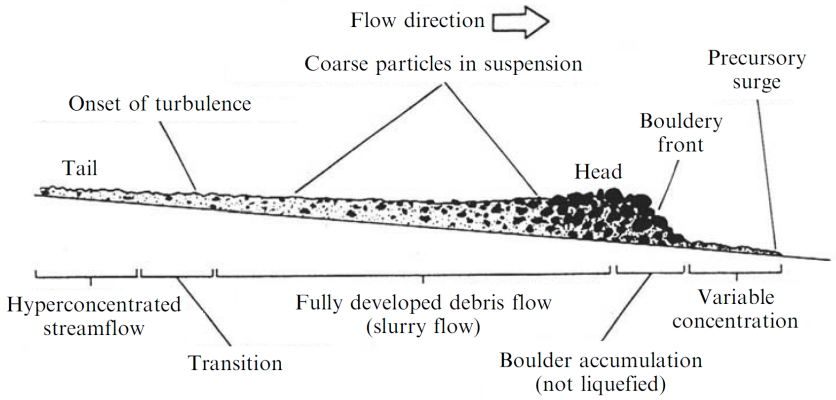

Figure 2.16: Longitudinal cross section of a granular debris flow. Figure reproduced from Jakob and Hungr (2005).

Takahashi (2014) describes three types of debris flows, the stony-type debris flow called also granular debris flow, the turbulent-muddy-type debris flow and the viscous debris flow. These types differ in terms of composition, sediment sorting and flow behaviour, i.e. the stony-type debris flow is characterised by the accumulation of large boulders at the front which is not observed for the other two types. Fig. 2.16 shows an illustration of a stony-type debris flow as it can often be observed in the alpine environment.
The debris load, including the amount and the size of debris material, plays an important role for the destructive power of a debris flow (Takahashi, 2014; Bhambri et al., 2016). Another aspect why debris flows and floods constitute a serious hazard is their fast and high mobility. Debris flows belong generally to very rapid mass movements where velocities exceed the speed of a person running (Jakob and Hungr, 2005). Takahashi (2014) gives a velocity range of around $20m/s$ to $0.5m/s$ for debris flows. Concerning high mobility, large travel distances could already be detected in the Himalayas by Richardson and Reynolds (2000) who measured distances exceeding $200km$.

A further reason why GLOFs are a serious threat for people living downstream is the virtual impossibility to predict their time of occurrence. In some cases, where GLOFs are triggered regularly on an annual or sub-annual basis, i.e. if lakes are dammed by ice and empty regularly, the flood periodicity can be used as an indicator to predict the approximate date of future floods (Carrivick and Tweed, 2016). However, in most situations predicting the occurrence of a GLOF remains unfeasible.

2.5.1 Natural dams

The stability of natural dams is decisive as it governs the outburst volume of a GLOF which can be huge in case of dam failure (Huggel, 2004). Stability depends mainly on dam geometry, the internal dam structure, material properties, and particle size distribution (Korup and Tweed, 2007; Worni et al., 2014). It can be influenced by glacier thinning and retreat, meltwater production, freeboard, and outburst triggers such as earthquakes, avalanches, debris flows, landslides, glacier calving or heavy rain (Watanabe et al., 2009; Benn et al., 2012; Schwanghart et al., 2016). If driving forces related to the weight of the impounded lake or shear stresses from overtopping flow, displacement waves or seepage exceed the material strength of the dam a collapse will be the result (Korup and Tweed, 2007). In general, overtopping waves are reported to be the most common trigger for moraine dam failures (Richardson and Reynolds, 2000; Takahashi, 2014); in the Himalayas estimates exist that more than 50% of moraine dam collapses are related to large impacts of ice or rock (Allen et al., 2016b).

As mentioned in the beginning of section 2.5, different types of natural dams exist which can hold a glacial lake. Depending on their composition different factors can cause an outburst. Ice-dammed lakes are prone to generate an outburst due to dam floatation, enlargement of subglacial drainage channels or overspill (Clague and Mathews, 1973; Clarke, 1982; Tweed and Russell, 1999; Huggel, 2004). They can also fail through a sudden break, particularly, if the ice is fractured as is the case in surging glaciers or for ice avalanche deposits (Haeberli, 1983; Walder and Costa, 1996). Carrivick and Tweed (2016) found that 70% of the glacier floods recorded around the globe in the past are from ice-dammed lakes. Floods from moraine-dammed lakes account only for 9% of the registered occurrences.

In mountainous regions, many lakes have emerged since the end of the Little Ice Age which are impounded by lateral or terminal moraine dams that remained after the glacier retreat (Haeberli and Whiteman, 2015). Takahashi (2014) describes three types of moraine dam failures, one being related to the erosive destruction which follows an overtopping, the second a sudden sliding collapse related to larger dam permeability and consequently stronger seepage and the last being a retrogressive failure. The last case may apply if permeability of the dam is very high and water oozes out the moraine triggering retrogressive erosion. Fig. 2.17 shows the three types of collapse mechanisms. Once dam failure is initiated, a self-reinforcing cycle of erosion and water discharge takes place; high flow rates accelerating erosion and the enlargement of the break leading in turn to a higher discharge. Dam incision proceeds vertically as well as laterally up to the point when lake discharge decreases and no sediment is transported anymore (Worni et al., 2014).

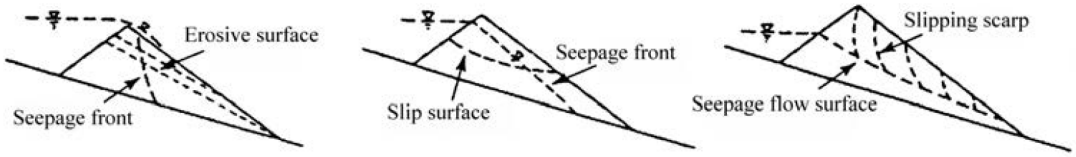

Figure 2.17: Three types of natural dam collapse (from left to right): erosive destruction due to overtopping; sudden sliding collapse; and retrogressive failure. Figure reproduced from Takahashi (2014).

The last category of natural dams are the bedrock dams. These are generally considered as safe from failure. Yet, mass movement impacts into bedrock-dammed lakes can still provoke impact waves which could overtop the dam and generate a GLOF (Huggel, 2004). Considering future glacier retreat, it can be expected that many of the new lakes will be dammed by bedrock rather than by large moraine dams as the development of moraines requires the glacier to remain stationary over a certain period of time (Frey et al., 2010; Allen et al., 2016b).

2.5.2 Flow transformations

GLOFs are unsteady flows that typically experience pronounced changes on their way down valley. They can transform from a normal flood to a hyperconcentrated flow to a debris flow and vice versa (Kershaw et al., 2005; Worni et al., 2012; Worni et al., 2014). These transformations occur due to bulking processes and sediment deposition which are influenced by different factors such as gradient of the flood path, channel confinement, the stability of stream banks or the dilution of flow by water originating from a tributary stream (Worni et al., 2014).

Jakob and Hungr (2005) describe three flow types which can be distinguished based on their sediment concentration and flow behaviour. Water flows transport mostly fine sediment in small proportions to their total flow volume (4%). Therefore, suspended sediments have little effect on flow behaviour and the flood propagates downstream as a Newtonian fluid[3]. In contrast, a debris flow can transport more sediment than water (often >60%) and sediment is strongly influencing the flow behaviour (Jakob and Hungr, 2005). Hyperconcentrated flows represent the intermediate stage between water and debris flows. The transition from Newtonian to non-Newtonian fluid behaviour with the related onset of measurable yield strengths[4] was used by several authors to define the lower limit of hyperconcentrated flows (Pierson and Costa, 1987; Rickenmann, 1991; Jakob and Hungr, 2005). The upper limit where hyperconcentrated flows transform to

[3]viscosity is not dependent on shear rate and shear stress.
[4]the potential to erode volume along the channel

debris flows can also be defined in terms of yield strength as the point where particles in the size of gravels are suspended in the flow (Pierson and Costa, 1987). Fig. 2.18 illustrates the three idealised flow types according to their sediment concentration and yield strength.
An example where several flow transitions could be observed is the Casita volcano disaster, Nicaragua, in 1998 (Wieczorek, 2000). A debris slide transformed into a debris avalanche, then into a hyperconcentrated flow, a debris flow and into a hyperconcentrated flow again. Sediment entrainment and deposition alternated several times during the downstream propagation of the event (Jakob and Hungr, 2005). During this disaster, where approximately 2000 people lost their life, a debris flow deposition volume nine times larger than the initial failure volume was recorded (Jakob and Hungr, 2005). As demonstrated by this example, sediment entrainment can largely affect downstream impacts. It appears that once the slope of a channel increases above $\sim 10°$ the bed itself might become unstable due to gravity and drag forces exerted by an over-riding water flow (Jakob and Hungr, 2005). If the fluid contains debris even greater drag forces are acting and can result in massive mobilisation and entrainment of debris into the flow. Material is entrained not only at the bed but also from collapsing stream banks that are undercut by bed erosion (Jakob and Hungr, 2005). Here, vegetation can help to stabilise the terrain to a certain degree. Once terrain slopes become shallow and potential flow diversion occurs sediments are deposited (Iverson et al., 2010).

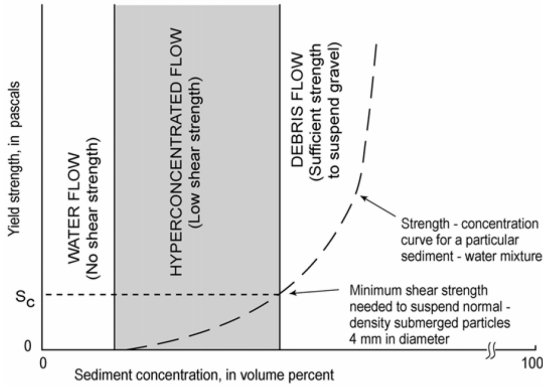

Figure 2.18: Definitions of three flow types for poorly sorted sediment-water mixtures based on an idealised yield strength curve. Figure reproduced from Jakob and Hungr (2005).

2.5.3 Modelling approaches

As mentioned in the beginning of section 2.5 GLOFs represent a serious hazard for down living population. To assess the exposure of inhabitants, current and planned infrastructure GLOF flood paths can be simulated with different models. This section

gives an overview of the common steps in the process of GLOF modelling. Please note that the described procedures constitute a part of the hazard assessment process which is described in section 2.6.

Remote sensing and GIS

Glacial hazards may emerge in remote areas without being noticed. The insufficient knowledge of their presence and distribution is a major problem for the delineation of potentially endangered areas. Therefore, remote sensing and GIS (geographic information system) based methodologies were developed which are capable of detecting glacial hazards over large and remote areas (Huggel, 2004; Wessels et al., 2002). The possibility to perform multi-hazard analyses within a GIS environment, i.e. detection of different hazard sources based on remote sensing data in combination with subsequent event path modelling is a large advantage (Huggel et al., 2004a). As lakes form mostly over several years, change detection studies based on remote sensing data are considered to be appropriate to monitor hazardous developments (Kääb et al., 2005).

To model GLOF paths lakes need to be mapped first. In addition, source zones of potential mass movements which could impact a lake are detected and related flow paths modelled. The normalised difference water index (NDWI) is commonly applied to map lakes semi-automatically (Allen et al., 2016b; Huggel, 2004). It uses the blue and near infrared channel of remote sensing instruments to distinguish between lake and no-lake areas based on a threshold. Despite the wide application of this technique, lake inventories from different studies should be compared with caution (Allen et al., 2016b). The reason is that the NDWI method is sensitive to scene specific properties and the selected lake/no-lake threshold. If lakes are covered by snow or frozen they are not detected by the NDWI and, moreover, the method struggles to differentiate between lake and blue glacial ice (Allen et al., 2016b). In case of availability of a digital elevation model (DEM) for the study area mapped lakes can be verified by determining the slope of lake areas. It should be 0° or very close to it. Once the lake area is delineated, empirical equations exist which estimate the lake volume based on the lake area (Huggel, 2004). Volume can then be empirically related to peak discharge and peak discharge to the angle of reach[5] of a potential outburst flood. These parameters are needed for certain models simulating a GLOF (more information on flow path modelling follows below).

Potential mass movement impacts into glacial lakes can be for example related to ice avalanches, rock falls or debris flows. In all three cases the procedure to detect starting zones include the determination of steep areas based on a DEM and a certain slope threshold defined. Source zones for ice avalanches can be mapped by different methods,

[5]The angle of reach is a concept introduced by Heim (1932). It represents the slope of the line connecting the source and the deposition zone.

i.e. the normalised difference snow index (NDSI) or band ratios (Allen et al., 2009; Bhambri et al., 2011; Huggel, 2004). Debris-covered glaciers are not detected, however, as steep glacier parts, where ice avalanches are potentially triggered, are debris-free source zones should still be recognised. The classification of unstable steep ice is based on a slope threshold. Generally, cold-based glaciers are stable at higher slope gradients than temperate glaciers (Allen et al., 2009). Therefore, an empirical value of 45°, respectively 25° can be applied to distinguish avalanche-prone glacier areas (Huggel, 2004). Alternatively, the mean annual air temperature can be taken into account to determine the critical stability slope based on an empirical relation (Huggel, 2004).

Areas in the glacial and periglacial environment which are neither classified as water, ice, snow or vegetation[6] are attributed to rock and debris slopes. Steep debris accumulations which can represent an initiation zone of a debris flow are more challenging to detect automatically. However, if high-resolution field, aerial or satellite images are available it is possible to identify and discern them from bedrock by using an image texture algorithm (Allen et al., 2008; Huggel, 2004). Compared to the rough and angular appearance of bedrock debris surfaces are rather uniform (Allen et al., 2009).

What can be detected from remote sensing images depends to a high degree on their spectral, spatial and radiometric resolution. If change detection studies shall be carried out temporal resolution of a sensor becomes important as well (Huggel, 2004). In complex mountain terrain, the use of a DEM may largely facilitate the detection and classification of objects (Huggel, 2004).

Flow path modelling

Different models exist which can be used for GLOF and debris flow simulations. Here, only two are briefly described, the first being the modified single flow model (MSF) (Huggel et al., 2003) and the second the rapid mass movement simulation (RAMMS) (Christen et al., 2010).

MSF is a hydrological flow routing algorithm that works in a GIS environment. For GLOF path modelling lake locations and a raster-based DEM is needed. Starting from lake pixels, flow direction is determined according to the steepest descent between each DEM pixel and its eight neighbours (O'Callaghan and Mark, 1984) and flow spreading is allowed up to 45°from the main flow direction (Huggel et al., 2003). Furthermore, for every pixel the qualitative probability is calculated whether it can be affected by a potential flood. This probability is based on the distance to the source area and the lateral deviation from the central flow path (Allen et al., 2016b). The flow path is modelled until a stop condition is fulfilled which in this case is the angle of reach[7]

[6] Vegetation is commonly detected by the normalised difference vegetation index (NDVI).

[7] The angle of reach can be estimated using empirical equations (see previous section Remote sensing and GIS). Alternatively, a predefined worst-case value can be applied.

(Noetzli et al., 2006). The MSF model has no strictly physical basis and relies strongly on digital terrain information (Huggel, 2004). Geological conditions such as presence and the amount of debris in the flow channel or friction parameters of surface materials along the channel are not considered. Therefore, it is impossible to estimate directly the expected debris flow volume, maximum discharge or the volume of sediment eroded and deposited (Huggel, 2004). However, areas where flow diversion is modelled likely belong to deposition zones and in contrast where flow conversion occurs sediment erosion is expected to dominate (Huggel, 2004). Further information on the MSF model is given in Huggel et al. (2003).

In contrast to MSF, RAMMS is a physically based model which calculates time-dependent flow heights, velocities, kinetic energy, momentum, frictional work rates, flow pressures and final deposition heights of mass movements (Christen et al., 2010; Schaub et al., 2015). The model is based on the Voellmy-Salm approach (Salm et al., 1990) and was extended by a random kinetic energy part which accounts for random movements of particles within a mass flow. Two frictional parameters are included, the velocity independent dry-Coulomb term μ which is proportional to the normal stress at the flow bottom, and the velocity dependent viscous or turbulent friction term ξ (Christen et al., 2010). The first term influences the runout distance of a modelled mass movement and the second viscous term the flow velocity (Schaub et al., 2015). For GLOF simulations a DEM, an assumed hydrograph and friction parameter values are required as input. Friction parameters can be varied along the channel depending on surface material. Originally developed by the Institute for Snow and Avalanche Research SLF for snow avalanches adapted model versions exist now for rock falls and debris flows.

The physical basis of RAMMS enables to simulate run-up, overtopping and deflection of mass movements which is a large advantage for local scale modelling (Allen et al., 2009). In addition, sediment entrainment and deposition are modelled and variations in flow rheology can be introduced by varying the friction parameters along the flow path (Christen et al., 2010; Schneider et al., 2014). Another convenience of using RAMMS for mass movement simulations is that flow heights and velocities are direct outputs and can be transformed into intensities which are needed for hazard mapping. However, there are also some disadvantages for RAMMS. The computational costs are considerably higher than for MSF and the estimation of input parameters such as friction values and hydrographs are difficult and require expert knowledge. In comparison, MSF requires little input data, is simple to apply and due to the low computational costs its use is especially suited for larger spatial scales (Allen et al., 2016b).

Results from both models, MSF and RAMMS highly depend on the quality and the resolution of the input DEM. If possible, high resolution DEMs should be preferred to achieve accurate results.

Process chains

It has been already mentioned that many GLOFs are triggered by mass movement impacts. A typical process chain of these flood events includes the impulse-wave generation by mass flow impact into the lake, dam overtopping and breaching, and lake drainage and flood propagation (Worni et al., 2014). Fig. 2.19 illustrates the individual stages of this process.

It is a subject of current scientific research to simulate these cascading processes and assess related hazards (Schneider et al., 2014; Worni et al., 2014; Schaub et al., 2015). In 2010, an ice-rock avalanche triggered at the Mount Hualcán impacted Lake 513 and the following outburst flood affected downstream communities and the city of Carhuaz, Peru (Schneider et al., 2014). Schneider et al. (2014) tried to reconstruct this event by coupling two numerical models. They used RAMMS to simulate the ice-rock avalanche, the outburst flood and debris flow, and IBER to model the impact wave, wave propagation in the lake and dam overtopping. RAMMS and IBER were related by their outputs and inputs. The output of RAMMS, which was a hydrograph estimated from the volume and density of the modelled avalanche, constituted the input for IBER and the output of IBER, which was a spillover hydrograph and water volume could then be passed to RAMMS as input.
Schaub et al. (2015) investigated the effect of variable values on the process chain simulation results for Lake 513 and the related propagation of uncertainties. Therefore, different ice avalanche scenarios were established where different release volumes were considered. Schneider et al. (2015) found that the assumed initial avalanche volume and the RAMMS friction calibration affected results to a considerably higher degree than the manual transformation of the RAMMS results to the IBER input hydrograph. Furthermore, the velocity of a mass movement, which is related to the friction parameters, seems to influence the generated overtopping wave more than the initial volume of the avalanche. Faster avalanches appear to have steeper impact fronts and with rising velocity higher wave heights and longer wave periods were observed in the simulation

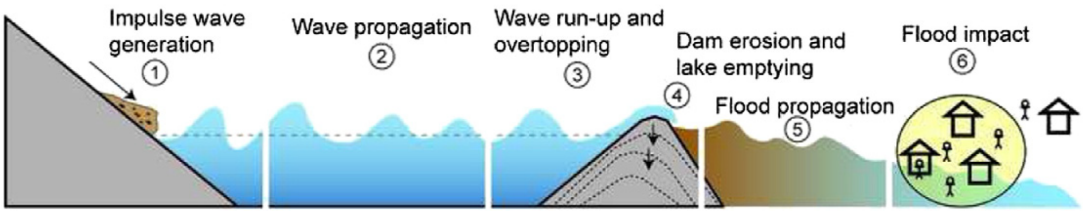

Figure 2.19: Sketch of a typical GLOF process chain. (1) A mass movement enters a lake, producing (2) an impulse wave that (3) overtops and (4) incises the dam, resulting in (5) a flood that propagates downstream and (6) eventually impacts inhabitad areas or infrastructure. Figure reproduced from Worni et al. (2014).

runs (Schaub et al., 2015).

The coupling of RAMMS and IBER is just one example how to simulate process chains for GLOFs. Instead of relating different models by their in- and output, an alternative would be to adapt an existing model to simulate process chains within a single model run (Worni et al., 2014). However, a single model might not be able to represent all processes optimally. A selection of models which can be used to simulate cascading processes of GLOFs is given in Worni et al. (2014).

2.5.4 Flood disaster 2013: Mandakini Valley

In June 2013, heavy rainfalls were recorded across the whole state of Uttarakhand and numerous mass movements were triggered including two large debris flows on June 16 and 17 in the Mandakini Valley (Allen et al., 2016a) (see fig. 2.3 for locations). The village of Kedarnath, and the settlements Rambara and Gaurikund were devastated by these events (Dobhal et al., 2013; Bhambri et al., 2016). Kedarnath is a significant Hindu pilgrimage site, its holy shrine being visited by thousands of people per day during the pilgrim season (Bhambri et al., 2016; Allen et al., 2016a). At the moment of the disaster, a high concentration of people in the valley, many of them pilgrims, led to an extremely high value of fatalities. Estimates indicate more than 6000 deaths due to the flash floods and landslides in the region, the Kedarnath disaster contributing to a large extent to this number (Guha-Sapir et al., 2016). This disaster belongs to the most severe ones which were ever recorded (Carrivick and Tweed, 2016; Bhambri et al., 2016).

Meteorological records indicate unusually high precipitation amounts preceding the disaster, i.e. $325mm$ rainfall within 24 h between 15 June (5:00 p.m.) and 16 June (5:00 p.m.) at Chorabari Glacier base camp (Dobhal et al., 2013). Already a week before the disaster occurred, heavy rainfalls were registered in the region which were related to the early onset of the monsoon in 2013. The total amount of June rainfall is estimated to correspond to at least a 100-year event (Singh et al., 2014). Meanwhile, snow cover depletion proceeded at higher rates than in other years between mid-May and mid-June (Allen et al., 2016a). Therefore, rivers were already running high before the heavy rainfalls occurred and the ground was saturated.

On June 16 at 7 p.m., a first debris flow struck Kedarnath and Rambara probably after transforming from a shallow landslide high above the terminus of Companion Glacier (Martha et al., 2015; Allen et al., 2016a). Then, on June 17 at 06:45 a.m. the most catastrophic debris flow followed which was triggered by an outburst of the Chorabari Lake. The Chorabari Lake was dammed by the western lateral moraine of Chorabari Glacier and experienced fast rising water levels due to high water input from rainfall and snow melt (Bhambri et al., 2016). Moreover, large debris amounts were deposited in the lake originating from erosion processes at the lateral moraine and rising the lake

level further (Allen et al., 2016a). Estimates exist that the level of the $\sim 400m$ long and $\sim 200m$ wide lake increased by $15 - 19m$ (Bhambri et al., 2016; Dobhal et al., 2013). Field evidences suggest that water surface reached the moraine crest and in consequence overflow and progressive erosion was initiated until the moraine dam failed completely (Allen et al., 2016a). The water entrained moraine material and sediment load increased as the debris flow passed through rather steep terrain upstream of Kedarnath (Allen et al., 2016a). The flat terrain around the pilgrimage site favoured in contrast sediment deposition. The area in and around Kedarnath was filled by debris to more than $5m$ thickness (Bhambri et al., 2016).

The damage caused by the flash flood events between June 16 and 17 is huge. Around 120 buildings in Kedarnath and all buildings in Rambara were washed away as this settlement was situated only $10m$ above the normal flow of Mandakini River (Bhambri et al., 2016). Devastation occurred also in the other settlements of Mandakini Valley. Moreover, large parts of roads and pedestrian treks were destroyed, obstructing rescue operations to evacuate pilgrims, tourists and local people after the disaster (Bhambri et al., 2016).

2.6 Hazard assessment

The definition of hazard includes the physical process involved as well as the magnitude and probability of occurrence of an event (Ragozin, 1994; Leroi, 1996; Heinimann et al., 1998). From a mathematical point of view, hazard can be defined as the product of magnitude and probability of occurrence (Fell, 1994). This section introduces the topic of frequency-magnitude relationships first before focussing on a possible parametrisation of these two quantities as implemented in this thesis. A link to risk assessment is given at the end.

Magnitude and frequency generally show a negative nonlinear relationship (Hungr, 1997; Liu and Lei, 2003); large magnitude events occurring less frequent than small magnitude events. This applies for hydrologically-driven hazards and certain glacial hazards such as ice avalanches from cliff-type glacier (Röthlisberger, 1987), regular filling and draining of ice-dammed lakes (Tweed and Russell, 1999), rainfall-triggered debris flows (Fan et al., 2003) and rock fall from permanently unstable rock faces (Huggel, 2004). However, most hazards in the glacial and periglacial environment cannot be described by magnitude-frequency relationships. The reason is that events, i.e. outburst floods from moraine-dammed lakes involving full dam failure (Haeberli et al., 1989) or large ice and rock avalanches, occur only once. For events that are recorded for the first time either due to missing data or because they indeed never happened before magnitude-frequency relationships fail as well (Huggel, 2004). The emergence of new hazards is often related to a system change induced by climate change (Huggel, 2004). A problem with glacial hazards is that the glacial system changes too rapidly

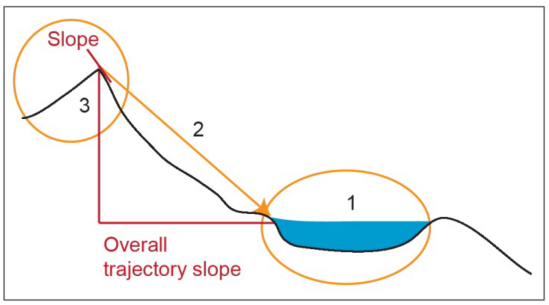

Figure 2.20: Schematic illustration of the concept of topographic potential. (1) A glacial lake is situated within the runout distance (2) of a potential mass movement triggered in the steep terrain (3). Figure reproduced from Allen et al. (2016b); modified from Schaub (2015).

to derive frequency characteristics. Low to very low frequencies and high magnitudes are common and therefore a negative relationship between magnitude and frequency cannot be established (Huggel, 2004).

Different options exist to assess the magnitude of an event, in the case of a GLOF the probable maximum discharge, volume and runout distance can be evaluated (Huggel, 2004). Allen et al. (2016b) analysed the future evolution of GLOF hazards for districts in Himachal Pradesh. They defined the magnitude as the potentially affected land area by a GLOF path. In this thesis lake volume is used as indicator for the magnitude of a potential future outburst flood. If no bathymetric field data exist which would allow to determine the lake volume, it can be approximated based on the lake area. Different scientists have established empirical equations which relate area to volume, the following was derived by Huggel et al. (2002): $V = 0.104A^{1.42}$ where V is the volume in m^3 and A the area in m^2. It should be kept in mind that this formula may underestimate volumes for larger lakes by up to 80% due to large natural variability of lake depths in relation to area (Huggel et al., 2004b; Allen et al., 2016b).
The assumption of total lake drainage is a worst-case scenario but partial emptying is possible. For moraine-dammed lakes, Fujita et al. (2013) developed an approach to estimate the potential flood volume based on the concept of steep lakefront area (SLA). According to them, moraine-dams with a surface slope below 10° on their downstream side will not collapse regardless of the triggering mechanism of the outburst flood. This value corresponds with the observed slope value where debris material starts to be eroded by overflowing water (see section 2.5.2). As the SLA determines the potential surface lowering of the dammed lake the potential flood volume can be estimated by assuming a cylindrical bathymetry. For more information see Fujita et al. (2013).

It is a difficult task to determine the probability of occurrence for outburst floods. Still, a probability estimation is necessary for the planning, design and construction of mitigation measures and therefore it is better to assign even an approximate and

subjective value than not to assign one at all (Fell, 1994). Considering GLOFs triggered by mass movement impacts a possible concept which enables to estimate the potential frequency is that of topographic potential. It determines the intersectional area where the slope is enough steep for rock and ice to detach and from where resulting mass movements could reach the glacial lake (Allen et al., 2016b). This area constitutes the lake impact predisposition area (Allen et al., 2016b). Fig. 2.20 illustrates the concept of topographic potential. If no information on further triggering processes and dam characteristics is available lake impact predisposition area can serve as a proxy to detect regions where GLOFs are expected to occur more frequently (Allen et al., 2016b).

A standardised method to assess the hazard posed by a glacial lake does not exist and therefore different strategies are revealed in studies. However, in the field of remote hazard assessment efforts are made to develop a holistic approach that would be objective and repeatable. Rounce et al. (2016) propose such an approach. They consider both failure types of natural dams, i.e. dynamic and self-destructive, and include multiple factors in their method such as snow/ice avalanche, rockfall, flood from an upstream lake, lake expansion, hydrostatic pressure and an ice-cored moraine dam. Simplistic models and globally available datasets are used to estimate these parameters. A detailed description is given in Rounce et al. (2016). Fig. 2.21 shows the flow chart used by Rounce et al. (2016) for the hazard classification of lakes.

A hazard map often constitutes an integral part of a hazard assessment. It depicts areas which are potentially exposed to a certain hazard. The calculated intensity for a site and the probability of being affected by an event determine the hazard level for a location. Debris flow intensities can be derived from flow heights and velocities (Schneider et al., 2014). According to Raetzo et al. (2002) no low intensities exist for debris flows. Although it is possible to generate hazard maps automatically based solely on numerical modelling it is strongly discouraged (Schneider et al., 2014). They should always be adapted in the field because smaller terrain structures, i.e. houses, are not present in the DEM but they still influence the flow of a mass movement (Schneider et al., 2014).

A hazard assessment is usually integrated within a risk assessment. The definition of risk includes the physical hazard intersecting with vulnerable and exposed people, infrastructure, or services (IPCC, 2012). Two components of risk assessment can be distinguished, risk analysis and risk evaluation (Huggel, 2004). Hazard assessment is a part of the first component whereas risk evaluation involves numerous political, social and economic aspects (Huggel, 2004). As human activities are constantly changing in time and space also the risk is changing (Carrivick and Tweed, 2016) what makes predictions of future risk evolution even more difficult. The aim of risk assessment is to enable risk management which involves prevention, i.e. active and passive mitigation measures, intervention and recovery from an event (Huggel, 2004).

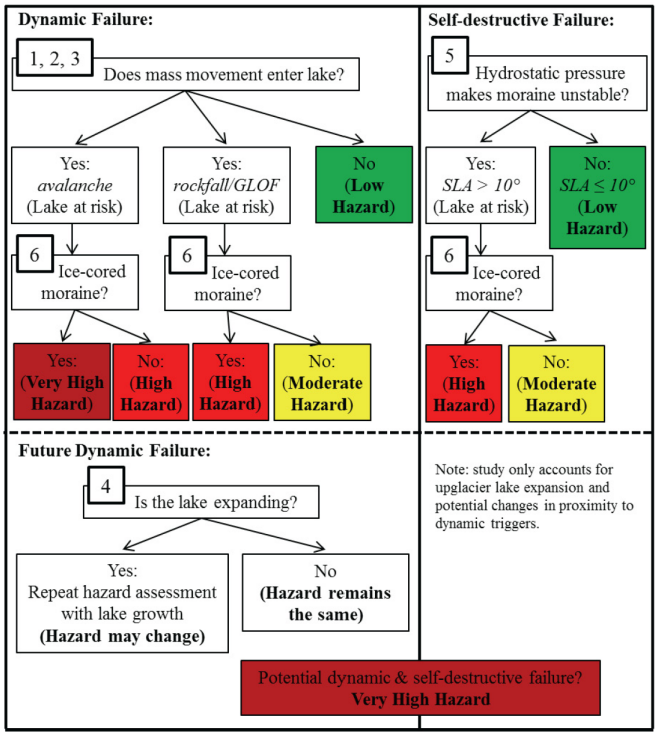

Figure 2.21: Hazard classification flow chart as proposed by Rounce et al. (2016) to determine the hazard posed by a glacial lake. Figure reproduced from Rounce et al. (2016).

3 Practical part

In order to analyse the temporal evolution of future GLOF hazards in the Bhilangna Valley and the exposure of hydropower stations to potential flow events a sequential approach was developed consisting of four parts: (1) past glacier thinning, (2) future glacier and lake evolution, (3) future GLOF hazard evolution, and (4) related downstream hazards. Fig. 3.1 visualises the individual steps and related outputs which serve as input for a following part. More details on the workflow are illustrated in fig. 5.2 and 5.1 in the appendix. This chapter gives first a brief overview of the data used and describes afterwards the methods and results of each of the four parts.

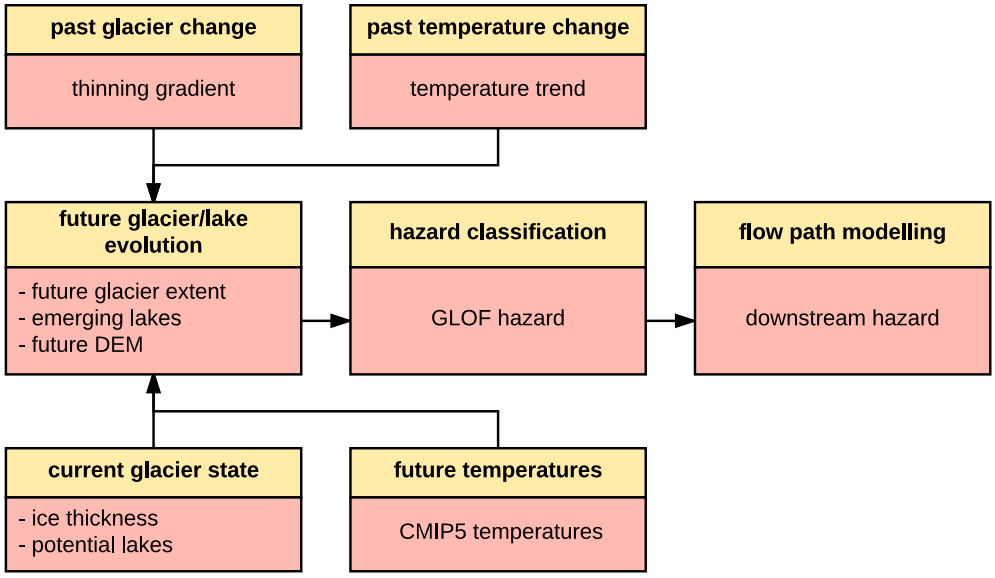

Figure 3.1: Workflow: A past temperature trend and an elevation-dependent thinning gradient are established for input to the future glacier evolution model. In addition, current ice thicknesses and future temperature projections are needed. The output of the future glacier evolution model, i.e. emerging lakes, glacier extents, and DEMs are used for the classification of GLOF hazards. The evolution of downstream hazard is analysed with flow path modelling.

3.1 Data

An aim of this master thesis was to establish methods that use open-source datasets with global coverage and which would therefore be applicable even for data-scarce mountain regions. Relatively few data were used including a digital elevation model,

mapped glacier outlines, modelled temperature data and the locations of hydropower stations.

ASTER GDEM

The following descriptions are based on information provided by MicroImages (2009), Earth Remote Sensing Data Analysis Center (2011), and Huggel (2004). ASTER GDEM is a global digital elevation model derived from the Advanced Spaceborne Thermal Emission and Reflection Radiometer and provided by METI (Ministry of Economics, Trade and Industry), Japan and NASA. It has a resolution of 1 arc-second ($\sim 30m$) although the effective spatial detail that is resolvable is on the order of $75m$. Therefore, small terrain features such as incised flow channels cannot be sufficiently represented whereas large scale spatial structures, i.e. main valley floors, are well recognisable. ASTER GDEM has a worldwide coverage between 83°N and 83°S and is referenced to the WGS84 coordinate system and the EGM96 geoid. Vertical units are meters and the overall accuracy is around $17m$. However, in rugged mountainous terrain larger elevation errors might be expected. The DEM is produced from stereo images taken in the near-infrared band by the nadir- and backward-pointing telescopes. After filtering cloud-areas, all DEMs from multiple years are stacked, residual bad values and outliers are removed and the average of the stacked pixel values is calculated. Where residual bad values persist they are replaced with elevations from reference DEMs. Artefacts in the ASTER GDEM may originate from poor coverage, cloud-contamination, water masking issues and the stacking process. In general, most problematic areas are steep northern slopes which are turned away from the sensor and mountain peaks where failed image matching may deliver wrong elevations. In comparison to the SRTM DEM where radar shadowing and foreshortening effects occur for steep terrain, the coverage of these areas is more complete for ASTER GDEM although accuracy is degraded.

Although high resolution DEMs are preferable for modelling glacial hazards data are not always available. Therefore, ASTER GDEM is of fundamental importance especially in remote high mountain terrain where data is lacking.

Glacier outlines

Glacier outlines were mapped manually by S. Mal for different years. In this thesis the first and the last glacier state were considered which belonged to 1968, respectively to 2015. The outline for 1968 was delineated using Corona imagery.
For Corona imagery, a best ground resolution of $\sim 2.8m$ can be attained in flat terrain (USGS, 2015). In mountain regions the resolution is worse but still very good (below $10m$) favouring detailed mapping. The main challenge of Corona data is the complex image geometry together with the absence of satellite camera specifications which

complicates image rectification (Bhambri et al., 2012). In consequence, distortions in several directions can lead to wrongly mapped glacier outlines at certain positions (see also section 3.2.2).

CMIP5 Temperatures

The Coupled Model Intercomparison Project Phase 5 (CMIP5) involves 20 climate modelling groups from around the world (McCoy, 2017). A gridded worldwide temperature dataset is provided, this thesis uses data simulated for the spatial extent 30-31°N and 78-79°E and the two warming scenarios RCP4.5 and RCP8.5 (see section 2.2.2 for more information on the two scenarios).

Hydropower stations

The hydropower stations are a point dataset with current (H1-H4) and planned stations (H5) (see fig. 3.24 for locations). They were digitised manually based on Google Earth imagery.

3.2 Past glacier retreat

In order to model future glacier evolution it is necessary to investigate past glacier behaviour first. For this reason an elevation-dependent ice thinning gradient was established for glaciers in the Bhilangna valley for the time period 1968-2015. Additionally, a linear temperature trend was determined based on northern India regional and local temperature data from the past. The calculated warming was thereafter compared to temperature warming data from the RCP scenarios of the IPCC report (IPCC, 2013) for this region. The aim of this first part is to empirically relate temperature changes to glacier ice elevation changes by establishing a temperature trend and an ice thinning gradient for a common historical time period.

3.2.1 Methods

Elevation change

The creation of a digital elevation model (DEM) is time consuming and financially expensive. Therefore, this master thesis examined whether elevation changes can be derived from a current DEM and digitised past glacier outlines. To estimate elevation changes in the field or using Google Earth is quite common, however, it was an objective to develop a replicable and automated approach. Elevation changes were calculated for the whole catchment and therefore resulting values represent a mean of all glaciers. Past

outlines were mapped manually based on a Corona scene acquired on 27. September 1968. Two approaches to estimate past rates of thinning were tested:

1. Plane approach:

   The idea of this approach was to approximate the old glacier surface by a plane connecting the old glacier outlines. The subtraction of this artificially created DEM and the current DEM would result in information about the minimal vertical surface elevation change.

   The area of analysis was restricted to the glacier tongue where glacier outlines differed in position. Obviously, no change in extent was mapped for the accumulation area and therefore this part was excluded from analysis. Moreover, the approximation of the old glacier surface by a plane is plausible for narrow glacier tongues but not for vast accumulation zones. Calculated elevation errors tend to increase if the plane spans a wider area. Furthermore, accumulation areas show rather a concave surface topography (Nielsen, 1955) and the approximation of the old glacier surface by a plane connecting the outlines would overestimate the past surface elevation. In contrast, glacier surface in ablation zones is characterised by a convex transverse profile (Nielsen, 1955). This means, that the elevation changes derived from the plane approach must be understood as a minimum change in surface elevation.

   A mask was created for areas where no change in extent was observed and overlayed with the current DEM. The output was a DEM with holes within the glacier tongue outlines of 1968. These holes were subsequently closed by various mathematical methods. In version 1 (v1), the elevation of a no data cell was calculated as the mean elevation of the preceding DEM cells. In this manner, the holes in the DEM were closed from top to bottom and from left to right. Consequently, the resulting cell values were strongly influenced by the topography of the two orientations. Version 2 (v2) used another technique to calculate the DEM values within holes. Here, once a no data cell was encountered, it was counted how many no data cells succeed in horizontal and vertical direction. The direction where less no data cells were found was used and the elevations at the margin were recorded. Afterwards, an imaginary straight line was put which connected the two marginal cells. The values along this line corresponded to the elevation values assigned to the no data cells. Version 3 (v3) is very similar to v1 with the difference that holes were closed continuously from the outside to the inside. In other words, after each iteration a new ring of calculated DEM cells was added until a hole disappeared completely. Figure 3.2 illustrates the three methods with test data.

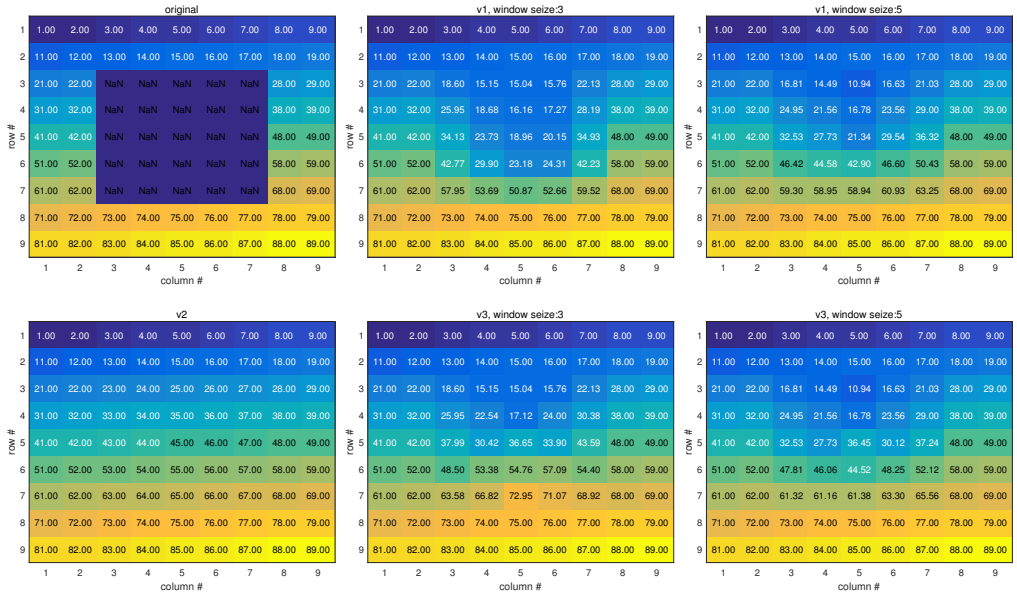

Figure 3.2: Filling of no data areas (NaN) in a test dataset using different methods of the plane approach. Two window sizes were tested for v1 and v3: a 3×3 and 5×5 window. The numbers represent the cell values.

2. Point approach:

   The second approach tries to derive elevation changes from an old glacier outline and a central flowline. A version with three flowlines was also tested. Points were generated in regular spacing along the old glacier outline which received the elevation of the underlying DEM as attribute. At the same time, the nearest point on the flowline was calculated for each point on the outline which again received the DEM elevation as attribute. In this manner, the elevation difference between the point on the outline and the corresponding point on the flowline could be derived.

In a next step, the elevation changes derived from the plane or point approach were summarised into a single value per elevation band. Only the area which was covered by ice in 2015 was analysed, otherwise values could underestimate the actual elevation change. The attribution to an elevation band was based on the elevation of a cell in the current DEM for the plane approach, respectively on the current DEM elevation of the points along the central flowline for the point approach. In this way, a cell with a DEM value of for example $3840m$ was attributed to the next upper $100m$ elevation band being in this case $3900m$. 100 meters were chosen as band width in order to have enough values within a single elevation band so that the resulting elevation

change per band is not dependent on too few values and less influenced by outliers. However, the resolution is still considered as high enough to show variations along the vertical direction. Another reason was that temperature differs enough between the single bands. Immerzeel et al. (2014) found that lapse rates range between -0.46 and $-0.64\,K/100m$ for the LangTang valley in Nepal depending on season. Unfortunately lapse rate measurements for this region are lacking.

The elevation change per band can be calculated as the maximum elevation change, the mean or the mean without considering negative values. The idea behind the maximum value was to derive the worst case thinning. The disadvantage of this method is that it is strongly influenced by outliers. The reason for calculating a mean excluding negative values is that glaciers flow over irregular topography and therefore negative values indicating elevation increase from past to present are only due to the simplifications made in the realisation of the plane or point approach. That is why values of elevation decrease are considered to be of further use whereas values of elevation increase resulting from the approaches, do not represent the real state and can be ommitted.

Thinning gradient

The aim of the plane and point approach was to derive a thinning gradient dependent on elevation. A linear and a quadratic regression was calculated for the summarised elevation change values per band. Additionally, the goodness of fit was determined which indicates how well the regression represents the values given. In order to have the elevation change expressed as an average annual rate, the thinning gradient was divided by the number of years between the two glacier states given. This is based on the assumption that thinning rates were constant during the period analysed.

Validation

Two different types of validation were made to assess the functionality of the methods and the accuracy of their results. On the one hand, transverse profiles were digitised manually within the old glacier outlines of 1968. Here, one profile was generated within each $100m$ elevation band of each glacier in the catchment. Afterwards, the two marginal points were connected by a straight line which represented the simplified glacier surface that should be modelled by the mathematical methods of the plane approach.

The elevation difference between the current DEM and the expected simplified glacier surface was calculated at the middle of the profile as ice thickness tends to be the largest along the central flowline. Moreover, the point approach was based on a central flowline and therefore also the results of this approach could be evaluated.

On the other hand, to study the error resulting from the assumption of a plane glacier surface instead of a convex surface DEM differencing data is required. As historical DEMs were not available for our Indian study region, the methodology was replicated and tested using DEM data from Findelen Glacier, Switzerland. The elevation change per band was calculated for the DEM differencing data as well as for the modelled data delivered by the plane or point approach. To quantify the difference between the datasets the root mean square error (RMSE) was used.

Temperature trend

A linear temperature trend was calculated for various station and model data after applying a filter to reduce variations from one year to another. A Savitzky Golay filter was applied for smoothing the data as it does not change the inclination of the regression line and delivers smoothed results which still represent well the original data. As the longterm temperature trend was of interest mean annual temperature data were used for analysis.

3.2.2 Results

Elevation change

Fig.3.3 shows the calculated elevation changes derived by the plane approach for glaciers in the Bhilangna valley between the years 1968 and 2015. All methods (v1, v2, v3) deliver a similar pattern of elevation change with overall lower values for Phating Glacier than for Khatling Glacier and two local maxima on Khatling Glacier, one situated on the lower part of the glacier tongue and the other south of Jogin Glacier around the confluence with another unnamed glacier. It can be observed that v1 delivers the heighest elevation changes of all three methods suggesting up to $337m$ elevation change for a steep contributary glacier of Khatling, the Ratangrian Glacier. Extraordinarly high elevation changes are also depicted at the former border of Jogin Glacier. Both values are unlikely and must be attributed to the calculation method. As elevations increase from north to south and from west to east for a southern contributary glacier of Khatling and for the Satling Glacier, the negative values which occur in these two cases are due to underlying calculations as well. Otherwise, glacier thinning derived from v1 is between $100m$ and $130m$ for the lower part of Khatling Glacier tongue, $110m$ to $170m$ around the confluence with the unnamed glacier, $20m$ to $30m$ for the upper section and $0m$ to $50m$ for the lower section of Phating Glacier tongue. The elevation changes for v2 range between $-97m$ and $102m$. The two larger areas of negative values which can be observed on Khatling and Jogin Glacier for the v2 method coincide with areas where these glaciers flow over convex topography, i.e. bumps. Therefore these results were an expected artefact of the methodology. The elevation changes for the steep part

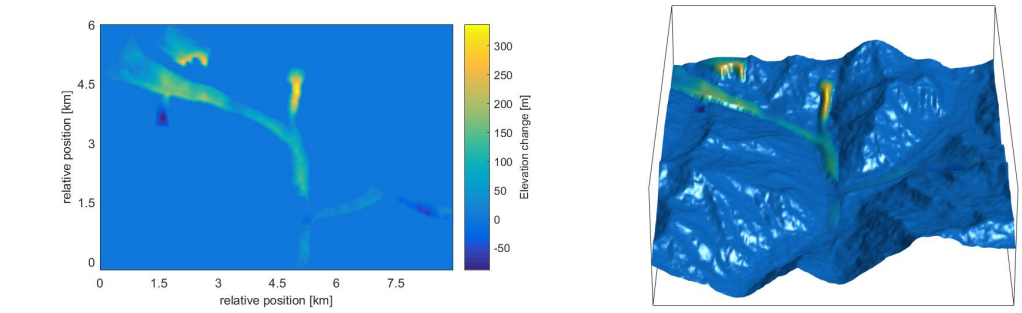

a)

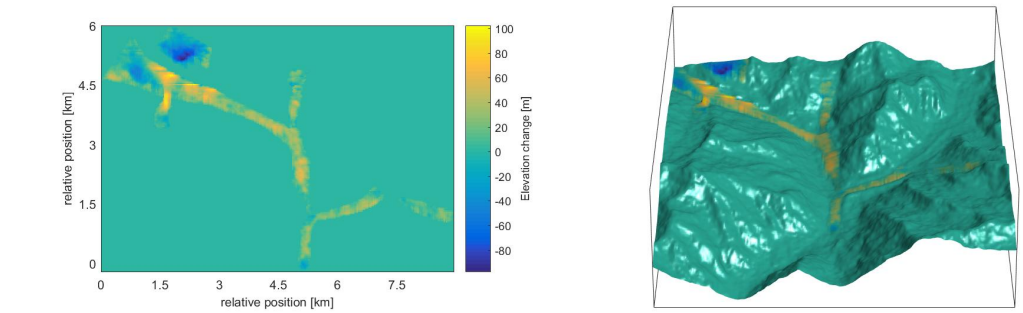

b)

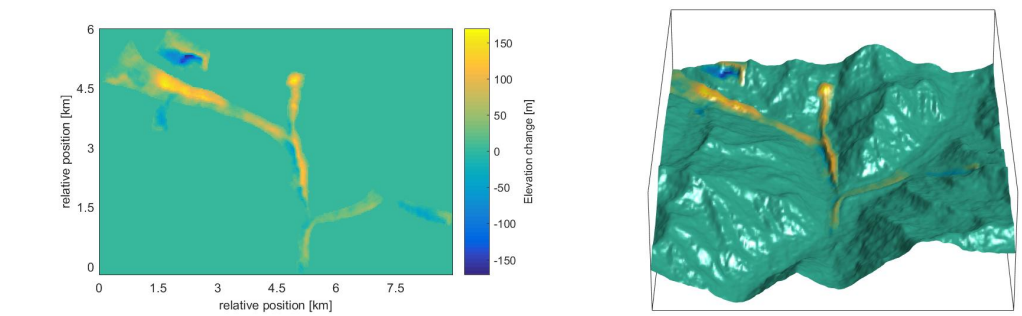

c)

Figure 3.3: Elevation change calculated for the plane approach, left in 2D, right in 3D draped over the calculated DEM for 1968. Results are based on the current ASTER GDEM. a) v1, b) v2 and c) v3. The colours indicate the order of magnitude of elevation change. Note, that the colour bars differ between v1, v2 and v3.

of the Ratangrian Glacier range mostly between $10m$ and $30m$ with low values in the steepest part and higher values in the lower situated flatter part. Elevation changes at the lowest part of the Khatling Glacier tongue from 1968 are between $30m$ and $60m$, those calculated for the Phating Glacier tongue range frequently between $20m$ and $30m$. Apart from the two larger negative areas mentioned, v2 delivers positive values for most of the glacier area in 1968. Results for v3 suggest $-171m$ to $169m$ elevation change. The distribution of negative values for v3 differs from those for v2, negative areas can be found on Jogin Glacier, the unnamed contributory glacier of Khatling, the lower part of Khatling Glacier tongue and on Satling Glacier. An interesting feature are the positive and negative elevation change values on the lower Khatling Glacier tongue situated close to each other. There are two reasons which lead to this result, one being the calculation method, the other being founded in the wrong mapping of the glacier tongue due to Corona optics. The western outline of the tongue in 1968 is situated at the bottom of the valley which is false as the central part of the tongue should occupy this position. Consequences of this can be found for v1 and v2 as well even though they are not as obvious as for v3. But 3D visualisations show that glacier surface seems to be tilted on the western side of Rudugaira ($5364m$) for all three methods (fig.3.3). However, since this part of the glacier tongue is not considered for the calculation of the thinning gradient no correction was done because this would lead to further large uncertainties. Elevation changes calculated by v3 are large for the Ratangrian glacier with a maximum value of $169m$, $110m$ to $140m$ around the confluence of Khatling Glacier and the unnamed glacier and $20m$ to $60m$ for Phating Glacier.

Thinning gradient

The elevation changes used for the calculation of the thinning gradient were established only for the common area situated within the outlines of both 1968 and 2015. Fig.3.4 gives an overview of the glacier thinning values per $100m$ elevation band for the plane and for the point approach respectively. All results have in common that most elevation change occurred between $4200m$ and $4600m$ with a maximum around $4500m$. At lower and higher elevations less glacier thinning was calculated. This form of the thinning gradient ressembles strongly to mass balance gradients of debris covered glaciers which were measured in different studies (Dobhal et al., 2013; Banerjee and Shankar, 2013). Fig.3.5 shows the mass balance profile for a bare ice glacier and a debris covered glacier. Khatling and Phating Glacier which are the main contributors to the computed elevation change values indeed show a considerable debris cover up to an elevation of $4300m$ for Khatling Glacier, for Phating Glacier only elevation changes below $4075m$ were calculated as no differing outlines were mapped above. However, the whole tongue of Phating Glacier is heavily debris covered. At higher elevations above $4300m$ where also other glaciers contribute to the summarised thinning

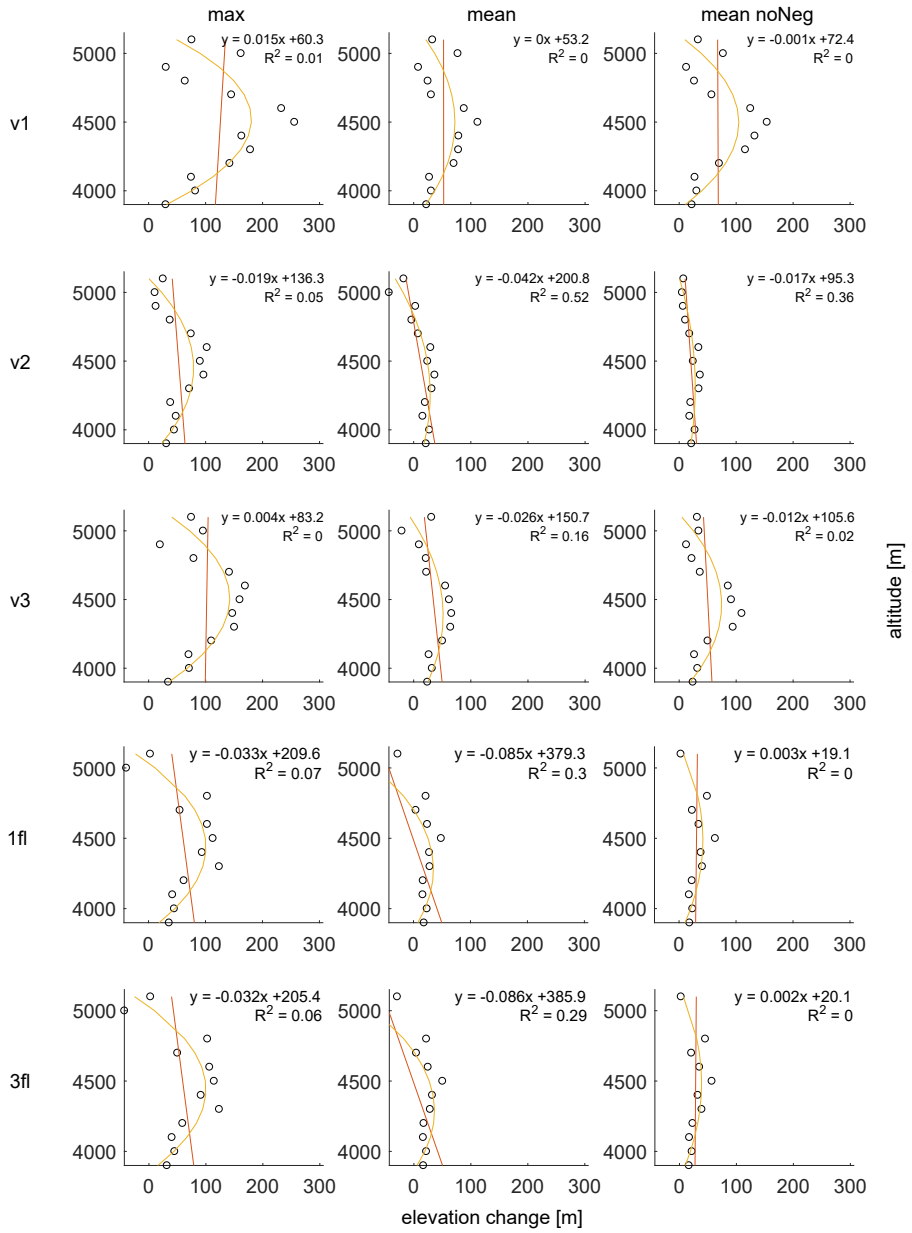

Figure 3.4: Change in elevation per 100m elevation band (black circles) over the time period 1968-2015 for methods of the plane approach (v1-v3) and of the point approach with one (1fl) and three flowlines (3fl). Linear, respectively quadratic regression lines are depicted in red respectively orange. The first column shows the maximum, the second the mean and the third the mean excluding negative values. The linear regression equation and the goodness of fit (R^2) are given. For visualisation purposes numbers are rounded.

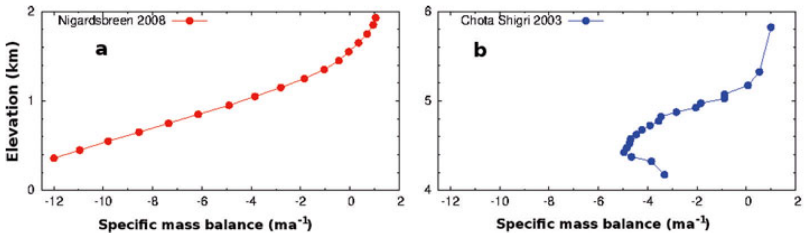

Figure 3.5: Mass balance profile for the clean ice glacier of Nigardsbreen, Norway (a) and the debris covered glacier Chota Shigri, Indian Himalaya. Figure reproduced from Banerjee and Shankar (2013).

values only little or no debris cover is found. According to satellite imagery (Google Earth and Landsat 8 scene from 08. Sept. 2015) Satling Glacier, Ratangrian Glacier, Jogin Glacier and the unnamed contributory glacier to Khatling are clean ice glaciers. Only Satling Glacier is debris covered at its lowest altitude between $4220m$ and $4310m$. Given the form of the thinning gradient, a quadratic regression line would be more appropriate to approximate the elevation change depending on elevation. However, as the aim was to establish a simplified glacier evolution model operating at a regional scale (see section 3.3) a linear approximation was selected to represent altitude-dependent elevation changes.

The linear regression slope of v1 max, v1 mean, v3 max and for the mean excluding negative values of the point approach (1fl and 3fl) is positive meaning an increase in thinning with increasing altitude. The calculation of positive gradients occurs because values are distributed non-linearly and low thinning values are found at the lowest elevations. Additionally, few values are used for line fitting. Since a gradient predicting less surface lowering with increasing altitude is needed for the future glacier evolution model (see section 3.3) the gradients mentioned were excluded in consequence. For the remaining thinning gradients of the plane approach surface lowering decreases by $0.1m$ to $4.2m$ for $100m$ elevation increase with the majority of values ranging between $1.2m$ and $2.6m$. For the point approach elevation change decreases by $3.3m$ or $8.5m$ per $100m$ altitude increase if the maximum, respectively the mean per band is calculated. The absolute minimum and maximum elevation change per band value of each method is summarised in table 3.1. Table 3.1 shows the same maximum value of $37m$ for v2 mean and v2 mean noNeg. Additionally, fig.3.4 illustrates that elevation changes per band of v2 mean are very close to those calculated for v2 mean noNeg. Therefore thinning values of v2 have to be less influenced by negative values. This is not the case for v1 and v3 where summarised elevation change values differ between mean and mean noNeg for the same band. In terms of the value range it can be stated that elevation change calculated by the point approach lies in between the values of v2 and v3 of the

plane approach. Overall the goodness of fit R^2 is the heighest for v2 (max, mean and mean noNeg).

Table 3.1: Global minimum and maximum elevation change (columns 1 and 2) with corresponding altitude band (columns 3 and 4). The elevation band $5000m$ contained only negative values for the point approach. This is the reason why these values were excluded by the mean without negative values and therefore higher minimum thinning values figure in 'mean noNeg' than in 'max'.

	method	min [m]	max [m]	min alt. [m]	max alt. [m]
max	v1	30	256	3900/4900	4500
	v2	11	102	5000	4600
	v3	20	170	4900	4600
	1fl	-39	124	5000	4300
	3fl	-43	123	5000	4300
mean	v1	8	112	4900	4500
	v2	-43	37	5000	4400
	v3	-21	66	5000	4400
	1fl	-181	49	5000	4500
	3fl	-186	50	5000	4500
mean noNeg	v1	11	154	3900	4500
	v2	5	37	5000	4400
	v3	13	110	4900	4400
	1fl	3	63	5100	4500
	3fl	3	57	5100	4500

As v2 mean noNeg seems to give the most reliable results for glacier thinning (see section 3.2.2), its linear regression equation was used for the future modelling part. To confirm these findings a validation with Findelen Glacier (Switzerland) data was carried out, see below.

Validation

The first part of the validation consisted of a comparison between an expected glacier surface for 1968 along manually digitised cross profiles and the calculated glacier surface from the plane approach at the same position. Fig.3.6 shows the position of all profiles and the results for two cross sections on Khatling, one on Phatling and one on Satling Glacier. It can be observed that all methods of the plane approach deliver results which differ from the expected glacier surface symbolised in the figure by a straight blue line. However, v2 seems to be closest to the target surface differing in most cases by less than $20m$ according to the four validation profiles in fig.3.6 and according to all additional profiles not visually presented in this thesis. Methods v1 and v3 show considerably larger discrepancies when compared to the target surface and are therefore

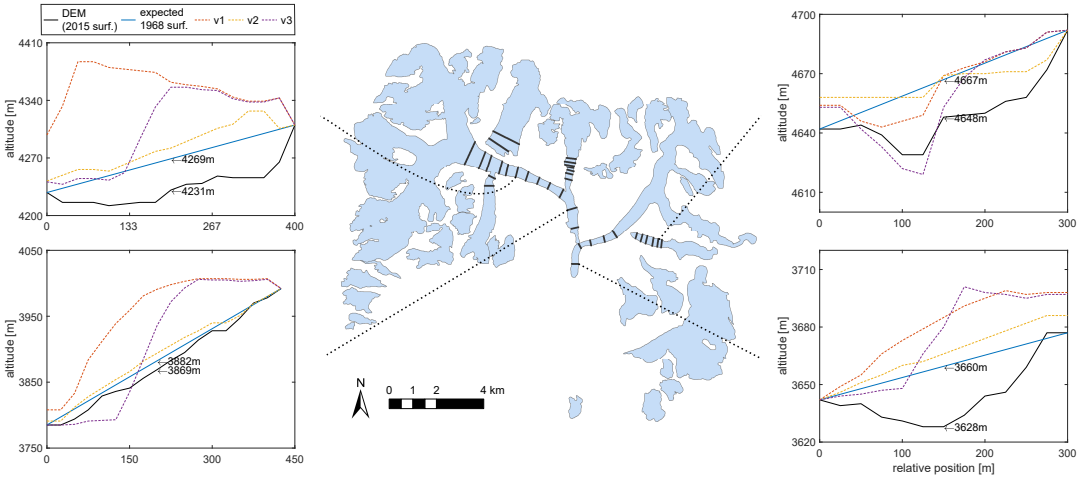

Figure 3.6: Position of manually drawn transects and the assumed and modelled glacier surface for different methods of the plane approach (v1, v2, v3) for the outline of 1968. Elevations of the ground and of the expected glacier surface are given for the centre of the cross sections. The sloped surface reflects the artefact errors in the mapped glacier outlines. Note the different scale used on the y-axis.

less appropriate for further use. In addition to cross-sectional profiles also elevation changes per $100m$ band derived from the different methods and the validation profiles were examined. The results for the mean and the mean excluding negative values can be consulted in fig.3.7. Validation elevation changes were calculated from the elevation differences between the expected glacier surface and the ground at the centre of the profiles. In this manner, the results could be compared to thinning values calculated by the point approach as well. While all methods show similar thinning like the validation data at the three lowest elevation bands ($3900m-4100m$) v1 and v3 clearly overestimate the changes for bands $4200m - 4600m$. Validation data at the heighest bands $5000m$ and $5100m$[1] consist exclusively of negative values therefore only the mean could be calculated in this case. In general, v2 and the point approach (regardless of the use of one or three flowlines) show overall the closest values to the validation data. Similarly as for the previous profile analysis, values differ by around $20m$ for v2 and the point approach except for the heighest elevation bands. However, as validation data for the bands $5000m$ and $5100m$ are based on a single value the larger discrepancy to modelled data can be explained.

In order to assess more quantitatively the accuracy of the methods in deriving elevation changes, thinning was calculated by the plane and the point approach for the Findelen Glacier in Switzerland and compared to DEM differencing results for the years

[1] no validation data is available for the band $4900m$

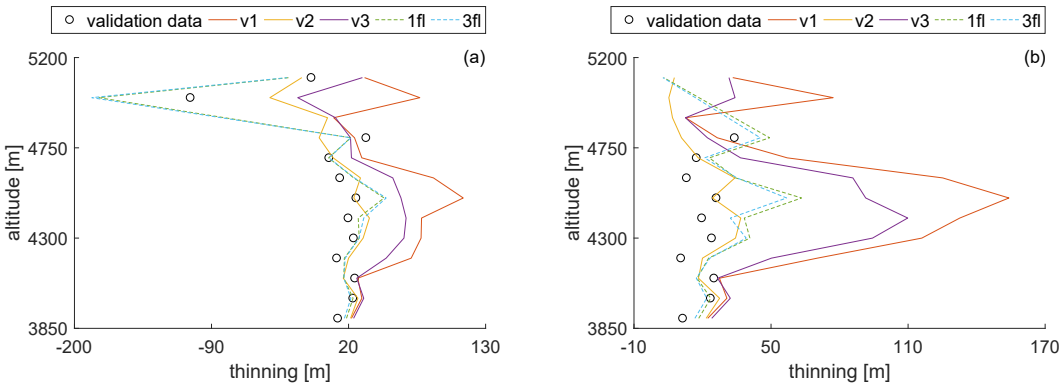

Figure 3.7: Elevation change per $100m$ band for various methods of the plane and point approach and for validation data based on cross section profiles. The thinning was calculated as the mean (a) and the mean excluding negative values (b) from values within each elevation band. Note the different x-axis range.

1965 and 2005. DEM differencing values were calculated by Rastner et al. (2016). For 1965 they used a national map of Switzerland from which they created a DEM based on the contour lines, for 2005 the dataset used was a laserscan DEM with $1m$ resolution. As glacier surface is not planar but rather convex in the ablation zone and concave in the accumulation zone differences between the plane or point approach and the DEM differencing results are expected. Fig.3.8 shows the thinning between 1965 and 2005, for a period of 40 years. It can be observed that thinning patterns of the various methods applied ressemble each other with a strong underestimation of thinning for the lowest bands ($2600m - 2800m$). Here values can differ up to 50% compared to elevation changes derived from DEM differencing data which suggest up to $80m$ elevation decrease. Between $2800m$ and $3000m$ results of v2 (plane approach) and 1fl and 3fl (point approach) match the DEM differencing results more or less. Above $3000m$ all methods rather overestimate actual thinning which should be around $10m$ according to DEM differencing data.

The similar pattern of the curves is striking therefore the question arised whether it is due to underlying topography. To test this assumption a version was calculated where a plane was put also in between the glacier outlines of 2005. The results can be seen in the central plot of fig.3.8 and the corresponding RMSE values in the right section of table 3.2. Apparently, thinning values derived from a plane approach using two planes are closer to elevation changes derived from DEM differencing data underpinned also by the smaller RMSE values. However, the form of the curve still persists (fig.3.8. Therefore topography has some influence but cannot explain the form of the thinning pattern. Another role could possibly play the mentioned convex respectively concave surface

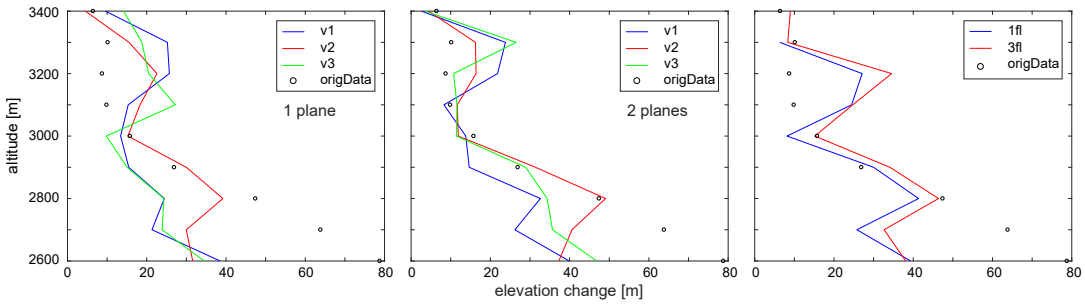

Figure 3.8: Change in elevation per 100m elevation band for DEM differencing data (black circles) and modelled data (colour lines) for Findelen glacier between 1965 and 2005. The data given represent the mean excluding negative values. Values are derived by the methods of the plane approach (left and centre) and point approach (right) (section 3.2.1). The central plot represents the results when also a plane in between the new glacier outlines was put and therefore the elevation change was calculated for two artificially created DEMs.

of the glacier. According to Bauder et al. (2014) the ELA was situated at $3275m$ in 2007/08 and at $3215m$ in 2008/09. Recent aerial imagery (SWISSIMAGE, (Swisstopo, 2015)) supports these findings that the ELA ranges somewhere around $3200m$. The left image in fig.3.9 shows the state of the Findelen Glacier in 1964. The ELA is not detectable in this case but it is likely that it is situated somewhere close above the two zones characterised by many crevasses which would correspond to an altitude between $3000m$ and $3100m$. Interestingly it is at $3000m$ where we find the break in the thinning curves of all methods (fig.3.8). Is it possible that the methods underestimate thinning in the lower ablation zone where glacier surface topography is convex, calculate it more or less correctly in the upper ablation zone close below the ELA and overestimate thinning at and above the ELA where glacier surface topography tends to be concave? This is a daring hypothesis which further studies outside the scope of this thesis could explore where multiple DEMs are available.

RMSE values (table 3.2) range for all methods around $20m$ with v2 showing the lowest values for the plane approach and 3fl even lower values for the point approach. $20m$ correspond to the contour line aequidistance of the national map and is valid for a time period of 40 years. Therefore this value is considered to be acceptable. However, as the DEM accuracy of 2005 is very high and therefore small mapping inaccuracies should not have a large impact a lower RMSE value could be expected and would be preferable.

The findings of this validation section support the choice of the thinning gradient derived by the v2 of the plane approach for the future modelling part. Therefore all future glacier evolution calculated will be based on its linear regression equation.

Table 3.2: Findelen RMSE values for elevation change data per 100m elevation band derived from DEM differencing and modelled by the methods of the plane and point approach (v1-v3 are methods of the plane approach; 1fl is the point approach with 1 flowline, 3fl the point approach with 3 flowlines). The analysis was done for a mean excluding all negative values as it is considered as the most sensible option (see section 3.2.1). The RMSE was determined for modelled data, modelled linear regression data (lr), modelled data when two planes were put (2p) - one in between the old, the other in between the new glacier outlines - and modelled linear regression data for two planes (2p lr).

method	RMSE [m]	RMSE lr [m]	RMSE 2p [m]	RMSE 2p lr [m]
v1	22.72	23.25	20.20	20.68
v2	20.39	19.24	16.34	15.81
v3	23.18	23.61	15.96	16.93
1fl	21.43	19.63		
3fl	19.94	17.32		

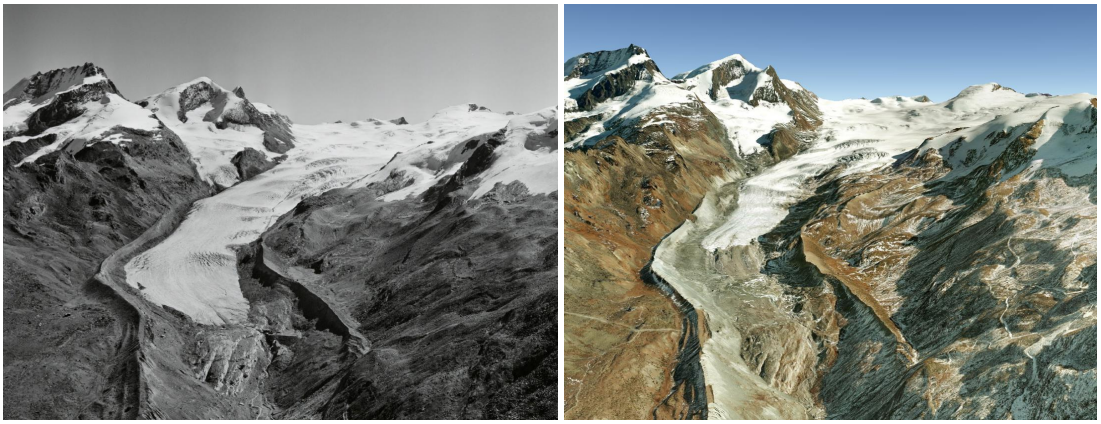

Figure 3.9: Photo of Findelen Glacier in September 1964 (Swissair Photo AG, 1964) and Google Earth view of the same scene for the year 2009.

Temperature trend

In order to model future glacier evolution temperature change was determined for three time frames in the past. Table 3.3 gives a review of calculated changes for different model based temperature datasets for the grid cell over the study region. Apparently, the time frame chosen has a strong influence on the results, all datasets show a considerably lower temperature increase for the period 1950-2000 than for 1965-2015 although both periods span 50 years. Only the 20th Century Reanalysis V2 dataset has a temperature change differing by less than $0.5K$ between the two periods. The reason for such large differences can be explained to some degree by analysing fig.3.10 which depicts the temperature course for RCP4.5 and RCP8.5. Around the year 1950 mean annual temperatures are higher than in the following years where a decrease occured until the minimum in 1967. Secondly, a distinct continuous temperature increase can be observed for years after 1993. Therefore it is clear that a linear regression line fitted to data between 1950 and 2000 delivers a rather small temperature change compared to the change resulting from a regression line fitted to data between 1965 and 2015. Another observation is that for the period of 1965-2005 the mean warming occured after 1990. This can be deduced by comparing temperature changes for 1965-2015 and 1961-1990 (table 3.3). Although 1990 marks with 25 years difference to 1965 and 2015 the half of this 50-year period, warming from 1961-1990 is considerably less than half of the warming determined for 1965-2015 for many of the datasets. The only exceptions are NCEP/DOE AMIP-II Reanalysis and GISS 30°-31°N, 78°-79 which shows a cooling for 1961-1990. However, a considerable degree of uncertainty persists for the temperature changes determined from the latter dataset as data reach back to 1979 and therefore linear regression lines were fitted to less data and temperature changes had to be extrapolated. For the period 1965-2015 all calculated temperature changes (table 3.3) are positive. 20th Century Reanalysis V2 and the two RCPs lead to very similar results with $\sim 1.45K$ warming for this period. It is expected that the RCPs will show near identical results for the historical period, because the model runs are tuned to the same historical observations. It is only towards the mid-21st century that the modelled temperatures start to diverge as a result of different emission scenarios (see fig. 3.10). Other studies presented similar past temperature change values for the Himalayan region as those derived for the two RCPs. Bolch et al. (2012) determined a warming of $0.03K$ per year for the Mount Everest region for the period 1959-2007 meaning an overall temperature increase of $1.44K$ for this 48-year long period. Bhutiyani et al. (2007) stated a warming of $1.6K$ for the northwestern part of the Indian Himalayas during the last century with minimum temperature rising at a lower rate than the maximum temperature. Furthermore they found that real warming has started at a modest rate in the decade of 1961-1970 and continued till the end of the investigated period with an exception of the decade of 1981-1990. Warming rates appeared to be higher for

Table 3.3: Change in mean annual temperatures for different time frames. The temperature differences are given in [K] and were derived from linear regression lines fitted to the different datasets for the time frames given.

Data source	1950-2000	1965-2015	1961-1990	Data time span
20th Century Reanalysis V2	1.01	1.45[1]	0.65	1871-2010
GISS 30°-31°N, 78°-79°E	−0.27	0.39	−0.46	1881-2016
GISS station data New Delhi	−0.24	0.93	0.37	1931-2016
NCEP/DOE AMIP-II Reanalysis	0.52[1,2]	1.60[1]	1.04[1,2]	1979-2016
NCEP/NCAR Reanalysis	−0.58	0.72	0.06	1948-2016
RCP4.5	0.57	1.44	0.55	1861-2100
RCP8.5	0.55	1.45	0.56	1861-2100

the period 1991-2002 (Bhutiyani et al., 2007) compared to previous decades. These observations made by Bhutiyani et al. coincide well with the observations made in this thesis.

Table 3.4 shows the temperature changes calculated for ground based station data. The results are wide spread and especially data for Mukhem do not seem to be trustworthy as negative temperature trends were computed for all periods. The very high temperature change of $1.8K$ at Dehradun for the period 1965-2015 appears to be remarkable when compared to the low temperature changes for the other two periods ($0.01K$ for 1950-2000 and $0.06K$ for 1961-1990). However, as Dehradun experiences a phase of strong growth after becoming the capital of the newly established state of Uttarakhand in 2000 with a resident population growth of about 114% from 1991-2011 (Singh et al., 2013), this could be an explanation for the calculated temperature changes. Nevertheless, Singh et al. (2013) derived a temperature increase of $0.43K$ for the period 1967-2007 for Dehradun which questions the reliability of the station data available in this thesis. Mukteshwar which is located in Uttarakhand in the lower Himalayas at an elevation of $2284m$ shows a negative temperature change of $-0.4K$ for 1950-2000 and an increase of $1.4K$ for 1965-2015 which is very close to the temperature changes determined for the RCPs and the 20th Century Reanalysis V2 dataset for this period.

The future glacier evolution model (described in section 3.3) uses projected temperatures for the two RCP scenarios. Therefore, RCP temperature trends determined for the period 1965-2015 were used as past temperature change input. In addition, derived RCP temperature trends were similar to those determined by other studies as mentioned above. Fig.3.10 illustrates the temperature datasets for the two RCP scenarios. Until 2030, RCP4.5 and RCP8.5 show very similar temperatures. Afterwards, RCP8.5

[1] Temperature change is extrapolated beyond the data span based on the linear regression line.
[2] Less than half of the years in this period are covered by data.

Table 3.4: Evolution of mean annual temperatures for different time frames for ground based weather stations. The temperature differences are given in [K] and were derived from linear regression lines fitted to the different datasets. Data were analysed in India.

Station	Coord.	Alt. [m]	1950-2000	1965-2015	1961-1990	Data time span
Dehradun	30.32°N/78.02°E	643	0.01	1.83	0.06	1929-2013
Mukhem	-	-	−1.73	−1.30	−0.23	1957-2007
Mukteshwar	29.47°N/79.65°E	2284	−0.40	1.42	0.11	1901-2013

is characterised by a faster warming which lasts until the end of this century. RCP4.5 in contrast presents the same rate of warming between 2000-2065 with a subsequent flattening of the curve and a temperature increase of only $\sim 0.3K$ afterwards until 2100. The overall temperature increase until 2100 compared to the reference period of 1986-2005 is $\sim 3.3K$ for RCP4.5 and $\sim 6.7K$ for RCP8.5 respectively.

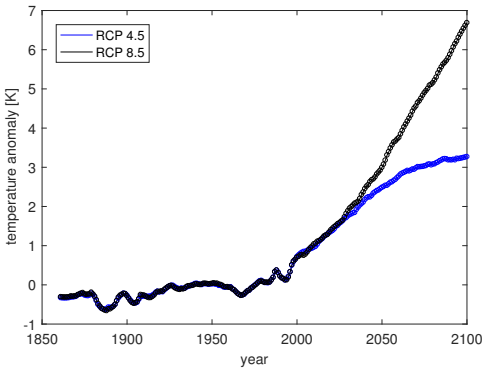

Figure 3.10: Temperature anomalies (reference period: 1986-2005) for 30°-31°N and 78°-79°E as modelled for the RCP4.5 and RCP8.5 (IPCC, 2013). The data were smoothed with a Savitzky-Golay filter.

3.3 Future glacier evolution

The modelling of future glacier thinning gives indication about the time frame when glaciers will have retreated to the position of future glacier lakes. The position and extent of the lakes can be modelled with GlabTop (Paul and Linsbauer, 2012) but not their time of occurence. It is the scope of this master thesis to develop on this research gap. The knowledge of the time frame of occurence is valuable for the planning of mitigation measures and the allocation of ressources.

Different warming scenarios were taken into account. On the one hand RCP4.5 from

the IPCC report (IPCC, 2013) was considered as a middle warming scenario, on the other hand RCP8.5 was used as the worst case warming scenario. As many uncertainties persist in future glacier evolution modelling, only the decadal time frame was of interest for the determination of future lake development.

3.3.1 Methods

This thesis follows the approach of Linsbauer et al. (2013). First, ice thickness has to be modelled for each glacier cell. This is done by applying the GlabTop model which assumes ideal plasticity of ice neglecting basal sliding. It uses local surface slope, total vertical extent and basal shear stress to calculate local ice thickness (Paul and Linsbauer, 2012; Cuffey and Paterson, 2010). The basal shear stress τ is derived from the elevation range Δh of a glacier as follows:

$$\tau = 0.005 + 1.598\Delta h - 0.435\Delta h^2 \tag{3.1}$$

If the elevation range exceeds $1.6km$ τ is set to a constant value of $150kPa$. The calculated shear stress τ can then be used to determine the ice thickness d using the following formula:

$$d = \frac{\tau}{\rho g f \sin\alpha} \tag{3.2}$$

where ρ is the density of ice ($900\,kg/m^3$), g the gravity acceleration ($9.81\,m/s^2$) and f the shape factor (a value of 0.8 is used for the GlabTop model (Paul and Linsbauer, 2012)). Two versions of the GlabTop model exist. For this thesis the original version was used which uses a DEM, current glacier outlines and additionally digitised branch lines as input. The result can be seen in Fig. 3.11.

In a next step, the future lowering of surface elevation was calculated for each cell depending on its DEM value using the thinning gradient derived in section 3.2.2. Thereby, the elevation change was subtracted from the current ice thickness. At the same time, the new elevation of the cell in the DEM was calculated. This leads to a feedback where glacier melt results in lower elevations of glacier ice at the same position and in consequence this leads again to intensified glacier melt. As soon as the ice thickness of a cell was below zero after the subtraction, the ice thickness was set to zero and the glacier has disappeared at this position.

The thinning gradient was determined only for glacier tongues (see section 3.2.1). Therefore, it was applied up to the elevation where elevation change equaled zero. For higher altitudes no information about elevation change was available and therefore no elevation changes were modelled for these parts. Considering, that we have positive

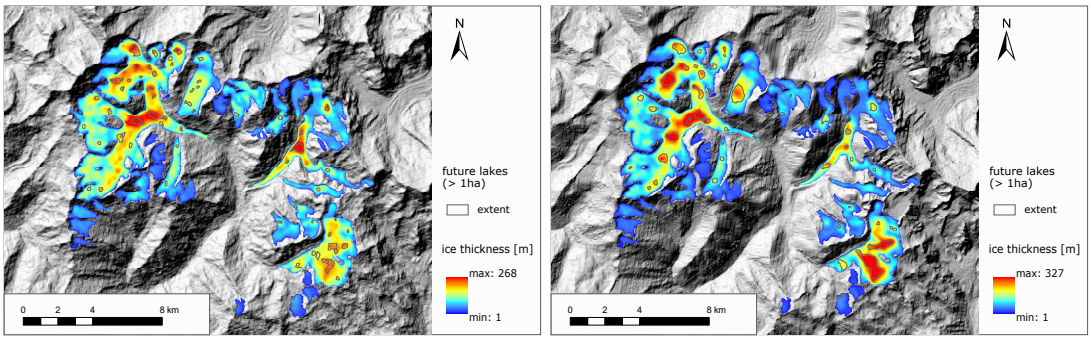

Figure 3.11: Ice thickness in 2015 and the position of future lakes modelled by the GlabTop model using ASTER GDEM (left) and SRTM (right) as input. Results for ASTER show lower ice thickness values with a maximum thickness of 268m. Ice thickness calculated for the SRTM dataset ranges up to 327m. For Dudhganga Glacier remarkably higher values were calculated using the SRTM DEM. The number of lake is higher for ASTER but their size tends to be smaller than for SRTM.

mass balances in the accumulation zone but also subsidence and melt of snow, the assumption that elevations of higher positioned ice cells remain the same, seems to be justified. There is no justification for using a quadratic function of elevation decrease above a certain elevation as done by Linsbauer et al. (2013) because data are simply missing and also the climatic and environmental setting of the Himalayas is different compared to the Alps.

A linear thinning gradient was selected which shows decreasing elevation change with increasing altitude. As v2 of the plane approach delivers the most reasonable results (see section 3.2.1), its thinning gradient was used for modelling future glacier evolution. The reason for the choice of a linear gradient was the way of coupling the thinning gradient to climate warming. A parallel shift of the gradient with climate warming was implemented. This is in accordance with the observation that spatial distribution and therefore also the elevation gradient of specific mass balances remains highly similar over several years and shifts only depend on the weather circumstances of a specific year (Singh et al., 2011).

For this reason, the approach was adapted by two points: First, the same elevation change was attributed to different time steps depending on the warming scenario used as implemented by Linsbauer et al. (2013). This was realised by adapting the number of iterations of elevation change being subtracted from the DEM and the ice thickness. The number of iterations was adjusted by multiplying the number of modelled years with a factor consisting of the division of $T_{\text{fut}}/t_{\text{fut}}$ and $T_{\text{past}}/t_{\text{past}}$. Secondly, it was accounted for the fact that warming climate leads to intensified ice and snow melt and as the form of the thinning gradient was assumed to not change strongly (Singh et

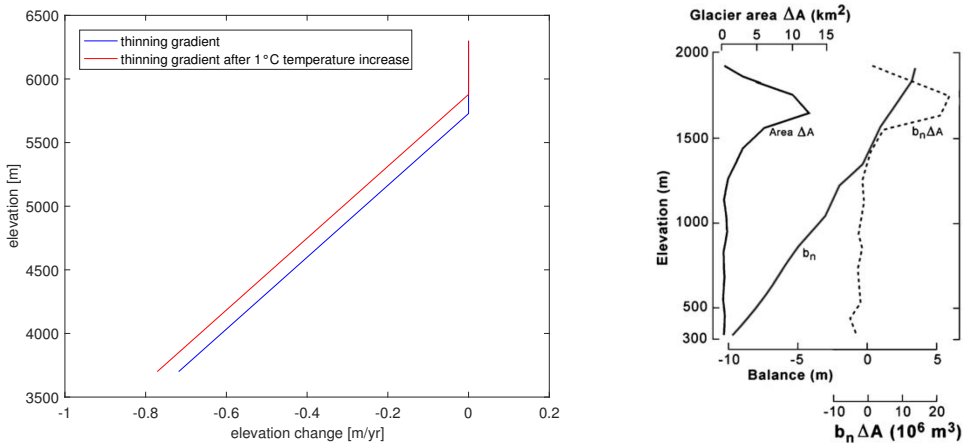

Figure 3.12: Elevation change gradient as implemented in the future modelling part (left). The gradient shifts by $150m$ for a temperature increase of $1K$. The right plot shows the area-altitude distribution and the specific mass balance for the Nigardsbreen Glacier in Norway, 1963-1964 (reproduced from Cuffey and Paterson (2010)). The profile of the specific mass balance is close to linear justifying the use of a linear thinning gradient for modelling future glacier evolution. However, it should be noted that Nigardsbreen is a clean ice glacier and glaciers in Bhilangna valley show debris cover. Therefore differing forms of the thinning gradient may be expected (see section 2.1.2 and 3.2.1 for further information).

al., 2011), a parallel shift of the thinning gradient was implemented. The shift of the thinning gradient was defined so that a $1K$ temperature increase induced a rise of the ELA by 150m meaning that after $1K$ warming the same amount of elevation change can be found at an elevation 150m higher than initially. The value of 150m/K is based on the ELA increase triggered by temperature increase as determined by Kuhn (1981).

Transferred into an equation the thinning Δe at iteration i is defined as follows:

$$\Delta e_i = \frac{m \cdot e_{i-1} + q + q_{\text{incr}} + (h_{\text{rise}} \cdot \frac{T_{\text{fut}}}{t_{\text{fut}}} \cdot \frac{t_{\text{period}}}{n}) \cdot i \cdot (-m)}{t} \tag{3.3}$$

with m being the regression slope, e the elevation, q and q_{incr} constants (q_{incr} changes during the modelling therefore it is separated from q), h_{rise} the elevation increase of the ELA per $1K$ warming, $\frac{T_{\text{fut}}}{t_{\text{fut}}}$ future temperature increase per time frame, t_{period} the modelled time step, n the number of iterations during this time step, i the iteration number and t the time frame of the past thinning gradient which is in this case 47 years (1968-2015). The variables used were for ASTER $m = -0.0166$ and $q = 95.322m$ and for SRTM $m = -0.006$ and $q = 45.521m$.

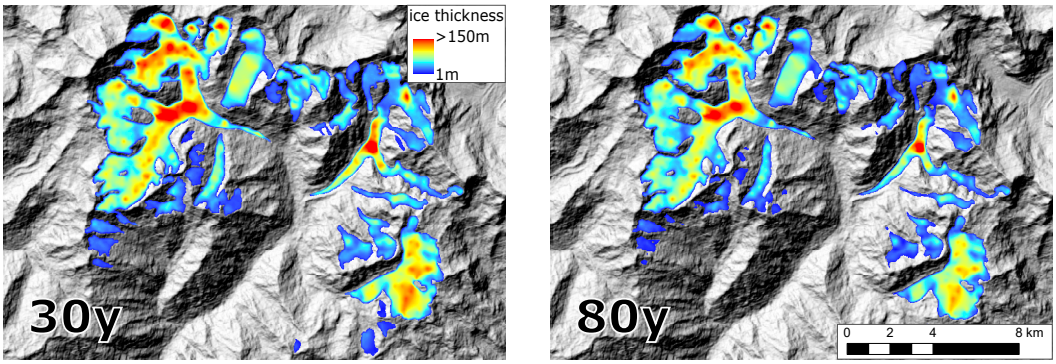

Figure 3.13: Future glacier ice thickness and extent in the Bhilangna Valley for the warming scenario RCP4.5, in year 2045 (left) and 2095 (right). Glacier evolution was calculated with an adapted version of the model proposed by Linsbauer et al. (2013).

3.3.2 Results

Fig. 3.13 shows the future glacier evolution for the RCP scenario 4.5. As half of the warming has already occured after 30 years the situation after this time step and the final state for 80 years is illustrated. It can be observed that little change in glacier extent occures compared to the state in 2015 (fig. 3.11), glacier retreat being most visible for smaller unnamed glaciers with low ice thicknesses. Between 30 and 80 years the tongue of Satling Glacier shrinks. Furthermore, ice thickness decreases on all glaciers. This is well visible for example on Dudhganga Glacier or around the confluence on Khatling and Phating Glacier. The thickness loss, which in this thesis is always in reference to the ice thickness in 2015, ranges after 30 years between $0m$ for sites above $6000m$ situated just below the heighest peaks in the catchment such as for example below Thaley Sagar, Bhartekhunta or on the northeastern flank of Jaonli and up to $29m$ at the lowest elevations on Phating Glacier tongue. Up to the confluence with Bhartekhunta Glacier, Phating Glacier shows thinning values of $29m$ to $22m$. At the tongue of Khatling Glacier a thinning of $27m$ was modelled. For the state after 80 years, elevation decrease is up to $54m$ on Phating Glacier tongue with a value of $43m$ around the confluence with Bhartekhunta Glacier. The tongue of Khatling Glacier thinned up to $49m$ and $32m$ can be found around the confluence between $4700m$ and $4800m$. Even the heighest elevations experienced thinning in 80 years although the value of $1m$ is negligible. The whole future evolution of glaciers for RCP4.5 can be consulted in fig. 5.4 in the appendix.

Larger changes of glacier extent and ice thicknesses can be observed for the RCP scenario 8.5 (fig. 3.14). Already after 40 years Phating Glacier tongue appears to be disconnected from its current accumulation zone as the ice thickness was low in this

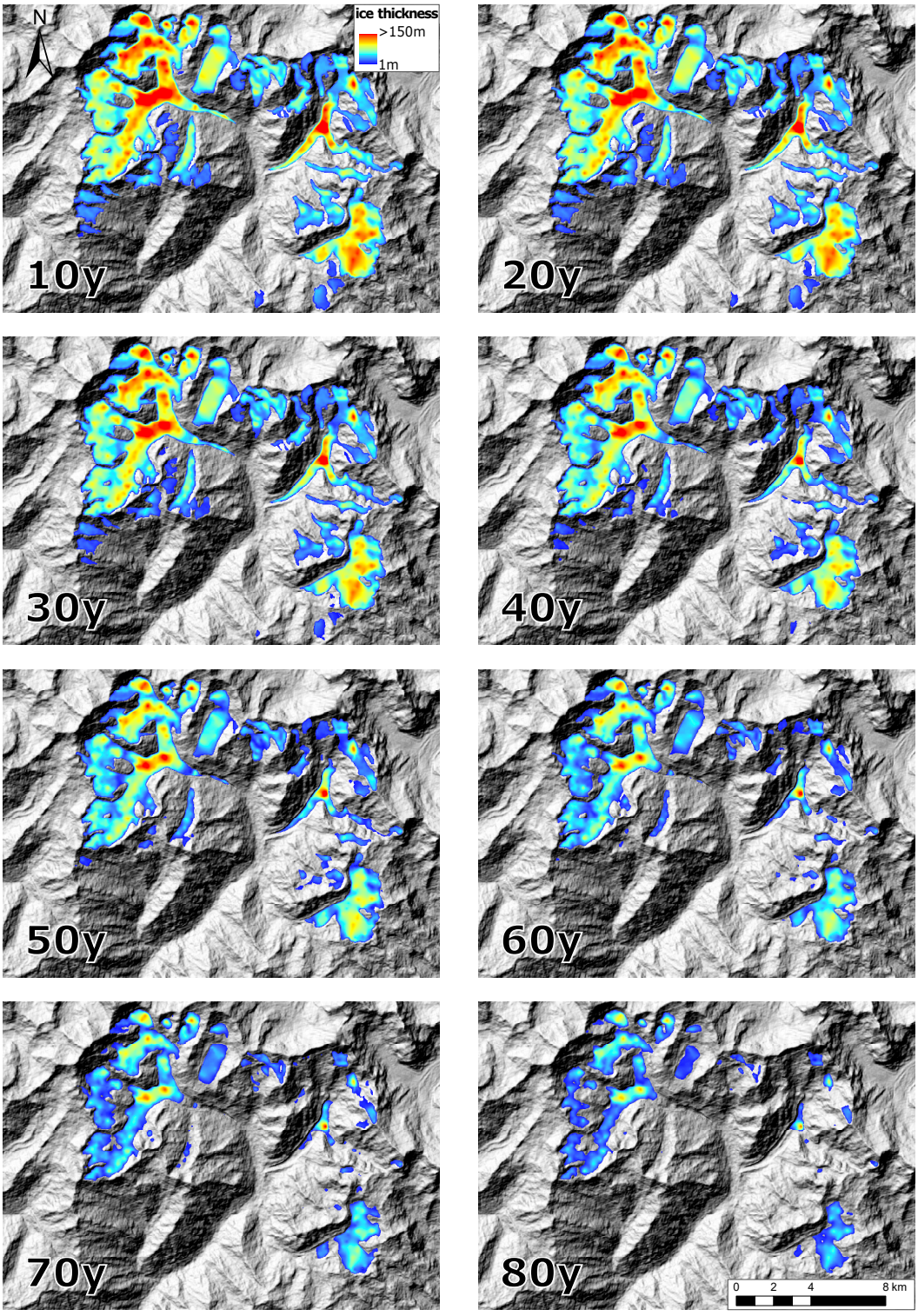

 Figure 3.14: Same as fig. 3.13 but for RCP8.5 and the years 2025-2095.

steep section of the glacier. The connection between Bhartekhunta Glacier and Phating Glacier tongue still exists, however, Bhartekhunta has shrunk remarkably. After 50 years the lower part of the Khatling Glacier tongue becomes isolated from the rest of the glacier. The tongue of Satling Glacier has disappeared completely. By the time of 60 years most of the small unnamed glaciers do not exist anymore and the tongue of Khatling Glacier has retreated below the confluence (above the bump) at an elevation of around $4600m$. For Phating Glacier only the upper part of the glacier tongue remains as well as some disconnected glacierised areas at the heighest elevations. Bhartekhunta Glacier has mostly vanished; only ice patches are left. Jogin Glacier is splitted into two and Ratangrian Glacier into numerous parts. In 70 years even the tongue of Phating Glacier has disintegrated. Dudhganga Glacier appears separated from its former tongue and also Khatling Glacier shows zones of separation where steeper terrain is present. In 80 years time a large part of the present glacierised area has disappeared, larger ice accumulations being found only for Khatling and Dudhganga Glacier. However, some ice patches from Jogin, Ratangrian and Phating Glacier persist. Concerning ice thickness loss, up to 30 years values are comparable to those of RCP4.5 as the evolution of RCP temperatures until this point is similar. In this way the minimum thinning is $0m$ and the maximum $38m$ though only $9m$ difference to the values of RCP4.5 (30 years). After 50 years maximal thinning is already $81m$ measured for Phating Glacier tongue. The tongue of Khatling Glacier has experienced an elevation decrease of around $75m$. At the heighest altitudes Khatling Glacier has lost between $2m$ and more often around $20 - 25m$; close to the confluence the values range around $50m$. Glacier surface of Jogin and Ratangrian Glacier has been lowered between $\sim 20m$ and $\sim 45m$, those of Dudhganga Glacier between $\sim 30m$ and $\sim 55m$. The greatest differences in ice thickness loss shows as usually Phating Glacier with its large elevation extent. Here, elevation decrease was $1m$ to $\sim 35m$ in the upper part and $\sim 60m$ to $81m$ for the glacier tongue. Elevation change values for 80 years depict more or less the ice thickness in a smoothed way with the heighest values around the confluence of Phating and Bhartekhunta Glacier. Here, ice loss amounts to $139m$. On Khatling Glacier thinning around the confluence ranges between $\sim 100m$ and $\sim 110m$ and between $\sim 60m$ and $\sim 80m$ for upper parts of the glacier which are still present in 80 years.

3.4 Lake exposition to gravitational impact and overall GLOF hazard

The presence of glacial lakes produces a hazard for downvalley living population and infrastructure. Besides factors which determine the dam stability (such as dam geometry and composition), also the probability of mass movements impacts into a lake plays an important role whether a lake is more or less prone to generate a GLOF. In

this thesis this aspect was examined by calculating the topographic potential for lakes emerging at a certain point in time. In this way, the overall evolution of the changing hazard for the Bhilangna valley could be studied.

3.4.1 Methods

The concept of topographic potential includes two components: on the one hand, the potential of rock or ice to detach, on the other, the potential for these generated rock and ice avalanches to reach a glacial lake (Allen et al., 2016b). The first component can be approximated by the calculation of slope, the latter by the angle of reach. A threshold of 30°was applied to select areas where ice and rock potentially detach. For the angle of reach a value of 25% ($\sim 14°$) for rock and 31% (ca. 17°) for ice avalanches was chosen (Huggel et al., 2004b).

The hazard at a certain point in time was evaluated for each lake individually. In order to achieve this, the lakes modelled by the GlabTop model (see section 2.3.2 for more information on modelling potential future lake positions) were overlayed with the ice extent of a specific decade and where no overlap was present, these lakes were regarded as having emerged. These lakes served as pour points in the following watershed calculation. The trajectory slope was calculated as the fraction of the elevation difference between pour point and the DEM value of a cell and the flowpath length. The trajectory slope values were calculated only for areas where the slope exceeded 30°. The selection of cells based on their trajectory slope value (rock: cells with a value > 0.25; ice: cells with a value > 0.31) delivered a subset of cells where mass could potentially detach and reach the lake. Therefore, the simplest approach to classify the exposition of a lake to gravitational impact was to build the sum of all trajectory slope cell values within a lake watershed. This results in high values if a large area is considered to potentially generate mass movements or if steep ice or rock walls surround the lake at close distance which automatically leads to high trajectory slope values.

In order to quantify the GLOF hazard posed by a lake it is also necessary to incorporate the lake volume. As the GlabTop model delivers a depth value for each lake cell the lake volume was computed by summing up all lake depth values and multiplying them with the cell area. Where no depth values were available which was the case for current lakes (not modelled by GlabTop) the lake volume was approximated by applying an area-volume-relation equation (Huggel et al., 2002):

$$V = 0.104A^{1.42} \tag{3.4}$$

with V being the volume and A the area of the lake. The probability of mass movement entering the lake and the magnitude of a potential GLOF were then classified in five classes ranging from 'very low' to 'very high' expressed as numbers from 1 (=

very low) to 5 (= very high). The probability was parametrised by the sum of the trajectory slopes of potential starting zones for ice and rock avalanches; the magnitude by the lake volume. It has to be noted, that a lake does not have to drain completely in the case of a GLOF and therefore the parametrisation of the GLOF magnitude by lake volume is a rough approximation and represents the worst case. The classification is based on natural breaks classes calculated for RCP8.5 for the latest stage of the analysis period (80 years). Natural breaks is a statistical procedure that groups the values in a way that internal differences of classes are minimised and differences to other classes maximised (Wikipedia, 2016).

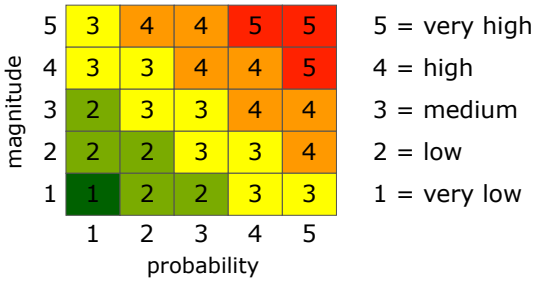

Figure 3.15: Hazard concept: Magnitude is parametrised by the lake volume and probability by the sum of all trajectory slope values within a lake watershed, indicating the probability of mass movement impacts into the lake. The concept was adapted based on the hazard concept developed by Raetzo et al. (2002).

The hazard posed by a lake was evaluated by adapting the risk concept developed by Raetzo et al. (2002). There, two variables are considered: the probability and the magnitude. In contrast to Raetzo et al. not the probability of an event is used but the probability of mass movement impacts into the lake. The implementation can be seen in fig. 3.15. The final GLOF hazard is calculated as the rounded mean of the magnitude and the probability level. It is important to consider that the classification made is only valid for the study area of the Bhilangna Valley and the hazard values here cannot be transferred and compared to rankings from other studies.

3.4.2 Results

At present, several lakes exist in the Bhilangna Valley most of them are located either around Shastru or around Masuri Tal (see fig. 2.5). All of these lakes are situated at positions where the probability of mass movements entering these lakes is low (2 lakes) or very low (10 lakes). A different value range can be observed for the volume classes. Here, all levels are present (very low: 5 lakes; low: 3 lakes; medium: 1 lake; high: 2 lakes; very high: 1 lake). This leads to overall GLOF hazard levels which range between very low and medium. Two lakes could be inspected during field work and to give an overview what the classification means transferred into reality, pictures are shown in fig. 3.16.

The lake situation after 30 years assuming a medium climate warming scenario is given in the left image of fig. 3.17. In comparison to the initial state five new lakes

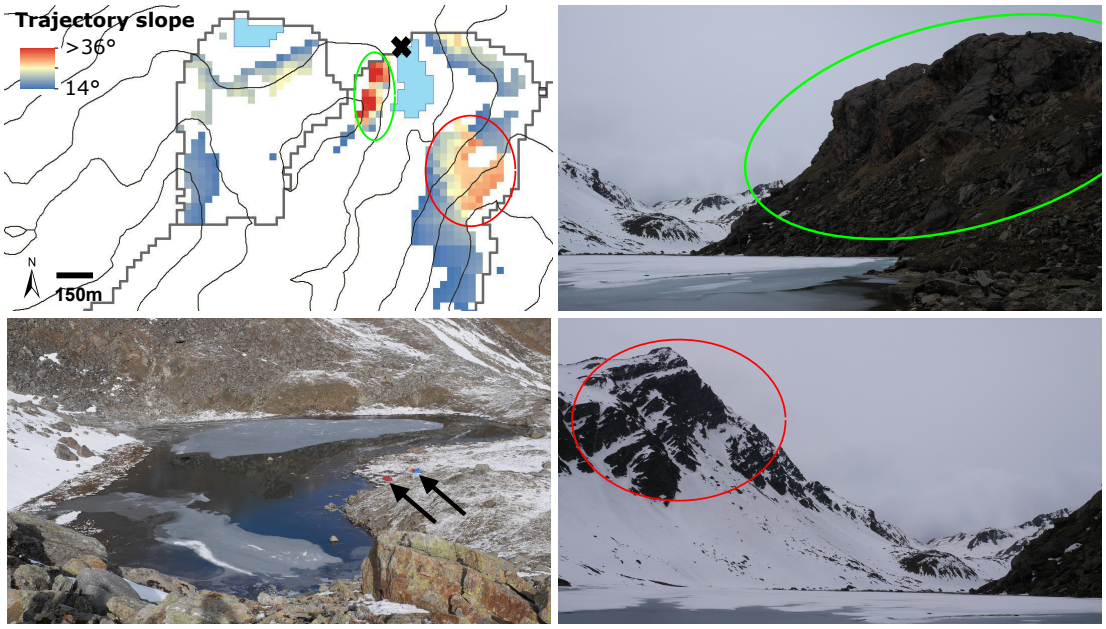

Figure 3.16: Modelled trajectory slopes for two lakes visited in May 2016 (top left), the cross indicating the approximate position from which pictures at the right were taken. Areas with high trajectory slope values are marked with an ellipse (top left) and the corresponding position of these areas is marked in the pictures (top right and bottom right). The smaller lake (top left and bottom left) belongs to the volume class 2 (= low) and the impact probability class 1 (= very low), arrows mark the position of tents indicating the proportions. The larger lake belongs to volume class 3 (= medium) and impact probability class 2 (= low).

have emerged (the initial state is identical with the state after 10 years which can be consulted in fig. 5.5 in the appendix). All new lakes are located at glacier termini of 2015 which means that an elevated level of uncertainty is inherent concerning their development. This is due to possible GlabTop modelling artefacts and because GlabTop averages slope in $50m$ elevation bins even if glacier boundaries are exceeded at the glacier termini (Allen et al., 2016b). All new lakes have low volumes most of them only several thousands m^3. The largest lake can be found south of Dudhganga Glacier with a volume of $100800m^3$ which belongs to the volume class 2, all other lakes are in class 1. In contrast, the impact probability for the lake at Khatling and Phating Glacier tongue is high leading to a final medium GLOF hazard value for these lakes. After 80 years four new lakes will have emerged compared to the situation after 30 years: one lake below Maiali ($5097m$), one below Kairi ($5435m$), and two next to Masuri Tal (see fig. 2.5 for place names). However, it is probable that the current lake at Masuri Tal will be connected with the future lower lake. Lakes which were present after 30 years

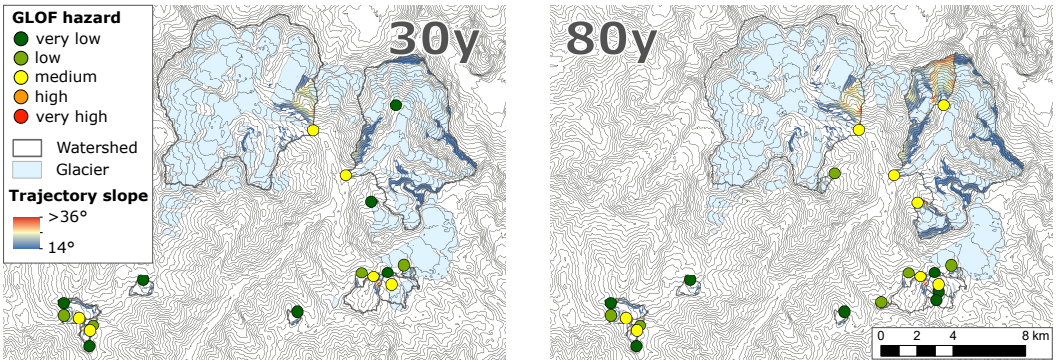

Figure 3.17: Future GLOF hazards posed by emerging glacial lakes in the Bhilangna Valley for the warming scenario RCP4.5, in year 2045 (left) and 2095 (right). Points indicate lake positions and the colour the related GLOF hazard. Hazard levels are based on the probability of mass movement impacts into the lake and the lake volume. Watersheds (gray outline) show the upstream area where flow is directed towards the lake. The trajectory slope values indicate the angle derived from the flow path length and the elevation difference between lake and potential starting zone of a mass movement. For more information on trajectory slope values and the calculation of the GLOF hazard see section 3.4.1.

have grown and their volume ranges now between 83700m^3 and 158400m^3. For newly developed lakes between 30 and 80 years volumes span a larger range from several thousands m^3 up to 155700m^3 for the lake below Maiali. Due to lake growth also watersheds have changed for some of the lakes and water bodies get closer to potential source areas of mass movements. This is the case for example for the lake north of the confluence of Phating and Bhartekhunta Glacier, lake 130 (see fig. 5.7 for lake numbers) which changes its impact probability class from very low to high between 30 and 80 years in future. Similarly, the probability of mass movements impacting the lake south of Phating Glacier tongue, lake 252 (fig. 5.7), rises between 30 and 80 years from a very low to a medium level. Together with the higher volume this leads to an overall increase in the GLOF hazard level for these two lakes from very low to medium.

For RCP8.5 lake development proceeds at considerably higher rates than for RCP4.5 (fig. 3.18). Already after 40 years the state of the lakes is the same as for RCP4.5 after 80 years. During the first decade no change occurs. After 20 years three new lakes have developed, one at Phating Glacier tongue, one at the glacier terminus of an unnamed glacier south of Phating Glacier (lake 252) and the last at an unnamed glacier tongue south of Dudhganga Glacier (lake 317). Medium GLOF hazard is the highest hazard level which can be found for this period, new lakes covering all hazard levels from very low to medium. Their volume is still very low so the low and medium GLOF hazard has to be attributed to medium and high impact probability. After 30 years

lake 317 changes its GLOF hazard class from very low to low due to volume increase. Furthermore three new lakes have emerged: the lake below Maiali, lake 130 and a lake at the front of Khatling Glacier. The two latter lakes and the lake at Phating Glacier tongue have all a very low volume but are highly susceptible that mass movements enter them. Especially in the watershed of lake 130 the probability of descending ice avalanches seems to be high as steep glacier ice is situated in the mountain flank above the lake. The situation after 40 years changes slightly compared to 30 years. A new lake is situated below Kairi, two new lakes are located close to Masuri Tal and the lake below Maiali and lake 252 have changed their GLOF hazard class due to volume growth. In terms of lake existence and the GLOF hazard classes the situation for RCP8.5 after 40 years is identical to the situation for RCP4.5 after 80 years. However, lake volumes are definitely larger for RCP8.5 (up to $63000m^3$ more). Two additional lakes are present after 50 years, one situated northeast of the confluence of Khatling and Sangli Glacier, the other east of lake 253 at an unnamed Glacier. For the first time a lake with a high GLOF hazard level can be found in the catchment which is lake 130. Its hazard increased due to the simultaneous increase of volume and impact probability. The impact probability is now very high and the volume at a medium level. As can be observed the watershed area has grown due to the lake area increase. This in turn leads to the heightened opportunity of mass movements reaching the lake. Although the glacier above lake 130 has retreated remarkably its upper parts are still present posing a serious ice avalanche hazard. In 60 years, lake 130 has grown so far that it is attributed to the volume class high and therefore the overall GLOF hazard level for this lake changes to very high. Its volume is $592200m^3$. New lakes in 60 years have emerged at the tongue of Jogin Glacier, a second lake at the former position of the Khatling Glacier tongue and another lake upstream of lake 252. The change between 60 and 70 years is remarkable: in total 8 new lakes have developed during this decade. Two of them are situated where the former unnamed glacier south of Khatling Glacier was located, one emerged above and one below the bump in the bed of the former Khatling Glacier tongue. Three of these four lakes belong to the low GLOF hazard class, the lake situated below the bump shows a medium hazard level. Further new lakes can be found at the ancient position of Ratangrian Glacier (lake 128), another one west of lake 130 (lake 135), one below the confluence of Phating and Bhartekhunta Glacier and the last at the place liberated by Bhartekhunta Glacier (lake 215). All these lakes have very low volumes but their surroundings are rather steep and though the probability of mass movement impacts is high leading to an overall medium GLOF hazard. Another observation is that the glacier above lake 130 has disappeared completely in 70 years though no ice avalanches only rock fall and rock avalanches can enter lake 130 at this point in time. Between 70 and 80 years again numerous lakes develop. Many of them are situated in the area vacated by the Dudhganga Glacier, Jogin Glacier, Satling and Sangli Glacier. Overall 11 new lakes have emerged but most of them show low or even

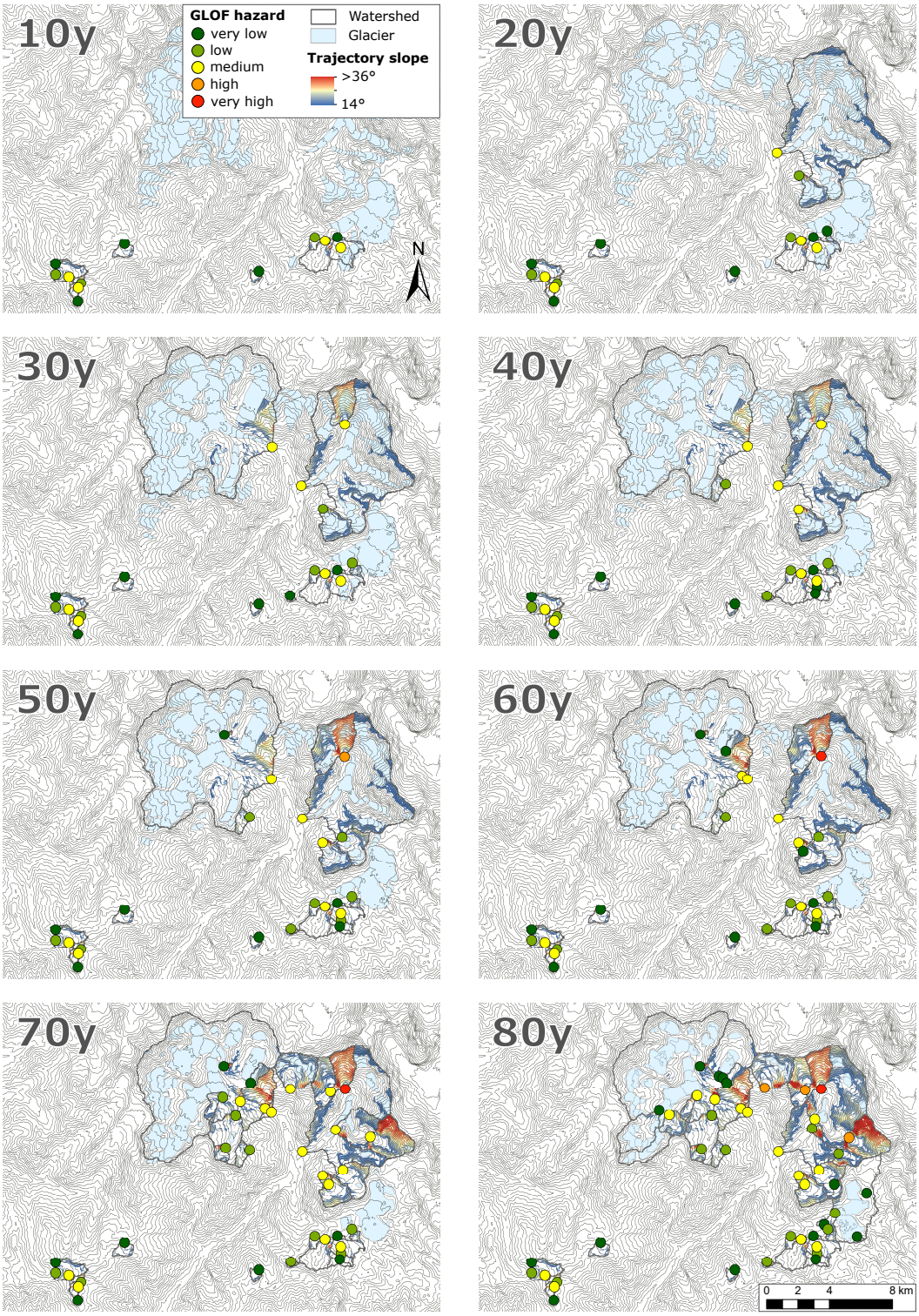

Figure 3.18: Same as fig. 3.17 but for RCP8.5 and the years 2025-2095

very low GLOF hazard levels. The probably most interesting development during this last decade is the change of the hazard class of the lakes 128, 135 and 215 which now show a high hazard level. Lake 215 (former Bhartekhunta Glacier) has grown rapidly skipping a volume class and belonging to the the medium sized lakes now. But also its impact probability level has increased due to lake growth. As the watershed of the lake remained the same higher trajectory values must be the cause for this class change. Even more rapidly than lake 215 has grown lake 128 (former Ratangrian Glacier) which changed from volume class 1 to class 4 between 70 and 80 years. The impact probability class remained the same being high at both stages in time, however, as can be seen in fig. 3.18, surrounding potential source areas are more red than for 70 years indicating higher trajectory slope values. Increasing trajectory slope values due to lake growth can be well observed also for lake 135 where a steep mountain flank is located above the lake which shows a color shift to red between 70 and 80 years. But just as lake 128, lake 135 did not change its GLOF hazard class because of its impact probability class but because of its volume growth. Now this lake belongs to the medium volume class.

In summary, the lake development for RCP8.5 seems to accelerate after 60 years. Particular attention should be paid to lake 130 which represents a high GLOF hazard in 50 years and a very high hazard in 60 years. The state in 80 years shows many lakes with a medium to very low GLOF hazard, however, three lakes with a high level and one with a very high level are present. Increasing GLOF hazard levels are the result of rising impact probabilities as well as volume growth.

3.5 Downstream hazard

A high magnitude GLOF can be a low risk if it occurs in a remote region without infrastructure and population. In contrast, a low to medium magnitude GLOF can already cause substantial damage if infrastructure, cultivated land or populated areas are crossed by its path. Therefore, it is necessary to evaluate the potential flow path of a GLOF in order to estimate the exposition of a site to such a debris flow event. In the case of the Bhilangna Valley, this was done for the locations of current and future hydropower stations. Again, the temporal evolution was examined to inform about the point in time when these infrastructures could be exposed to a future GLOF.

3.5.1 Methods

The scope of this thesis was to give a broad overview and a first order assesment of the future GLOF hazard evolution. This is the reason, why the Modified Single Flow (MSF) model was used to determine potential flow paths. The MSF model (Huggel et al., 2003) is based on the D8 single-flow-direction model (O'Callaghan and Mark, 1984) which routes the flow along the steepest descent. As debris flows, rock and ice

avalanches deviate from the direction of the steepest descent a spreading function was implemented in the MSF model which allows horizontal diversion of flow up to 45°from the central flowline which follows the steepest descent (Noetzli et al., 2006).

To account for the different GLOF hazards posed by the various lakes, the modelled MSF paths were weighted by the lake hazard value. Hence, a modelled GLOF originating from a lake with an overall hazard value of 3 (= medium) received this value as an attribute and it was assigned to all cells affected by the modelled debris flow. In this way, the lake volume figured at least indirectly in the results as it was included in the lake hazard value. However, it should be considered that actual flow dynamics of a mass movement are dependent on volume and that this aspect was not included in the MSF modelling part. Instead, a single angle of reach of 11°was used as a maximum runout criterion for all GLOFs modelled as debris flows and 3°for GLOFs modelled as floods. These numbers were derived by Haeberli (1983) and are commonly used to model worst case runout distances.

In order to account for the increasing probability of a site being affected by a GLOF if a higher number of lakes are located upstream in the catchment, the MSF paths of all lakes were overlaid. The sum of these weighted paths was computed and provides an indication about the exposition of a site to a future GLOF. In particular hydropower stations can be affected by a GLOF due to their proximity to river channels. Therefore, a timeline of the changing hazard was established for current and planned stations located in the Bhilangna Valley. Further points along the river channel were added upstream to increase the level of detail of the downstream hazard evolution with the first point being placed at a comparable position as Kedarnath in the neighbouring valley (Kedarnath and P_{0km} are both $1km$ downstream to the closest current glacier tongue, Kedarnath at an altitude of $\sim 3540m$ and P_{0km} at $3631m$). The location of points and hydropower stations is represented in fig. 3.24.

3.5.2 Results

Fig. 3.19 shows the MSF model results for the current state. The numbers are dimensionless and represent only a relative susceptibility of sites being affected by a GLOF. East of Shastru ($5150m$) three lakes could generate a debris flow descending to Bhilangna River. In $2km$ distance from their source at an approximate altitude of $3800m$ all paths overlay each other and are channelised. After reaching the Bhilangna River all debris flows travel for another $5km$ downstream where the mass movement of the lake with the medium GLOF hazard stops, the debris flow from the low hazard lake continues $300m$ further downstream and the GLOF propagation of the very low hazard level lake ceases after a total distance of around $6km$. These model results appear to coincide well with reality as past debris flows seem to have stopped approximately at these locations not far upstream of Gangi (fig. 2.3). GLOFs triggered at lakes north

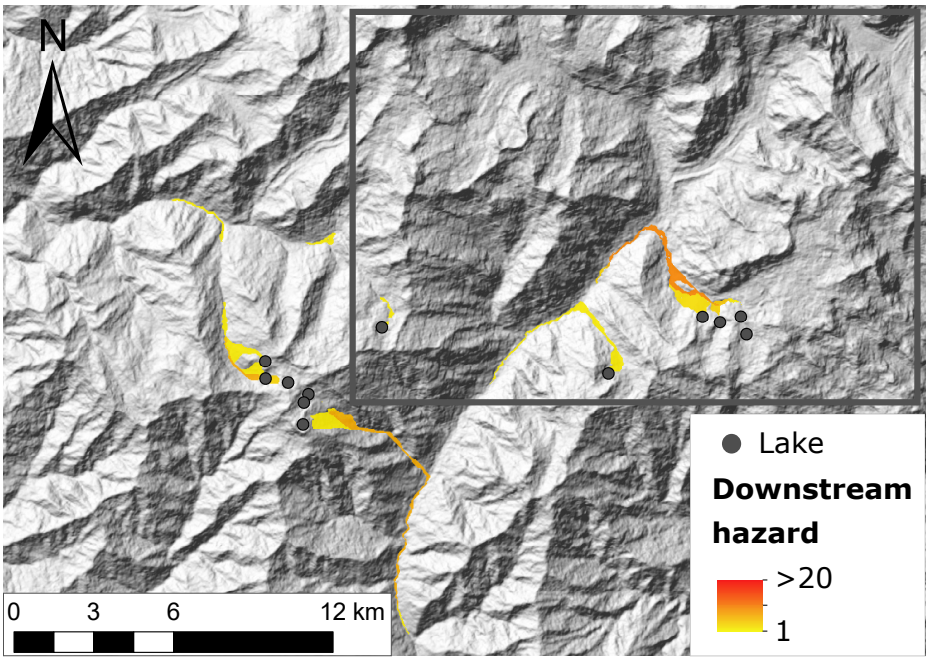

Figure 3.19: Potential of cells being affected by a current GLOF (modelled as debris flow) in the Bhilangna Valley. Values represent the sum of all weighted MSF paths which were overlaid. Therefore they are unitless and give only a comparative measure of the site exposure to potential GLOFs. The box marks the area where changes in MSF paths are expected to occur in future and shows the enlargement for fig. 3.21 and 3.22.

of Shastru will travel to another valley where rivers finally drain to Bhagirathi River. The disrupted debris flow paths which can be observed in this region are due to the fact that the trajectory slope rises from below 11°above this threshold again. It is an artefact of the model implementation, however, it can be argued that erosion occurs for the modelled areas and where a disruption is present the GLOF will still continue as a flood downstream. This is reasonable as transformations of debris flows to floods and vice versa can be observed in nature. Fig. 3.23 and 3.24 show that there is indeed a continuous propagation of GLOFs if the model is run for a flood and a debris flow. The most susceptible areas to debris flows at current stage are located downstream of Masuri Tal and at and below the confluence with Bhilangna River. Fig. 3.20 shows the lower section of these potential GLOF path areas in May 2016 for a vast sediment filled plain. It is possible that many debris flows will already stop in this plain due to the low gradient. Downstream hazard values range up to 9 at these locations as flow paths of four lakes overlay each other. The exposure to potential GLOFs originating from

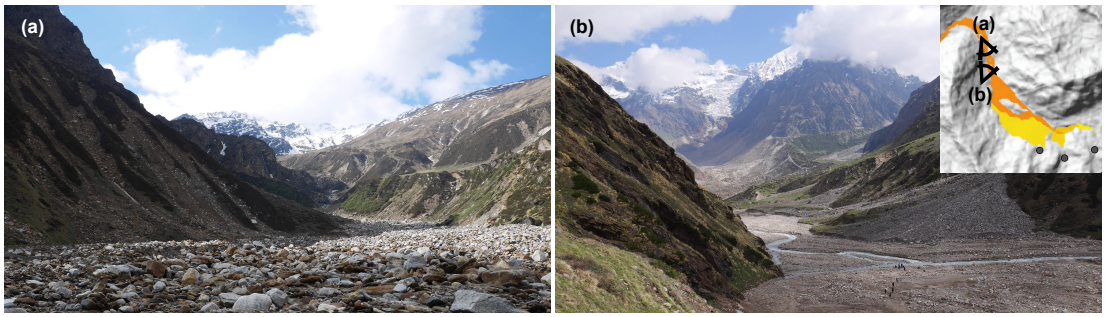

Figure 3.20: An upstream and a downstream view of the area below Dudhganga Glacier and Masuri Tal affected by potential debris flows. The approximate position where pictures were taken and the view angle is given in the small image at the top right corner.

lakes situated around Masuri Tal starts to diminish close to Tambakund and no GLOFs should propagate to Bhumka, located approximately $1km$ downstream of Tambakund (see fig. 2.5 for place names). Another current lake (lake 508, see fig. 5.7 for lake numbers) is situated west of Maiali but its hazard is very low and therefore also sites within the modelled path have a very low likelihood of being affected by a GLOF.

Fig. 3.21 illustrates the evolution of downstream affected areas by GLOF paths in 30 and 80 years for a medium warming scenario RCP4.5. Sites downstream of Masuri Tal are negligibly more exposed (value increase of two due to the appearance of a new lake). A new MSF path emerges for the lake south of Phating Glacier tongue (lake 252) and for lake 130 north of the Phating and Bhartekhunta Glacier confluence. The former shows a continuous propagation in direction of Phating Glacier where its path is deviated to the southwest due to the present lateral moraine. At the valley bottom it joins the Bhilangna river rising slightly in this way the exposure of these sites and travels further downstream until Bhumka where it rejoins the path of lake 508 for another $200m$ and stops. For lake 130 a GLOF would not propagate very far due to the flat surrounding. Although lakes have also emerged at the front of Khatling and Phating Glacier debris flows do not propagate as the progracial area is flat. After 80 years new MSF paths emerge together with the new lakes. At Masuri Tal two very low hazard lakes could generate debris flows which would most likely stop in the vast plain shown in fig. 3.20. However, their flow path would have to travel through rather flat terain first. Further new affected areas appear downstream of a lake below Maiali ($5097m$) its path running to the same position as the MSF path of the current lake 508 (west of Maiali). The new lake below Kairi ($5435m$) shows a low hazard and a debris flow triggered here could travel down until Bhumka. Due to the lowering of Phating Glacier also the travel distance of the MSF path of lake 130 increases slightly (fig. 3.21). The overall heighest increase in downstream hazard values between 30 and 80 years can be registered for the area along the Bhilangna River channel between

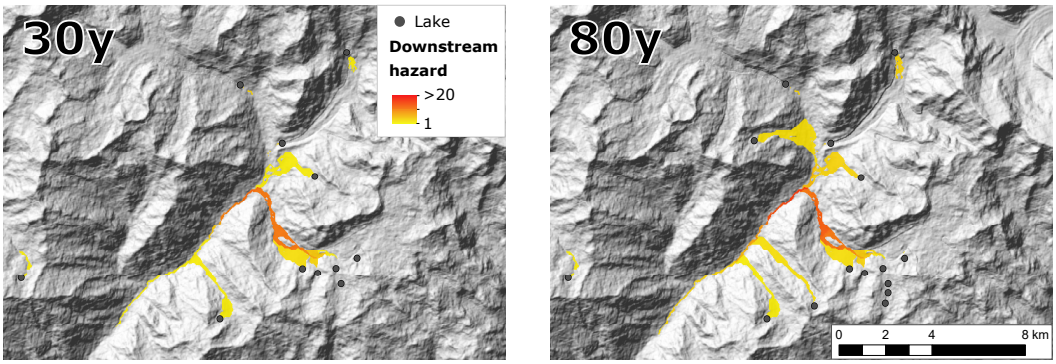

Figure 3.21: Potential of cells being affected by a future GLOF (modelled as a debris flow) in the Bhilangna Valley for the warming scenario RCP4.5, in year 2045 (left) and 2095 (right). The paths were modelled with MSF. Downstream hazard values represent the sum of all weighted MSF paths which were overlaid. Therefore they are unitless and give only a comparative measure of the site exposure to potential GLOFs.

Khatling and Bhelbagi (see fig. 2.5 for place names). Here, values range between 5 and 16 and increased by 4 to 7 during this 50 year period.

For the worst case warming scenario RCP8.5 downstream hazard increases more rapidly (fig. 3.22). Similarly as for the lake development the downstream hazard situation after 40 years considering RCP8.5 appears quasi identical as for RCP4.5 after 80 years. The main change between 10 and 40 years includes the new MSF paths originating at lake 252, at the lake below Maiali and at the lake below Kairi which appear after 20, 30 and 40 years respectively. Additionally, lake 130 emerges after 30 years together with the ongoing downstream hazard. In 50 years the appearance of the lake north of the confluence of Sangli and Khatling Glacier leads to new affected areas along the Khatling Glacier and in the liberated bed in front of its snout. This debris flow could potentially travel up to $6.5km$ downstream of its source, however, the lake has a very low GLOF hazard. Another lake positioned south of the Phating Glacier tongue and east of lake 252 could generate a GLOF with a modelled MSF path continuing downstream for $5.9km$ up to the MSF paths coming from the valley of Masuri Tal where it stops. A slight increase can be observed in the runout distance of a debris flow triggered at lake 130 between 40 and 50 years. After 50 years a new lake emerges upstream of lake 252 and therefore the exposure along the path of lake 252 increases by a small amount. Furthermore, a debris flow initiated at the new lake could travel up to $570m$ more downstream than one starting at the lower lake 252. A new modelled GLOF path appears also for a lake situated at the front of Jogin Glacier. As terrain shows rather an evenly sloped or convex topography between the lake and the liberated bed of Khatling Glacier a wide spread of possible debris flow trajectories

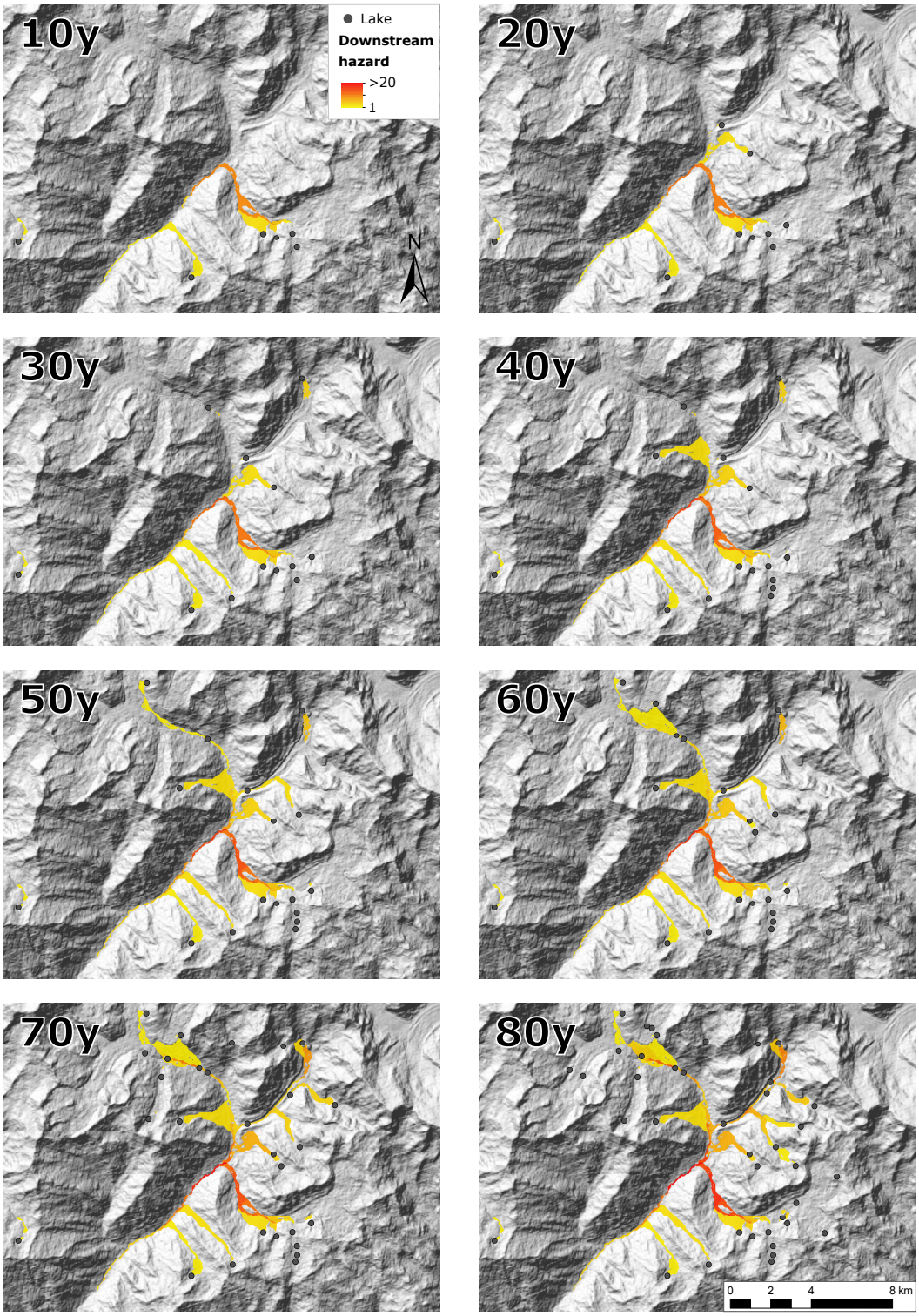

Figure 3.22: Same as fig. 3.21 but for RCP8.5 and the years 2025-2095.

is modelled. From the former Khatling Glacier bed downwards the flow is channelised. The maximum travel distance of this mass movement would be down to the place named Khatling (fig. 2.5) respectively close to the point where debris flow paths from Masuri Tal join the Bhilangna River. A new lake has emerged $0.5km$ upstream of the Khatling Glacier terminus in 2015. Although the potential of mass movement impacts in this lake is high a debris flow would not propagate due to the surrounding flat terrain. For the case of a GLOF originating from lake 130 the exposure of affected areas downstream increased due to the hazard level change of the lake which is now very high. After 70 years many sites register a higher susceptibility being affected by GLOFs. Increased hazard levels of lakes are the cause, i.e. for lakes 260 and 249 which now belong both to the medium hazard class, as well as the appearance of numerous new lakes. West and upstream of lake 130 a new medium hazard lake is located which could generate a GLOF with a $4.8km$ long trajectory path, exceeding the path of lake 130 by $2.2km$ further downstream. In the overlapping area the downstream hazard increased. The lake situated within the former boundaries of Bhartekhunta Glacier shows a medium hazard and its MSF path extends $2.9km$ downstream as the terrain is rather flat. Interestingly no GLOF propagates from the lake which emerged after the retreat of Ratangrian Glacier although downstream terrain is steep. The greatest change in downstream hazard between 60 and 70 years occured in the former bed of Khatling Glacier tongue. The GLOF paths of four new developed lakes overlap adding a value up to 9 to the downstream hazard leading to an overall value of 11 at this place. This value is comparable to downstream hazards measured in the valley below Masuri Tal, around Khatling and between Tambakund and Bhumka. Higher values are present only for the Bhilangna River section between Khatling and Tambakund. Comparing the values here which range up to 19 with the value of 9 for the state in 2015 a doubling of the exposure of these sites will take place within the next 70 years. During the eighth decade new lakes develop in the area vacated by Dudhganga, Satling, Phating, Jogin and Sangli Glacier. Related to this the hazard increases or emerges for corresponding downstream areas, i.e. within former boundaries of Satling Glacier new terrain could be affected by a GLOF. A debris flow developing from a GLOF event at lake 239 (former Satling Glacier area) could travel relatively far downstream because of its high altitude position at $5000m$. Its maximum runout can be found close to Tambakund though at a distance of $8.8km$ from the source. The two new lakes placed at the former position of Jogin Glacier show a very similar trajectory path as their neighbouring lake which has emerged after 60 years. Therefore downstream hazard increases uniformly for affected areas. A GLOF does not propagate from the lakes located around Sangli Glacier. Overall, many of the exposed sites in 70 years experience a rise in the downstream hazard by a value between 1 and 3 in 80 years. The only exception is the section between Khatling and Tambakund. Here, a value increase of 6 can be found due to new overlapping debris flow paths originating from

lakes found at the former Dudhganga Glacier tongue, lake 239 (former Satling Glacier area) and lake 258 (see fig. 5.7 for lake numbers). The section between Khatling and Tambakund is also the area with the overall heighest downstream hazard after 80 years. But also the downstream area of Masuri Tal shows higher hazard values.

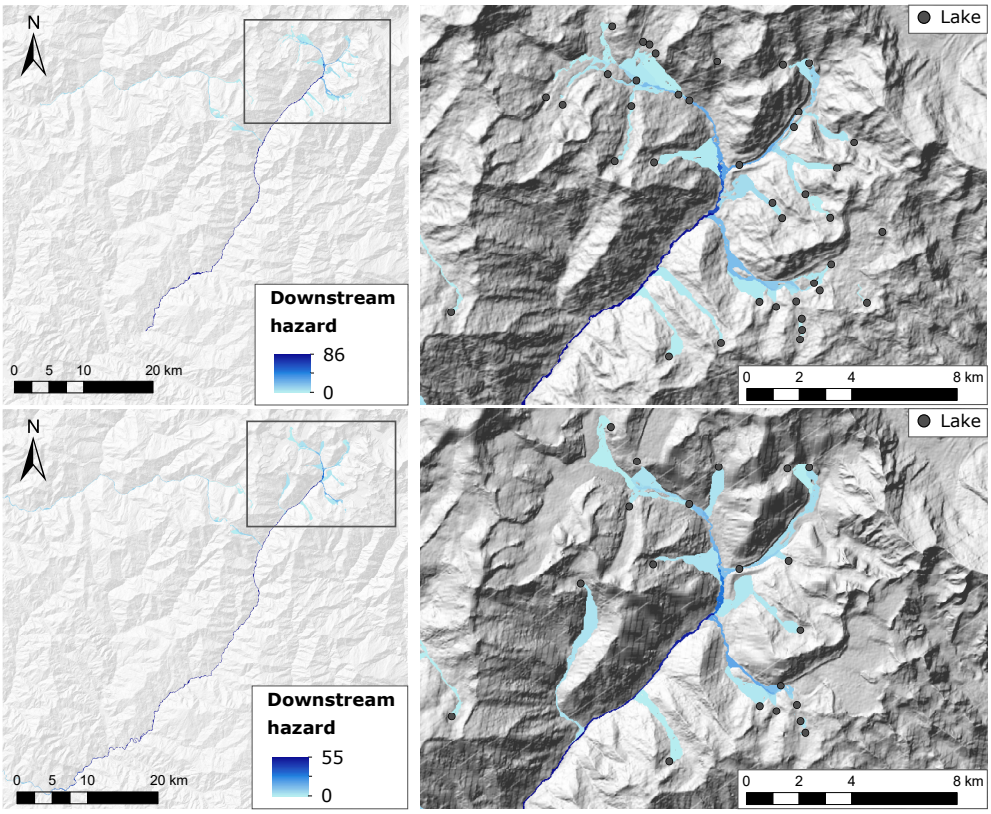

Figure 3.23: Same as fig. 3.21 but for RCP8.5 in year 2095 and the GLOFs are modelled as floods. Results for two DEMs are shown: ASTER (top); SRTM (bottom).

Fig. 3.23 illustrates the downstream hazard for flood events using ASTER and SRTM as the underlying DEM dataset. Glacier thinning, lake development and GLOF hazard was also determined separately for ASTER and SRTM (SRTM results can be consulted in fig. 5.3 in the appendix). Therefore the number of lakes differs between the two datasets as can be seen in fig. 3.23. First of all, it can be observed that floods can travel considerably further downstream than debris flows. For ASTER the flood stops not far upstream of Ghansali, for SRTM it continues further down even entering the water reservoir of Tehri dam (see fig. 2.3 for locations). Compared to debris flow simulations the flood propagates also in flatter areas as can be seen for example for the two lakes around Sangli Glacier in the zoomed section of fig. 3.23. Concerning

the pattern, downstream affected areas are similar for ASTER and for SRTM. An exception is the modelled flood from the lake located within the former Ratangrian Glacier area. A MSF path appears for SRTM but not for ASTER. Another difference between these two datasets is that MSF results for SRTM appear more smooth. In general, downstream hazard values are higher for ASTER but this is primarily due to the higher number of lakes.

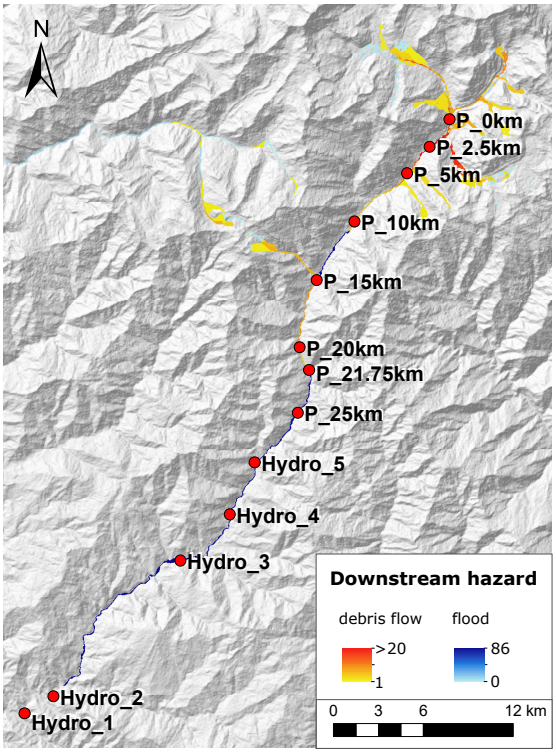

Figure 3.24: Locations of hydropower stations and points for the downstream hazard evolution in the Bhilangna Valley. Hydropower station 5 is planned, stations 1-4 are constructed.

The temporal evolution of the downstream hazard for several points along the Bhilangna River (see fig. 3.24 for point locations) can be studied in fig. 3.25. Apparently, downstream hazard increases with time for points upstream of P_{15km}. The hazard values for P_{15km} and P_{20km} stay constant during the next 80 years. This is due to the fact that no debris flows generated at future lakes will travel far beyond P_{10km} and therefore hazard remains the same for downstream areas. P_{25km} is located beyond the reach of modelled debris flow paths. It can be observed that downstream hazard values increase more rapidly for RCP8.5 than for RCP4.5 for the first four points. During the first

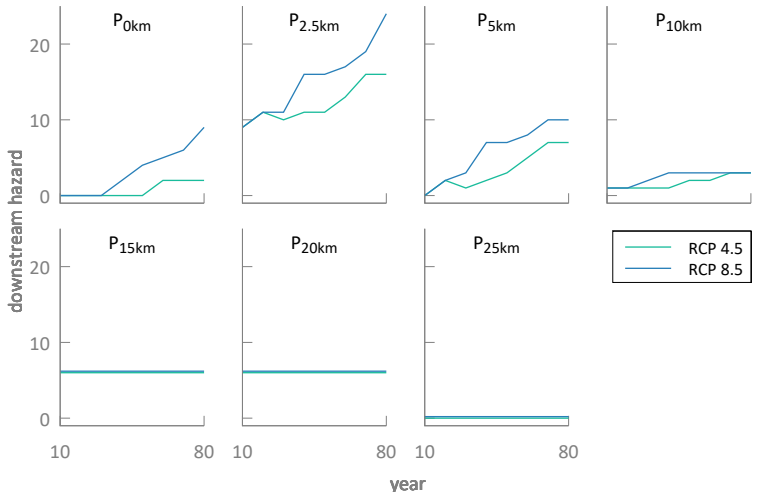

Figure 3.25: Future evolution of the downstream hazard from debris flows for different points along the Bhilangna River for the years 2025-2095 (see fig. 3.24 for point locations). Numbers are dimensionless, calculated as the sum of the overlapping weighted MSF paths. Therefore they give only a relative estimate on the exposure of a site to a potential GLOF compared to other sites.

20 years the evolution is identical for RCP4.5 and RCP8.5 where no changes occur for P_{0km} and P_{10km} and an increase is registered at $P_{2.5km}$ and P_{5km}. Then, after 30 years downstream hazard values start to differ for the two warming scenarios. The decrease in hazard which can be observed in the RCP4.5 curve for $P_{2.5km}$ and P_{5km} between 20 and 30 years can be ascribed to the downgrade of the GLOF hazard posed by the lake 252. This in turn is caused by the watershed calculation which determines a much smaller watershed extent in 30 years than in 20 or 40 years. As the DEM changes for every decade watersheds may change as well. Considering RCP8.5, a remarkable increase in downstream hazard seems to occur between 30 and 40 years for the first three points. This is due to the emergence of a new lake (lake 229), the increased GLOF hazard of two lakes (lake 252 and 342) and the longer runout distance of a debris flow originating at lake 317 now reaching $P_{2.5km}$. After 40 years the downstream hazard for RCP8.5 continues to rise for P_{0km}, $P_{2.5km}$ and P_{5km} although for the latter two at a slower rate. Between 70 and 80 years the RCP8.5 curves of the first two points steepen the primary cause being the emergence of many new lakes. For P_{5km} the hazard stays constant after 70 years and for P_{10km} the value is already constant since four decades. If temperatures of RCP4.5 are considered downstream hazard values are lower for the same point in time than for RCP8.5. A remarkable change in the slope of the RCP4.5 curves for the first three points is situated at 50 years. The reason is the appear-

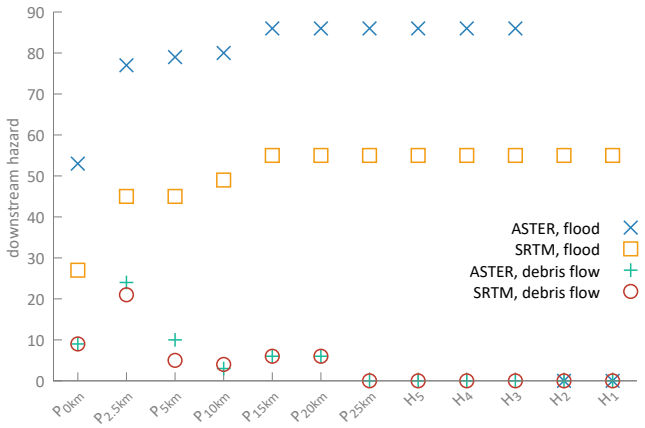

Figure 3.26: Downstream hazard along the Bhilangna River for the scenario RCP8.5 in 80 years (year 2095). Results are shown for different DEMs (ASTER and SRTM) and different mass movement types (flood and debris flow). Numbers are dimensionless, calculated as the sum of the overlapping weighted MSF paths. Therefore they give only a relative estimate on the exposure of a site to a potential GLOF compared to other sites.

ance of a low hazard lake between 50 and 60 years (lake 229). For P_{0km} the hazard stays constant afterwards, for $P_{2.5km}$ and P_{5km} it continues to increase until 70 years. Between 70 and 80 years downstream hazard values for RCP4.5 stay constant for all points. Fig. 3.25 shows further that hazard may vary considerably along the channel of Bhilangna River. $P_{2.5km}$ is the most exposed site to potential debris flows originating from GLOFs. P_{0km} and P_{5km} have a similar value range although downstream hazard emerges later at P_{0km} and if RCP4.5 is considered lower values are found for P_{0km}. P_{10km} appears to be less exposed to debris flows emerging from GLOFs, even less than P_{15km} and P_{20km} located further downstream.

A similar pattern can be seen in fig. 3.26. Here, downstream hazard values of all points and hydropower stations in 80 years are compared for different flood types and different datasets. In the case of a debris flow the results based on the ASTER and on the SRTM DEM show a very similar behaviour with differing values only for $P_{2.5km}$, P_{5km} and P_{10km}. However, the general pattern of ASTER and SRTM results ressembles each other strongly. The site with the heighest downstream hazard for debris flows is $P_{2.5km}$. In contrast the lowest hazard in the upper section can be found at P_{10km} for ASTER as well as for SRTM and for points located at and downstream of P_{25km} no hazard persists that debris flows reach these sites. If a flood is considered instead of a debris flow the situation of downstream hazard changes. Values increase in downstream direction before the flood stops. Even if downstream hazard values differ between ASTER and SRTM which is caused by the higher number of lakes present in

the ASTER dataset the overall pattern still remains very similar. A rapid increase can be observed between P_{0km} and $P_{2.5km}$, than a section follows where values increase less rapidly and at and downstream of P_{15km} downstream hazard remains constant along the Bhilangna River channel. The modelled flood stops earlier for the ASTER dataset somewhere between H_3 and H_2. For SRTM the flood propagates even beyond H_1.

4 Discussion

This thesis applies a remote-sensing and GIS-based approach to evaluate emerging GLOF hazards in the remote Bhilangna Valley, Indian Himalaya. In a first step, past glacier retreat was evaluated in terms of surface elevation change by establishing an automated technique to derive lowering. Over a period of 47 years glaciers in the Bhilangna catchment seem to have thinned between $5m$ and $37m$ depending on elevation with highest rates around $4400m$. The form of the thinning gradient resembles mass balance gradients observed for debris-covered glaciers (Dobhal et al., 2013; Benn and Lehmkuhl, 2000) with an inverted form for the lowest parts. Glaciers in Bhilangna Valley show indeed a debris cover up to $4300 - 4400m$. The mean surface lowering for the whole glacier area over the time period 1968-2015 was estimated to be $0.2m/yr$. Kaab et al. (2012) calculated elevation changes from 2003 to 2008 using two elevation data sets, SRTM and sparse laser measurements from the Ice, Cloud and land Elevation Satellite (ICESat). For Uttarakhand, they obtained a thinning trend of around $0.6m/yr$ which is three times higher than the longer-term mean elevation change rate determined in this thesis. However, in West Nepal which is rather close to the Garhwal Himalaya a mean rate of around $0.3m/yr$ was calculated (Kaab et al., 2012). It has to be considered that the sample size available for this thesis and for the study of Kaab et al. (2012) differs as well as the period analysed. Dobhal et al. (2013) measured thickness changes at different altitude bands for the Chorabari Glacier in the neighbouring Mandakini Valley between 2003-2010 (fig. 4.1). The pattern of elevation decrease seems to be similar to those observed in this thesis (fig. 3.4) with a maximum around $4300m$ to $4400m$ and the lowest values around $5000m$. The thickness loss within an elevation band between $3900m$ and $4000m$ ranged between $18 - 19m$ for the 7-year period (fig. 4.1). When extrapolated to a 10-year period a value of $26 - 27m$ is obtained which is approximately three times higher than the decadal elevation change of $9m$ obtained for these elevation bands in this thesis. However, it should be considered that glacier retreat has significantly increased over the last two decades (see section 2.3 and Kulkarni and Karyakarte (2014)). Therefore, it is not surprising that thinning rates derived in this thesis for a longer time period are considerably lower than those calculated by Dobhal et al. (2013) for 2003-2010.

Based on a careful comparison with other published results it appears that the method developed underestimates actual elevation changes for glaciers. The main reason might be the assumption of a flat glacier surface in areas where elevation changes are derived. In fact, glacier surface in the ablation zone shows a convex topography. Moreover, glaciers flow over irregular terrain and their surface reflects the underlying bed in a smoothed manner (Oerlemans, 2001). Hence, the modelling of a flat surface is problematic for areas where bumps are present at the glacier bed because current glacier surface might then be located above the modelled past flat surface. Although

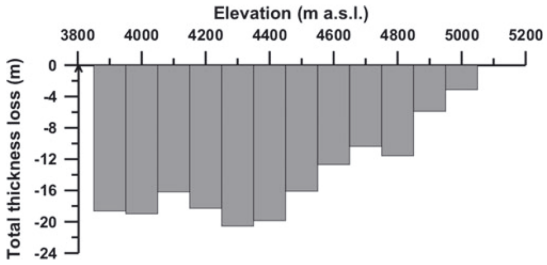

Figure 4.1: Total thickness changes for Chorabari Glacier at different altitude bands. Figure reproduced from Dobhal et al. (2013).

areas where this case occurred were excluded it can be expected that derived elevation changes represent a minimum value. Another source of uncertainty is related to the mapped glacier outlines. The rectification of Corona imagery is a complex procedure and remaining distortions can lead to errors in glacier outline mappings (see section 3.1). In combination with the ASTER GDEM where elevation differences between neighbouring pixels can be considerable large in areas of steep terrain a false position of an outline can have substantial implications on derived elevation changes.

The underestimation of past glacier thinning has consequences for future projections. Less glacier retreat is modelled for future time steps than can be expected and therefore also lakes emerge at a later point in time. This in turn means that future GLOF and downstream hazards are increasing at a slower rate in the model than can be assumed in nature. Resulting implications for hazard management and planning are that the temporal emergence of hazards might be faster than derived by the presented approach requiring a rather early application of potential mitigation measures.

For this reason, DEM differencing data would be preferred if available, as demonstrated in the validation section (section 3.2.2). Additionally, the method to calculate elevation changes can only be applied in the case of valley glaciers and not for ice caps.

The linear thinning gradient derived is rather flat showing a decrease from $0.65m$ for the elevation band $3800 - 3900m$ to $0m$ thinning at $5729m$ and above. The altitude where no elevation change was calculated seems to be reasonable as the ELA position is located at around $5100m$ in the catchment. Fig. 4.2 (Huss and Farinotti, 2012) illustrates that even above the ELA, where mass balances are positive, surface elevations are expected to decrease due to processes such as snow subsidence and glacier flow. The flat gradient calculated could be related to the debris cover on the glaciers which diminishes melting in the lower altitudes and increases it at higher altitudes.

Future glacier evolution was modelled on a decadal scale. An empirical model was established which relates past thinning to past temperature changes and calculates future surface lowering. The approach was based on the model proposed by Linsbauer et al. (2013). In contrast to their model, temperature changes calculated by the CMIP5

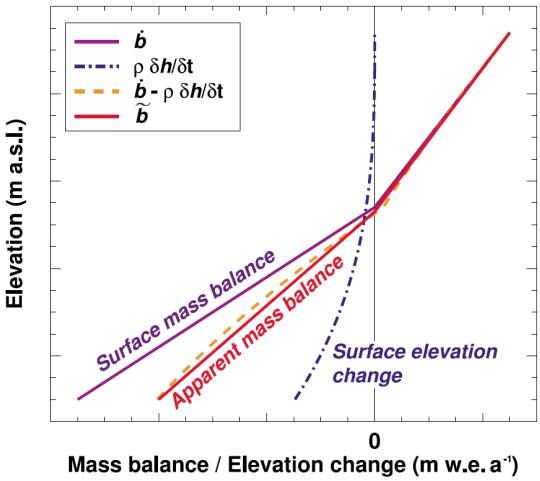

Figure 4.2: Schematic illustration of the altitudinal distribution of surface mass balance, surface elevation change and apparent mass balance (considers ice emergence in the ablation zone). Figure reproduced from Huss and Farinotti (2012).

models for the warming scenarios RCP4.5 and RCP8.5 (IPCC, 2013) could be included directly in the simulation of future glacier states. The model implementation is simple requiring few input data (i.e. past thinning gradient, past temperature change, current ice thicknesses and a DEM). The altitude-mass-balance feedback is considered as well as an increase in thinning with rising temperatures, the latter point being a complement to the model of Linsbauer et al. (2013) where no modification of thinning rates is included. The results suggest a similar glacier thinning for the next 30 years for both warming scenarios and an acceleration for RCP8.5 thereafter. Glacier disintegration starts in 40 years for RCP8.5 for Phating Glacier and in the following decades an increasing number of glaciers appears to produce dead ice bodies which are expected to melt considerably faster than modelled. In 80 years, larger ice bodies are likely to exist only at higher situated areas for Khatling, Sangli and Dudhganga Glacier if a worst case warming scenario is considered. In contrast, if RCP4.5 is applied, where a stabilisation of temperatures is assumed, glacier extent change is comparably small and almost the same as in 30 years.

The modelling of glacier retreat permits to estimate the time of occurrence of future glacier lakes. Potential lake positions are modelled for glaciers around the world but few studies investigate their time of development (Frey et al., 2010; Linsbauer et al., 2016; Nussbaumer et al., 2014). Moreover, a quantitative classification technique of future lakes which are prone to generate a GLOF was not found in other studies. However, modelling the occurrence and the GLOF hazard posed by future lakes offers the possibility to identify locations which might be more important to survey than others.

This is important if limited resources shall be used efficiently (ICIMOD, 2011). Ives et al. (2010) recommend to rank current lakes based on their apparent level of instability to determine sites where field studies are needed. In case of future lakes, the dam stability cannot be evaluated, although it can be assumed that a large number of lakes will form in bedrock depressions and therefore they can be considered to be stable (Frey et al., 2010). Nevertheless, it is widely recognised that mass movements of ice and rock are the most common trigger for GLOFs in the Himalayas (Richardson and Reynolds, 2000). This is the reason why a classification of lakes was completed based on their impact predisposition area (Allen et al., 2016b) and their volume. The results show a considerably different GLOF hazard evolution for RCP4.5 and RCP8.5. The state after 80 years for RCP4.5 is equivalent to the situation after 40 years for RCP8.5. An acceleration in lake development seems to appear beyond 60 years if RCP8.5 is considered. GLOF hazards increase due to volume growth as well as increasing probabilities of mass movements reaching the lakes due to their expansion. Most of the new lakes are classified to pose a low to medium GLOF hazard, although three show a high and one a very high hazard within 80 years for RCP8.5. These results highlight that future human emissions of greenhouse gases, and any mitigation measures, will have a significant influence on the rate of future glacier retreat, and thereby, an influence on related GLOF hazard potential.

Planning of mitigation measures and the allocation of limited resources is dependent on the recognition of a hazard as well as the time frame available within which to plan and apply counter measures. The occurrence of a lake in itself does not necessarily lead to an increased exposure of downstream infrastructure and population. Therefore, modelling of lake development should always be accompanied by flood path simulations if hazard evolution for these sites shall be estimated. Ives et al. (2010) state that both aspects have to be evaluated separately, the hazard of lakes posed from a geophysical point of view and the potential of downstream damage and loss of life in the event of a GLOF. This latter aspect was investigated by running the MSF model (Huggel et al., 2003) for all current and potential future lakes in the Bhilangna catchment. It could be observed that debris flows originating from future lakes will most likely not run further downstream than $\sim 12km$ from the current position of Phating Glacier tongue. The most exposed sites are located between Khatling and Tambakund (see fig. 2.5 for place names). During the first 20 years the downstream hazard evolution is the same for RCP4.5 and RCP8.5, afterwards a faster increase can be observed for RCP8.5. Current or planned hydropower stations are not exposed to debris flows from actual or future lakes, however, in case of floods several could be damaged (between 3 or 5 depending on the DEM that is used for downstream modelling). The impact was not evaluated for villages as these are situated relatively far downstream or at higher positions than the Bhilangna River.

According to these results, inhabited areas and infrastructure in Bhilangna Valley

should not be affected by debris flows originating from potential future glacier lakes. An exception is the pedestrian trek path towards Khatling Glacier which follows the river course at some places. In contrast to debris flows, floods show much larger runout distances and could therefore affect human settlements and roads. A more detailed investigation is needed in this case.

While infrastructure is not affected by debris flows in the Bhilangna Valley, the situation is potentially very different in the neighbouring Mandakini Valley. Here, Kedarnath is located exactly within a zone where modelling results for the Bhilangna Valley suggest a substantial increase in future hazard from debris flows. The pedestrian path towards Khatling Glacier used to see much more visitors but is now rarely used. In contrast, in the neighbouring valley, tourism has considerably increased.

5 Conclusion

Alpine environments are constantly changing and climate warming plays an important role in the evolution of hazards in mountainous regions. The number and extent of glacial lakes is increasing due to current global deglaciation (Gardelle et al., 2013; Wang et al., 2011; Carrivick and Quincey, 2014) and this trend will continue in future. Moreover, rising temperatures are responsible for the observed increase in rockfall activity in the European Alps (Huggel et al., 2012) and a change in frequency of ice avalanches is expected as well(Allen et al., 2016b). These facts indicate that the probability of mass movements entering a glacier lake will increase. On this background, this master thesis evaluated the temporal evolution of changing GLOF hazards for Bhilangna Valley, Indian Himalaya. A sequential approach was applied which determined the time of occurrence of new glacier lakes based on future glacier retreat. The concept of topographic potential could then be used to determine lakes which have a higher susceptibility to mass movement impacts. Finally, downstream impact was evaluated in the event of a GLOF. While uncertainties remain large, this study has provided a useful basis for decision makers to anticipate and prepare for future hazards. In Bhilangna Valley, these findings are of primary concern for the hydro-power industry, while lessons can also be transferred to neighbouring valleys where communities are directly threatened.

In a future study, more factors could be considered such as ice flow, which influences surface elevation change of a glacier, or interactions between water and ice as the contact of a glacier to a lake leads to intensified melt due to convection and calving. Moreover, in terms of scenario definition flood volumes could be included as well because lakes do not necessarily drain completely in case of an outburst flood. At the current stage of model implementation, glacier surface elevation changes were related to past temperature change over a common time period. However, it is known that ice flow, which contributes to surface elevation change, shows a delayed response to climate forcing (Cuffey and Paterson, 2010). Therefore, an investigation of the response time is advised to optimise the coupling of thinning gradients and temperature trends.

The complex interrelation of natural processes requires a multi-level analysis, however, it is de facto impossible to include all variables. Different studies have already made first attempts in simulating related processes such as mass movements entering a lake, subsequent impact wave propagation, dam overtopping and flood propagation (Schneider et al., 2014; Worni et al., 2014). The approach established in this thesis tried to relate future lake formation to glacier retreat. It might be used for a first order assessment of the temporal evolution of future GLOF hazards and is applicable on a regional scale. In case of local or individual event modelling a physically based approach would be preferred.

A multitude of models exist for most of the natural processes but few have been

integrated in a larger ensemble yet. Scientific collaboration and model combinations could open new possibilities and improve our understanding of process interactions, particularly within sensitive high mountain systems.

Bibliography

Allen SK, Rastner P, Arora M, Huggel C, Stoffel M (2016a) Lake outburst and debris flow disaster at Kedarnath, June 2013: Hydrometeorological triggering and topographic predisposition. *Landslides* 13:1479–1491.

Allen SK, Schneider D, Owens IF (2009) First approaches towards modelling glacial hazards in the Mount Cook region of New Zealand's Southern Alps. *Natural Hazards and Earth System Science* 9:481–499.

Allen S, Owens I, Sirguey P (2008) Satellite remote sensing procedures for glacial terrain analyses and hazard assessment in the Aoraki Mount Cook region, New Zealand. *New Zealand Journal of Geology and Geophysics* 51:73–87.

Allen SK, Linsbauer A, Huggel C, Randhawa SS, Schaub Y, Stoffel M (2016b) Current and Future Glacial Lake Outburst Flood Hazard: Application of GIS-Based Modeling in Himachal Pradesh, India In Singh RB, Schickhoff U, Mal S, editors, *Climate Change, Glacier Response, and Vegetation Dynamics in the Himalaya*, pp. 181–203. Springer International Publishing, Cham.

Bahuguna IM, Kulkarni AV, Nayak S, Rathore BP, Negi HS, Mathur P (2007) Himalayan glacier retreat using IRS ICPAN stereo data. *International Journal of Remote Sensing* 28:437–442.

Banerjee A, Shankar R (2013) On the response of Himalayan glaciers to climate change. *Journal of Glaciology* 59:480–490.

Bauder A, Steffen S, Usselmann S, Funk M, Hoelzle M, Huss M, Kappenberger G, Paul F (2014) *The Swiss Glaciers 2007/08 and 2008/09: Glaciological Report (Glacier) No. 129/130.*

Benn DI, Bolch T, Hands K, Gulley J, Luckman A, Nicholson LI, Quincey D, Thompson S, Toumi R, Wiseman S (2012) Response of debris-covered glaciers in the Mount Everest region to recent warming, and implications for outburst flood hazards. *Earth-Science Reviews* 114:156–174.

Benn DI, Evans JA (2010) *Glaciers & Glaciation* Routledge, London, 2 edition.

Benn DI, Lehmkuhl F (2000) Mass balance and equilibrium-line altitudes of glaciers in high-mountain environments pp. 15–29.

Bhambri R, Bolch T (2009) Glacier mapping: a review with special reference to the Indian Himalayas. *Progress in Physical Geography* 33:672–704.

Bhambri R, Bolch T, Chaujar RK (2012) Frontal recession of Gangotri Glacier, Garhwal Himalayas, from 1965 to 2006, measured through high-resolution remote sensing data 102:489–493.

Bhambri R, Bolch T, Chaujar RK, Kulshreshtha SC (2011) Glacier changes in the Garhwal Himalaya, India, from 1968 to 2006 based on remote sensing. *Journal of Glaciology* 57:543–556.

Bhambri R, Mehta M, Dobhal DP, Gupta AK, Pratap B, Kesarwani K, Verma A (2016) Devastation in the Kedarnath (Mandakini) Valley, Garhwal Himalaya, during 16–17 June 2013: A remote sensing and ground-based assessment. *Natural Hazards* 80:1801–1822.

Bhutiyani MR, Kale VS, Pawar NJ (2007) Long-term trends in maximum, minimum and mean annual air temperatures across the Northwestern Himalaya during the twentieth century. *Climatic Change* 85:159–177.

Bolch T, Buchroithner M, Pieczonka T, Kunert A (2008) Planimetric and volumetric glacier changes in the Khumbu Himal, Nepal, since 1962 using Corona, Landsat TM and ASTER data. *Journal of Glaciology* 54:592–600.

Bolch T, Kulkarni A, Kaab A, Huggel C, Paul F, Cogley JG, Frey H, Kargel JS, Fujita K, Scheel M, Bajracharya S, Stoffel M (2012) The state and fate of Himalayan glaciers. *Science* 336:310–314.

Bookhagen B, Burbank DW (2010) Toward a complete Himalayan hydrological budget: Spatiotemporal distribution of snowmelt and rainfall and their impact on river discharge. *Journal of Geophysical Research* 115:39.

Buechler S, Sen D, Khandekar N, Scott C (2016) Re-Linking Governance of Energy with Livelihoods and Irrigation in Uttarakhand, India. *Water* 8:1–22.

Carrivick JL (2010) Dam break – Outburst flood propagation and transient hydraulics: A geosciences perspective. *Journal of Hydrology* 380:338–355.

Carrivick JL, Quincey DJ (2014) Progressive increase in number and volume of ice-marginal lakes on the western margin of the Greenland Ice Sheet. *Global and Planetary Change* 116:156–163.

Carrivick JL, Tweed FS (2016) A global assessment of the societal impacts of glacier outburst floods. *Global and Planetary Change* 144:1–16.

Census Organisation of India (2011) Ghansali Population - Tehri Garhwal, Uttarakhand `http://www.census2011.co.in/data/village/42916-ghansali-uttarakhand.html` (accessed: 02.03.2017).

Christen M, Kowalski J, Bartelt P (2010) RAMMS: Numerical simulation of dense snow avalanches in three-dimensional terrain. *Cold Regions Science and Technology* 63:1–14.

Clague JJ, Mathews WH (1973) The Magnitude of Jökulhlaups. *Journal of Glaciology* 12:501–504.

Clarke G (1982) Glacier Outburst Floods From "Hazard Lake", Yukon Territory, and the Problem of Flood Magnitude Prediction. *Journal of Glaciology* 28:3–21.

Cuffey KM, Paterson W (2010) *The Physics of Glaciers* Butterworth-Heinemann, Amsterdam and Boston and Heidelberg, fourth edition.

Cui P, Zhou GG, Zhu XH, Zhang JQ (2013) Scale amplification of natural debris flows caused by cascading landslide dam failures. *Geomorphology* 182:173–189.

Diaz HF, Bradley RS (1997) Temperature variations during the last century at high elevation sites. *Climatic Change* 36:253–279.

Directorate of Census Operations Uttarakhand (2011) District Census Handbook: Tehri Garhwal `http://www.censusindia.gov.in/2011census/dchb/DCHB.html` (accessed: 08.04.2017).

Dobhal DP, Gergan JT, Thayyen RJ (2008) Mass balance studies of the Dokriani Glacier from to 1992 to 2000, Garhwal Himalaya, India. *Bulletin of Glaciological Research* 25:9–17.

Dobhal DP, Gupta AK, Mehta M, Khandelwal DD (2013) Kedarnath disaster: facts and plausible causes. *Current Science* pp. 171–174.

Dobhal DP, Mehta M, Srivastava D (2013) Influence of debris cover on terminus retreat and mass changes of Chorabari Glacier, Garhwal region, central Himalaya, India. *Journal of Glaciology* 59:961–971.

Earth Remote Sensing Data Analysis Center (2011) *ASTER GDEM 2 README*.

Easterling DR, Horton B, Jones PD, Peterson TC, Karl TR, Parker DE, Salinger MJ, Razuvayev V, Plummer N, Jamason P, et al (1997) Maximum and Minimum Temperature Trends for the Globe. *Science* 277:364–367.

Fan JC, Liu CH, Wu MF, Yu SK (2003) Determination of critical rainfall threshold for debris-flow occurrence in central Taiwan and their revision after the 1999 Chi-Chi great earthquake In Rickenmann D, Chen CL, editors, *Debris-Flow Hazards Mitigation: Mechanics, Prediction and Asssessment*, pp. 103–114, Rotterdam. Millpress.

Fell R (1994) Landslide risk assessment and acceptable risk. *Canadian Geotechnical Journal* 31:261–272.

Folland CK, Rayner NA, Brown SJ, Smith TM, Shen SSP, Parker DE, Macadam I, Jones PD, Jones RN, Nicholls N, Sexton DMH (2001) Global temperature change and its uncertainties since 1861. *Geophysical Research Letters* 28:2621–2624.

Fowler HJ, Archer DR (2006) Conflicting Signals of Climatic Change in the Upper Indus Basin. *Journal of Climate* 19:4276–4293.

Frey H, Haeberli W, Linsbauer A, Huggel C, Paul F (2010) A multi-level strategy for anticipating future glacier lake formation and associated hazard potentials. *Natural Hazards and Earth System Science* 10:339–352.

Frey H, Machguth H, Huss M, Huggel C, Bajracharya S, Bolch T, Kulkarni A, Linsbauer A, Salzmann N, Stoffel M (2014) Estimating the volume of glaciers in the Himalayan-Karakoram region using different methods. *The Cryosphere* 8:2313–2333.

Fujita K (2008) Influence of precipitation seasonality on glacier mass balance and its sensitivity to climate change. *Annals of Glaciology* 48:88–92.

Fujita K, Ageta Y (2000) Effect of summer accumulation on glacier mass balance on the Tibetan Plateau revealed by mass-balance model. *Journal of Glaciology* 46:244–252.

Fujita K, Sakai A, Takenaka S, Nuimura T, Surazakov AB, Sawagaki T, Yamanokuchi T (2013) Potential flood volume of Himalayan glacial lakes. *Natural Hazards and Earth System Science* 13:1827–1839.

Gardelle J, Berthier E, Arnaud Y, Kääb A (2013) Region-wide glacier mass balances over the Pamir-Karakoram-Himalaya during 1999-2011. *The Cryosphere* 7:1263–1286.

Glen JW (1955) The Creep of Polycrystalline Ice. *Proceedings of the Royal Society A: Mathematical, Physical and Engineering Sciences* 228:519–538.

Gruber S, Hoelzle M, Haeberli W (2004) Permafrost thaw and destabilization of Alpine rock walls in the hot summer of 2003 pp. 1–4.

Guha-Sapir D, Below R, Hoyois P (2016) EM-DAT: International Disaster Database `http://www.emdat.be/country_profile/index.html` (accessed: 12.04.2017).

Guhathakurta P, Rajeevan M (2008) Trends in the rainfall pattern over India. *International Journal of Climatology* 28:1453–1469.

Haeberli W, Alean JC, Müller P, Funk M (1989) Assessing Risks from Glacier Hazards in High Mountain Regions: Some Experiences in the Swiss Alps. *Annals of Glaciology* 13:96–102.

Haeberli W, Clague JJ, Kaeaeb A, Huggel C (2010) Hazards from lakes in high-mountain glacier and permafrost regions: climate change effects and process interactions. *Avances de la Geomorphología en Españ̃a* pp. 439–446.

Haeberli W, Hoelzle M (1995) Application of inventory data for estimating characteristics of and regional climate-change effects on mountain glaciers: a pilot study with the European Alps. *Annals of Glaciology* 21:206–212.

Haeberli W, Wegmann M, Vonder Muhll D (1997) Slope stability problems related to glacier shrinkage and permafrost degradation in the Alps. *Eclogae Geologicae Helvetiae* 90:407–414.

Haeberli W, Whiteman C, editors (2015) *Snow and Ice-Related Hazards, Risks and Disasters* Elsevier.

Haeberli W, Zemp M, Frauenfelder R, Hoelzle M, Kaeaeb A (2003) Fluctuations of Glacier 1995–2000 (Vol VIII). *International Commission on Snow and Ice of the International Association of the Hydrological Sciences* .

Haeberli W (1983) Frequency and Characteristics of Glacier Floods in the Swiss Alps. *Annals of Glaciology* 4:85–90.

Harris C, Arenson LU, Christiansen HH, Etzelmüller B, Frauenfelder R, Gruber S, Haeberli W, Hauck C, Hölzle M, Humlum O, Isaksen K, Kääb A, Kern-Lütschg MA, Lehning M, Matsuoka N, Murton JB, Nötzli J, Phillips M, Ross N, Seppälä M, Springman SM, Vonder Mühll D (2009) Permafrost and climate in Europe: Monitoring and modelling thermal, geomorphological and geotechnical responses. *Earth-Science Reviews* 92:117–171.

Harris C, Davies MC, Etzelmuller B (2001) The assessment of potential geotechnical hazards associated with mountain permafrost in a warming global climate. *Permafrost and Periglacial Processes* 12:145–156.

Heim A (1932) Bergsturz und Menschenleben. *Beiblatt zur Vierteljahrsschrift der Naturforschenden Gesellschaft in Zürich.* 77.

Heinimann HR, Hollenstein K, Kienholz H, Krummenacher B, Mani P (1998) *Methoden zur Analyse und Bewertung von Naturgefahren* Bundesamt für Umwelt, Wald und Landschaft (BUWAL), Bern.

Hewitt K (2005) The Karakoram Anomaly? Glacier Expansion and the 'Elevation Effect,' Karakoram Himalaya. *Mountain Research and Development* 25:332–340.

Hewitt K (2007) Tributary glacier surges: an exceptional concentration at Panmah Glacier, Karakoram Himalaya. *Journal of Glaciology* 53:181–188.

Hoelzle M, Haeberli W, Dischl M, Peschke W (2003) Secular glacier mass balances derived from cumulative glacier length changes. *Global and Planetary Change* 36:295–306.

Hoelzle M, Paul F, Gruber S, Frauenfelder R (2005) Glacier and permafrost in mountain areas: different modelling approaches, projecting global change impact and sustainable land use and natural resource management in mountain biosphere reserves (GLOCHAMORE). *Global Change Impacts in Mountain Biosphere Reserves* pp. 28–39.

Huber E (1985) Garhwal-Himalaya-West (Map 1:150,000) Schweizerischen Stifung fur alpine Forschungen.

Huggel C (2004) Assessment of Glacial Hazards based on Remote Sensing and GIS Modeling Dissertation, Universität Zürich, Zürich.

Huggel C, Allen S, Deline P, Fischer L, Noetzli J, Ravanel L (2012) Ice thawing, mountains falling-are alpine rock slope failures increasing? *Geology Today* 28:98–104.

Huggel C, Haeberli W, Kääb A, Bieri D, Richardson S (2004b) An assessment procedure for glacial hazards in the Swiss Alps. *Canadian Geotechnical Journal* 41:1068–1083.

Huggel C, Kaeaeb A, Haeberli W, Krummenacher B (2003) Regional-scale GIS-models for assessment of hazards from glacier lake outbursts: evaluation and application in the Swiss Alps. *Natural Hazards and Earth System Sciences* 3:647–662.

Huggel C, Kääb A, Haeberli W, Teysseire P, Paul F (2002) Remote sensing based assessment of hazards from glacier lake outbursts: A case study in the Swiss Alps. *Canadian Geotechnical Journal* 39:316–330.

Huggel C, Kääb A, Salzmann N (2004a) GIS–based modeling of glacial hazards and their interactions using Landsat–TM and IKONOS imagery. *Norsk Geografisk Tidsskrift - Norwegian Journal of Geography* 58:61–73.

Hungr O (1997) Some methods of landslide hazard intensity mapping In Cruden DM, Fell R, editors, *Landslide Risk Assessment*, pp. 215–226. Balkema, Rotterdam.

Huss M, Farinotti D (2012) Distributed ice thickness and volume of all glaciers around the globe. *Journal of Geophysical Research: Earth Surface* 117:1–10.

ICIMOD (2011) *Glacial Lakes and Glacial Lake Outburst Floods in Nepal* International Centre for Integrated Mountain Development, Kathmandu.

Immerzeel WW, Petersen L, Ragettli S, Pellicciotti F (2014) The importance of observed gradients of air temperature and precipitation for modeling runoff from a glacierized watershed in the Nepalese Himalayas. *Water Resources Research* 50:2212–2226.

IPCC (2007) *Climate Change 2007: Climate Change Impacts, Adaptation and Vulnerability. Working Group II Contribution to the Intergovernmental Panel on Climate Change—Fourth Assessment Report Summary for Policymakers* Cambridge University Press, New York.

IPCC (2012) *Managing the Risks of Extreme Events and Disasters to Advance Climate Change Adaptation: A Special Report of Working Groups I and II of the Intergovernmental Panel on Climate Change* Cambridge University Press, New York.

IPCC (2013) *Climate Change 2013: The Physical Science Basis. Contribution of Working Group I to the Fifth Assessment Report of the Intergovernmental Panel on Climate Change* Cambridge University Press, Cambridge, United Kingdom and New York, NY, USA.

IPCC (2017) History `https://www.ipcc.ch/organization/organization_history.shtml` (accessed: 18.04.2017).

Iverson RM, Reid ME, Logan M, LaHusen RG, Godt JW, Griswold JP (2010) Positive feedback and momentum growth during debris-flow entrainment of wet bed sediment. *Nature Geoscience* 4:116–121.

Ives JD, Shrestha RB, Mool PK (2010) *Formation of Glacial Lakes in the Hindu Kush-Himalayas and GLOF Risk Assessment* International Centre for Integrated Mountain Development, Kathmandu.

Jakob M, Hungr O (2005) *Debris-flow hazards and related phenomena* Springer, Berlin and New York.

Kaab A (2000) Photogrammetry for early recognition of high mountain hazards: New techniques and applications. *Physics and Chemistry of the Earth, Part B: Hydrology, Oceans and Atmosphere* 25:765–770.

Kääb A, Huggel C, Fischer L, Guex S, Paul F, Roer I, Salzmann N, Schlaefli S, Schmutz K, Schneider D, Strozzi T, Weidmann Y (2005) Remote sensing of glacier- and permafrost-related hazards in high mountains: An overview. *Natural Hazards and Earth System Science* 5:527–554.

Kaab A, Berthier E, Nuth C, Gardelle J, Arnaud Y (2012) Contrasting patterns of early twenty-first-century glacier mass change in the Himalayas. *Nature* 488:495–498.

Kargel JS, Abrams MJ, Bishop MP, Bush A, Hamilton G, Jiskoot H, Kaab A, Kieffer HH, Lee EM, Paul F, Rau F, Raup B, Shroder JF, Soltesz D, Stainforth D, Stearns L, Wessels R (2005) Multispectral imaging contributions to global land ice measurements from space. *Remote Sensing of Environment* 99:187–219.

Kattel DB, Yao T (2013) Recent temperature trends at mountain stations on the southern slope of the central Himalayas. *Journal of Earth System Science* 122:215–227.

Kershaw JA, Clague JJ, Evans SG (2005) Geomorphic and sedimentological signature of a two-phase outburst flood from moraine-dammed Queen Bess Lake, British Columbia, Canada. *Earth Surface Processes and Landforms* 30:1–25.

Klok EJ, Oerlemans J (2003) Deriving historical equilibrium-line altitudes from a glacier length record by linear inverse modelling. *Holocene* 13:343–351.

Korup O, Tweed F (2007) Ice, moraine, and landslide dams in mountainous terrain. *Quaternary Science Reviews* 26:3406–3422.

Kothawale DR, Rupa Kumar K (2005) On the recent changes in surface temperature trends over India. *Geophysical Research Letters* 32:1–4.

Kuhn M (1981) Climate and glaciers: Symposium at Canberra -Sea Level, Ice, and Climatic Change. *IAHS Publ.* 131:3–20.

Kulkarni A, Karyakarte Y (2014) Observed changes in Himalayan glaciers. *Current Science* 106:237–244.

Kulkarni AV, Bahuguna IM, Rathore BP, Singh SK, Randhawa SS, Sood RK, Dhar S (2007) Glacial retreat in Himalaya using Indian Remote Sensing satellite data. *Current Science* 92:69–74.

Leclercq PW, Oerlemans J, Cogley JG (2011) Estimating the Glacier Contribution to Sea-Level Rise for the Period 1800-2005. *Surveys in Geophysics* 32:519–535.

Leroi E (1996) Landslide hazard - risk maps at different scales: objectives, tools and developments In Senneset K, editor, *Proceedings of the 7th International Symposium on Landslides*, Rotterdam. Balkema.

Linsbauer A, Frey H, Haeberli W, Machguth H, Azam MF, Allen S (2016) Modelling glacier-bed overdeepenings and possible future lakes for the glaciers in the Himalaya-Karakoram region. *Annals of Glaciology* 57:119–130.

Linsbauer A, Paul F, Haeberli W (2012) Modeling glacier thickness distribution and bed topography over entire mountain ranges with GlabTop: Application of a fast and robust approach. *Journal of Geophysical Research: Earth Surface* 117:1–17.

Linsbauer A, Paul F, Machguth H, Haeberli W (2013) Comparing three different methods to model scenarios of future glacier change in the Swiss Alps. *Annals of Glaciology* 54:241–253.

Liu X, Lei J (2003) A method for assessing regional debris flow risk: An application in Zhaotong of Yunnan province (SW China). *Geomorphology* 52:181–191.

Luethi MP, Bauder A, Funk M (2010) Volume change reconstruction of Swiss glaciers from length change data. *Journal of Geophysical Research - Earth Surface* 115:1–8.

Machguth H, Paul F, Kotlarski S, Hoelzle M (2009) Calculating distributed glacier mass balance for the Swiss Alps from regional climate model output: A methodical description and interpretation of the results. *Journal of Geophysical Research* 114:1–19.

Martha TR, Roy P, Govindharaj KB, Kumar KV, Diwakar PG, Dadhwal VK (2015) Landslides triggered by the June 2013 extreme rainfall event in parts of Uttarakhand state, India. *Landslides* 12:135–146.

Mathison C, Wiltshire A, Dimri AP, Falloon P, Jacob D, Kumar P, Moors E, Ridley J, Siderius, C. Stoffel, M., Yasunari T (2013) Regional projections of North Indian climate for adaptation studies. *Science of the Total Environment* 468-469:4–17.

Matsuoka N, Sakai H (1999) Rockfall activity from an alpine cliff during thawing periods. *Geomorphology* 28:309–328.

McCoy RB (2017) CMIP5 - Coupled Model Intercomparison Project Phase 5 - Overview `http://cmip-pcmdi.llnl.gov/cmip5/` (accessed: 15.04.2017).

MicroImages (2009) ASTER Global Elevation Data `http://www.microimages.com/documentation/TechGuides/75asterDEM.pdf` (accessed: 14.04.2017).

Nielsen LE (1955) REGIMEN AND FLOW OF ICE IN EQUILIBRIUM GLACIERS. *Geological Society of America Bulletin* 66:1–8.

Noetzli J, Gruber S (2009) Transient thermal effects in Alpine permafrost. *The Cryosphere* 3:85–99.

Noetzli J, Huggel C, Hoelzle M, Haeberli W (2006) GIS-based modelling of rock-ice avalanches from Alpine permafrost areas. *Computational Geosciences* 10:161–178.

Nussbaumer S, Schaub Y, Huggel C, Walz A (2014) Risk estimation for future glacier lake outburst floods based on local land-use changes. *Natural Hazards and Earth System Science* 14:1611–1624.

O'Callaghan JF, Mark DM (1984) The extraction of drainage networks from digital elevation data. *Computer Vision Graphics and Image Proceedings* 28:323–344.

O'Connor JE, Costa JE (1993) Geologic and hydrologic hazards in glacierized basins in North America resulting from 19th and 20th century global warming. *Natural Hazards* 8:121–140.

Oerlemans J (2001) *Glaciers and Climate Change* Balkema, Lisse.

Oerlemans J (2007) Estimating response times of Vadret da Morteratsch, Vadret da Palü, Briksdalsbreen and Nigardsbreen from their length records. *Journal of Glaciology* 53:357–362.

Oerlemans J, Dyurgerov M, de van Wal RSW (2007) Reconstructing the glacier contribution to sea-level rise back to 1850. *Cryosphere* 1:59–65.

Office of the Registrar General & Census Commissioner India (2011) District Census HandBook - Uttrakhand: Tehri Garhwal `http://www.censusindia.gov.in/2011census/dchb/Uttarakhand_tables.html` (accessed: 08.04.2017).

Ohmura A (2001) Physical Basis for the Temperature-Based Melt-Index Method. *Journal of Applied Meteorology* 40:753–761.

Paul F, Maisch M, Rothenbühler C, Hoelzle M, Haeberli W (2007) Calculation and visualisation of future glacier extent in the Swiss Alps by means of hypsographic modelling. *Global and Planetary Change* 55:343–357.

Paul F, Linsbauer A (2012) Modeling of glacier bed topography from glacier outlines, central branch lines, and a DEM. *International Journal of Geographical Information Science* 26:1173–1190.

Pelto MS, Hedlund C (2001) Terminus behavior and response time of North Cascade glaciers, Washington, USA. *Journal of Glaciology* 47:497–506.

Pierson TC, Costa JE (1987) A rheologic classification of subaerial sediment-water flows In *Debris Flows/Avalanches: Process, Recognition, and Mitigation*, Vol. 7 of *Reviews in Engineering Geology*, pp. 1–12. Geological Society of America.

Raetzo H, Lateltin O, Bollinger D, Tripet J (2002) Hazard assessment in Switzerland - Codes of Practice for mass movements. *Bulletin of Engineering Geology and the Environment* 61:263–268.

Ragozin AL (1994) Basic principles of natural hazard risk assessment and management In *Proceedings 7th International Congress International Association of Engineering Geology*, Vol. 3, Rotterdam. Balkema.

Rangwala I, Miller JR (2012) Climate change in mountains: A review of elevation-dependent warming and its possible causes. *Climatic Change* 114:527–547.

Rao PN, Pati UC (1980) Geology and tectonics of Bhilangana Valley and its adjoining parts, Garhwal Himalaya, with special reference to the Main Central Thrust. *Journal of Himalayan Geology* 10:220–233.

Rastner P, Joerg PC, Huss M, Zemp M (2016) Historical analysis and visualization of the retreat of Findelengletscher, Switzerland, 1859–2010. *Global and Planetary Change* 145:67–77.

Richardson SD, Reynolds JM (2000) An overview of glacial hazards in the Himalayas. *Quaternary International* 65-6:31–47.

Rickenmann D (1991) Hyperconcentrated Flow and Sediment Transport at Steep Slopes. *Journal of Hydraulic Engineering* 117:1419–1439.

Rickenmann D, Zimmermann M (1993) The 1987 debris flows in Switzerland: documentation and analysis. *Geomorphology* 8:175–189.

Rimac A, van Geffen S, Oerlemans J (2017) Numerical simulations of glacier evolution performed using flow-line models of varying complexity. *Geoscientific Model Development Discussions* pp. 1–26.

Röthlisberger H (1987) Sliding phenomena in a steep section of Balmhorngletscher, Switzerland. *Journal of Geophysical Research* 92:8999–9014.

Rounce DR, McKinney DC, Lala JM, Byers AC, Watson CS (2016) A new remote hazard and risk assessment framework for glacial lakes in the Nepal Himalaya. *Hydrology and Earth System Sciences* 20:3455–3475.

Salm B, Burkard A, Gubler H (1990) *Berechnung von Fliesslawinen: eine Anleitung für Praktiker mit Beispielen*, Vol. 47 of *Mitteilungen des Eidgenossischen Institutes fur Schnee- und Lawinenforschung* Eidgenossische Institut fur Schnee- und Lawinenforschung.

Schaub Y (2015) Outburst floods from high-mountain lakes: risk analysis of cascading processes under present and future conditions Dissertation, Universität Zürich, Zürich.

Schaub Y, Huggel C, Cochachin A (2015) Ice-avalanche scenario elaboration and uncertainty propagation in numerical simulation of rock-/ice-avalanche-induced impact waves at Mount Hualcán and Lake 513, Peru. *Landslides* 13:1445–1459.

Scherler D, Bookhagen B, Strecker MR (2011) Spatially variable response of Himalayan glaciers to climate change affected by debris cover. *Nature Geoscience* 4:156–159.

Schild A (2008) ICIMOD's Position on Climate Change and Mountain Systems. *Mountain Research and Development* 28:328–331.

Schneider D (2011) On Characteristics and Flow Dynamics of Large Rapid Mass Movements in Glacial Environments Dissertation, Universität Zürich, Zürich.

Schneider D, Huggel C, Cochachin A, Guillén S, García J (2014) Mapping hazards from glacier lake outburst floods based on modelling of process cascades at Lake 513, Carhuaz, Peru. *Advances in Geosciences* 35:145–155.

Schwanghart W, Worni R, Huggel C, Stoffel M, Korup O (2016) Uncertainty in the Himalayan energy–water nexus: Estimating regional exposure to glacial lake outburst floods. *Environmental Research Letters* 11:074005.

Seyfferth G (2006) Die Berge des Himalaya `http://www.himalaya-info.org/Gesamtuebersicht.htm` (accessed: 28.03.2017).

Shekhar MS, Chand H, Kumar S, Srinivasan K, Ganju A (2010) Climate-change studies in the western Himalaya. *Annals of Glaciology* 51:105–112.

Singh D, Horton DE, Tsiang Mea (2014) Severe precipitation in Northern India in June 2013: Causes, historical context, and changes in probability: Explaining extreme events of 2013 from a climate perspective. *Bulletin of the American Meteorological Society* 95:58–61.

Singh O, Arya P, Chaudhary BS (2013) On rising temperature trends at Dehradun in Doon valley of Uttarakhand, India. *Journal of Earth System Science* 122:613–622.

Singh S, Kumar R, Bhardwaj A, Sam L, Shekhar M, Singh A, Kumar R, Gupta A (2016) Changing climate and glacio-hydrology in Indian Himalayan Region: a review. *WIREs Clim Change* 7:393–410.

Singh VP, Singh P, Haritashya UK, editors (2011) *Encyclopedia of Snow, Ice and Glaciers* Encyclopedia of Earth Sciences Series. Springer Science+Business Media B.V, Dordrecht.

Snehmani, Bhardwaj A, Singh MK, Gupta RD, Joshi PK, Ganju A (2015) Modelling the hypsometric seasonal snow cover using meteorological parameters. *Journal of Spatial Science* 60:51–64.

Softusvista Inc. (2017) Compare Rocks `www.comparerocks.com` (accessed: 05.03.2017).

Stoffel M, Huggel C (2012) Effects of climate change on mass movements in mountain environments. *Progress in Physical Geography* 36:421–439.

Swiss Re (2014) *Natur- und Man-made- Katastrophen 2013: Massive Schäden aus Überschwemmungen und Hagelstürmen; Haiyan verwüstet die Philippinen* Number 01 in sigma.

Swissair Photo AG (1964) Findelgletscher, Rimpfischhorn `http://ba.e-pics.ethz.ch/#1489141919543_49` (accessed: 10.03.2017).

Swisstopo (2015) SWISSIMAGE `https://map.geo.admin.ch` (accessed: 19.03.2017).

Takahashi T (2014) *Debris Flow: Mechanics, Prediction and Countermeasures* CRC Press, Leiden.

Tangari AK, Chandra R, Yadav S (2004) Temporal monitoring of the snout, equilibrium line and ablation zone of Gangotri glacier through remote sensing and GIS techniques – an attempt at deciphering the climatic variability. *Geological Survey of India* 80:145–153.

Thadani R, Singh V, Chauhan DS, Dwivedi V, Pandey A (2015) *Climate Change in Uttarakhand* Bishen Singh Mahendra Pal Singh, Dehradun.

Tweed FS, Russell AJ (1999) Controls on the formation and sudden drainage of glacier-impounded lakes: Implications for jokulhlaup characteristics. *Progress in Physical Geography* 23:79–110.

USGS (2015) Declassified Satellite Imagery - 1 `https://lta.cr.usgs.gov/declass_1` (accessed: 14.04.2017).

Vaidya R (2012) Water and Hydropower in the Green Economy and Sustainable Development of the Hindu Kush-Himalayan Region. *Hydro Nepal: Journal of Water, Energy and Environment* 10:11–19.

Villageprofile (2017) Ghansali Population `http://www.villageprofile.in/uttarakhand/tehri-garhwal/ghansali` (accessed: 07.04.2017).

Viviroli D, Dürr HH, Messerli B, Meybeck M, Weingartner R (2007) Mountains of the world, water towers for humanity: Typology, mapping, and global significance. *Water Resources Research* 43:1–13.

Vohra CP (1980) Some problems of glacier inventory in the Himalayas. *IAHS Publ.* 126:67–74.

Walder JS, Costa JE (1996) Outburst floods from glacier-dammed lakes: the effect of mode of lake drainage on flood magnitude. *Earth Surface Processes and Landforms* 21:701–723.

Wang W, Yao T, Yang X (2011) Variations of glacial lakes and glaciers in the Boshula mountain range, southeast Tibet, from the 1970s to 2009. *Annals of Glaciology* 52:9–17.

Watanabe T, Lamsal D, Ives JD (2009) Evaluating the growth characteristics of a glacial lake and its degree of danger of outburst flooding: Imja Glacier, Khumbu Himal, Nepal. *Norsk Geografisk Tidsskrift - Norwegian Journal of Geography* 63:255–267.

Wessels RL, Kargel JS, Kieffer HH (2002) ASTER measurement of supraglacial lakes in the Mount Everest region of the Himalaya. *Annals of Glaciology* 34:399–408.

Wieczorek GF, editor (2000) *Debris-flow hazards mitigation: mechanics, prediction and assessment: Proceedings of the Second International Conference on Debris-Flow Hazards Mitigation, Taipei, Taiwan, 16 - 18 August 2000* Balkema, Rotterdam.

Wikipedia (2016) Jenks-Caspall-Algorithmus `https://de.wikipedia.org/wiki/Jenks-Caspall-Algorithmus` (accessed: 14.03.2017).

Worni R, Huggel C, Stoffel M, Pulgarín B (2012) Challenges of modeling current very large lahars at Nevado del Huila Volcano, Colombia. *Bulletin of Volcanology* 74:309–324.

Worni R, Huggel C, Clague JJ, Schaub Y, Stoffel M (2014) Coupling glacial lake impact, dam breach, and flood processes: A modeling perspective. *Geomorphology* 224:161–176.

Xu J, Grumbine RE (2014) Building ecosystem resilience for climate change adaptation in the Asian highlands. *Wiley Interdisciplinary Reviews: Climate Change* 5:709–718.

Yang S, Zhang Z, Kousky VE, Higgins RW, Yoo SH, Liang J, Fan Y (2008) Simulations and Seasonal Prediction of the Asian Summer Monsoon in the NCEP Climate Forecast System. *Journal of Climate* 21:3755–3775.

Zekollari H, Fürst JJ, Huybrechts P (2014) Modelling the evolution of Vadret da Morteratsch, Switzerland, since the Little Ice Age and into the future. *Journal of Glaciology* 60:1155–1168.

Appendix

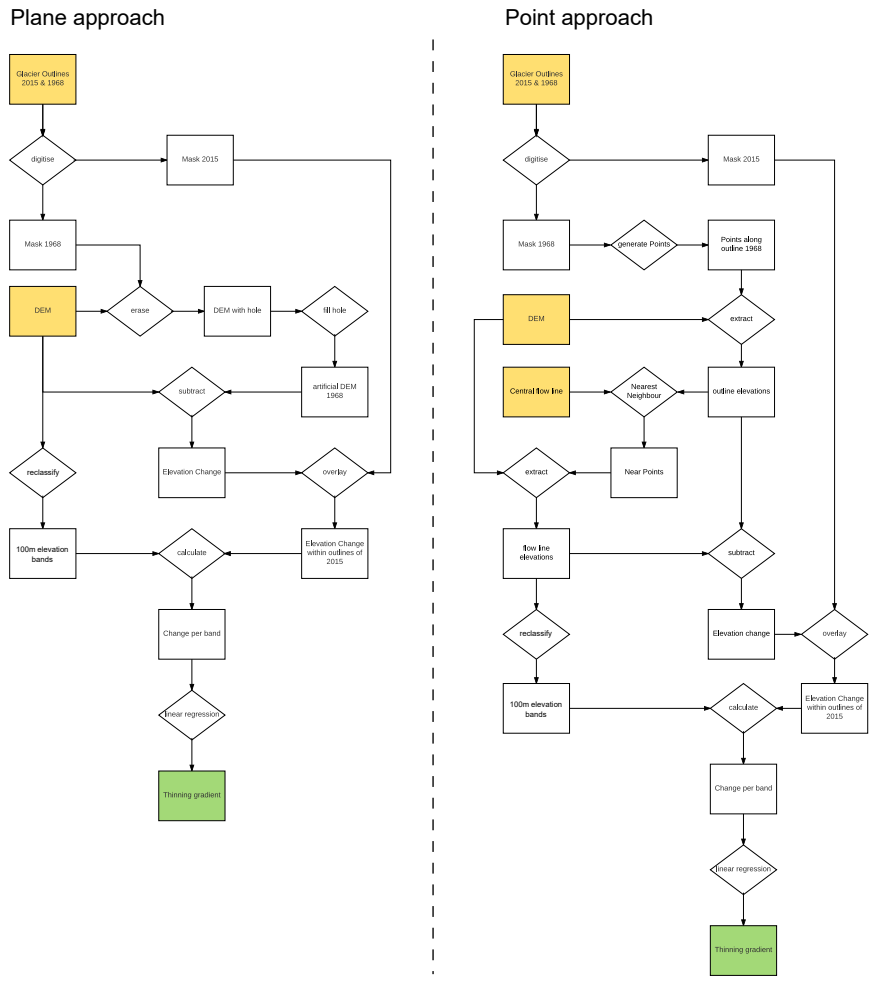

Figure 5.1: Sketch of the plane and point approach to derive the elevation-dependent thinning gradient. External input data (yellow), outputs which are reused in a following part (green), objects (boxes) and processes (diamonds).

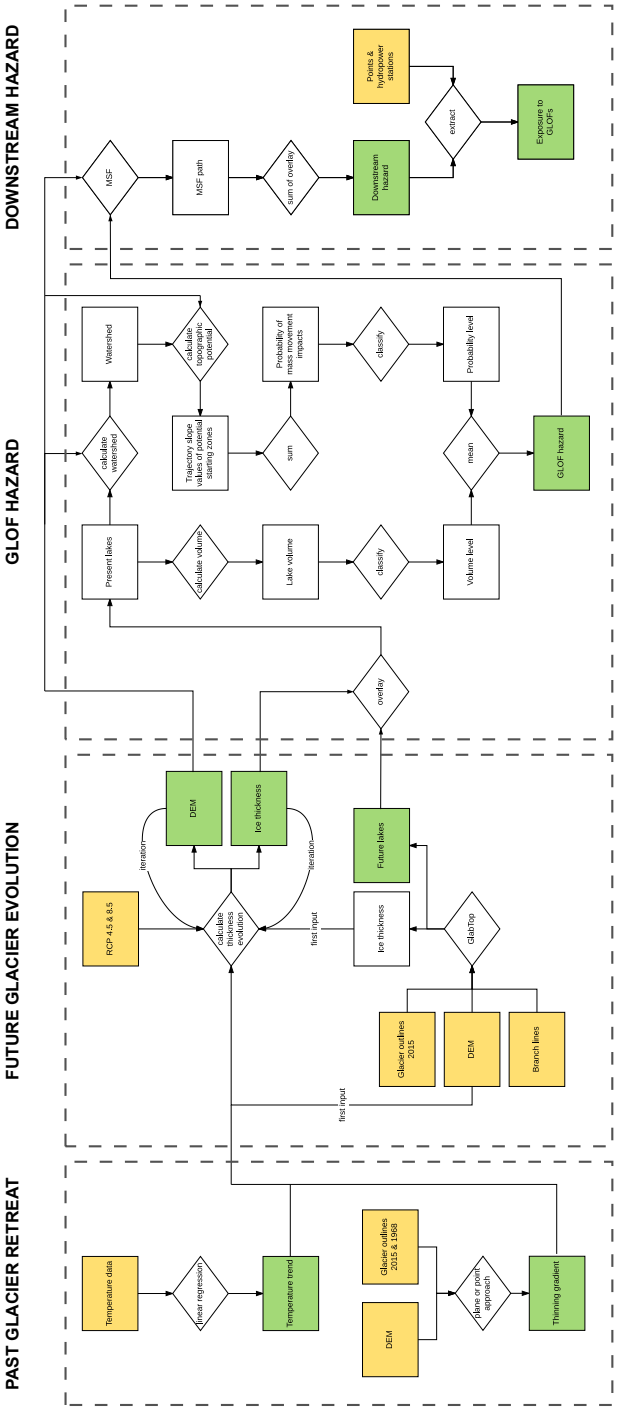

Figure 5.2: Sketch of the workflow: Within the first part (past glacier retreat) a temperature trend and an elevation-dependent thinning gradient is derived for the past which are input to the future glacier evolution model (second part). Modelled future lakes, glacier extents and DEMs are used to determine the future GLOF hazard within the third part. The last part (downstream hazard) includes debris flow and flood path modelling based on the GLOF hazard determined in part three. External input data (yellow), outputs which are reused in a following part (green), objects (boxes) and processes (diamonds).

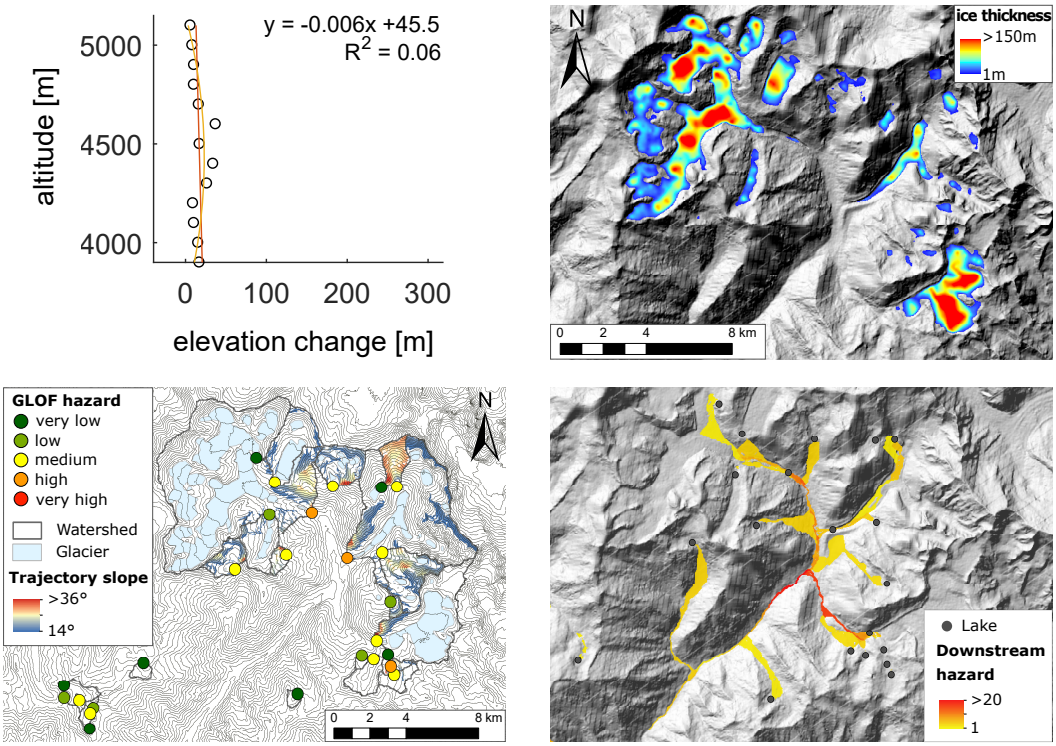

Figure 5.3: Thinning gradient (top left) based on the SRTM which was used for future glacier modelling (top right). Hazard classification (bottom left) and MSF path modelling (bottom right). All future projections were modelled with SRTM as the underlying DEM and illustrate the situation in 80 years (year 2095) using RCP8.5.

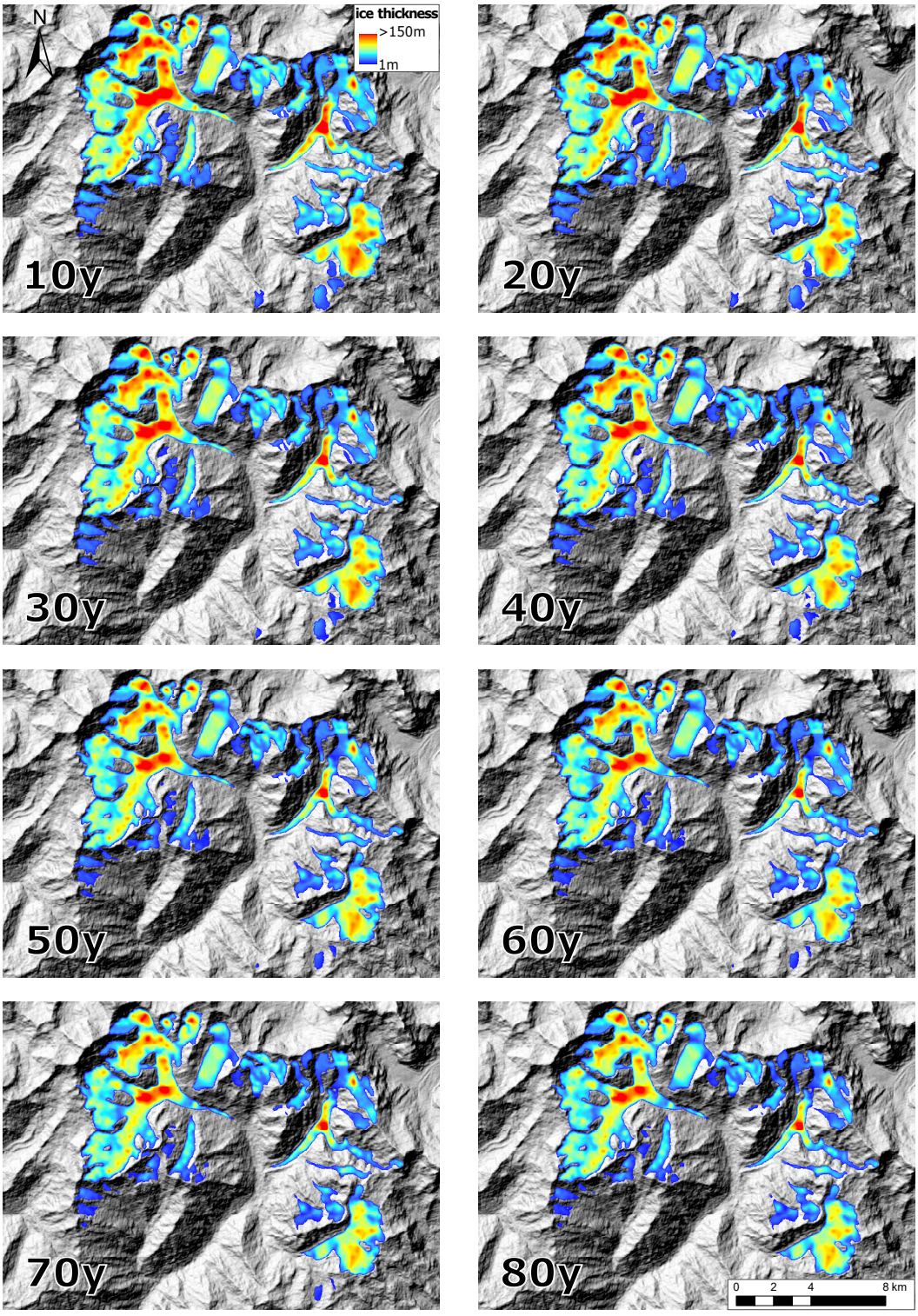

Figure 5.4: Same as fig. 3.13 but for the years 2025-2095.

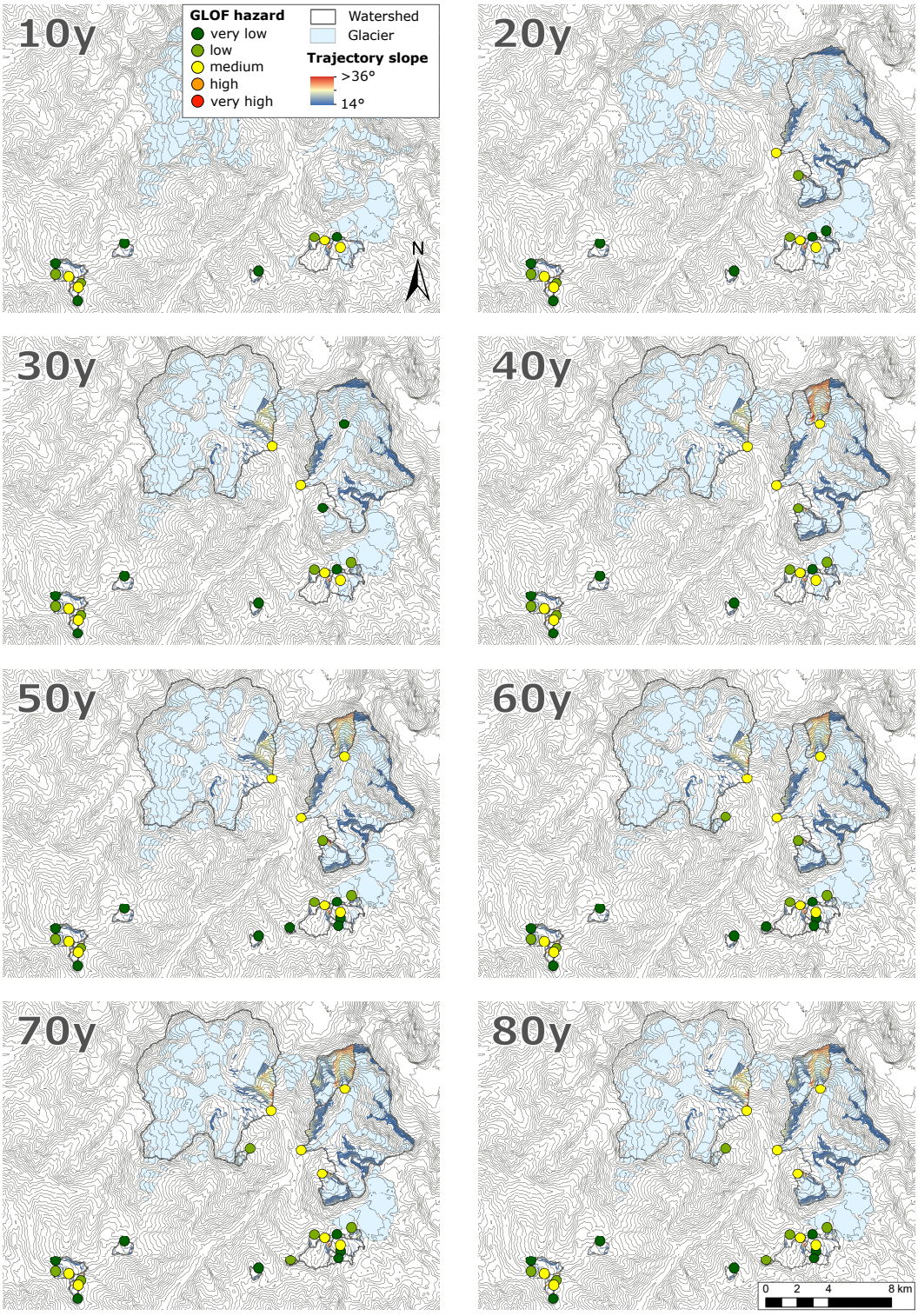

Figure 5.5: Same as fig. 3.17 but for the years 2025-2095.

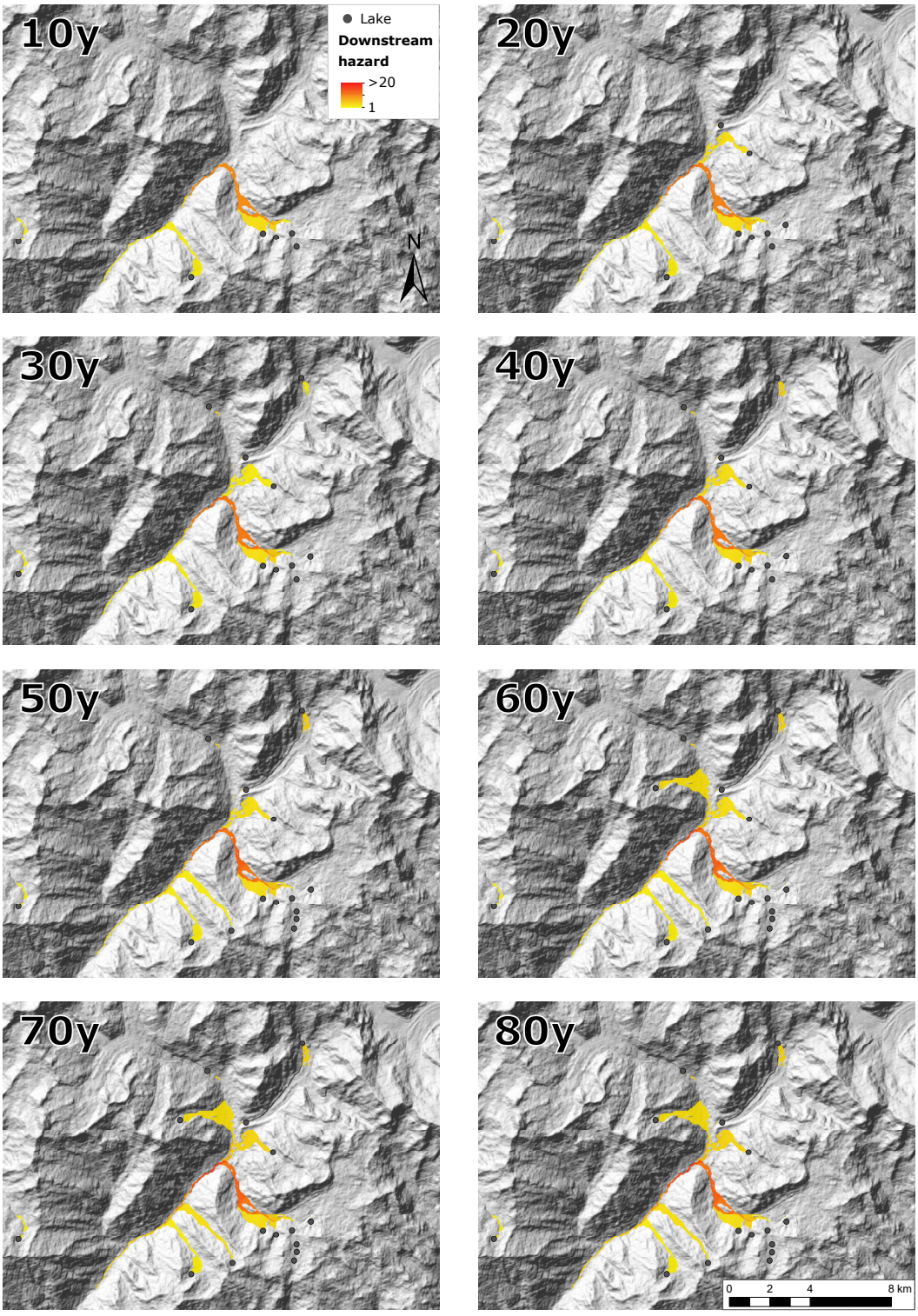

Figure 5.6: Same as fig. 3.21 but for the years 2025-2095.

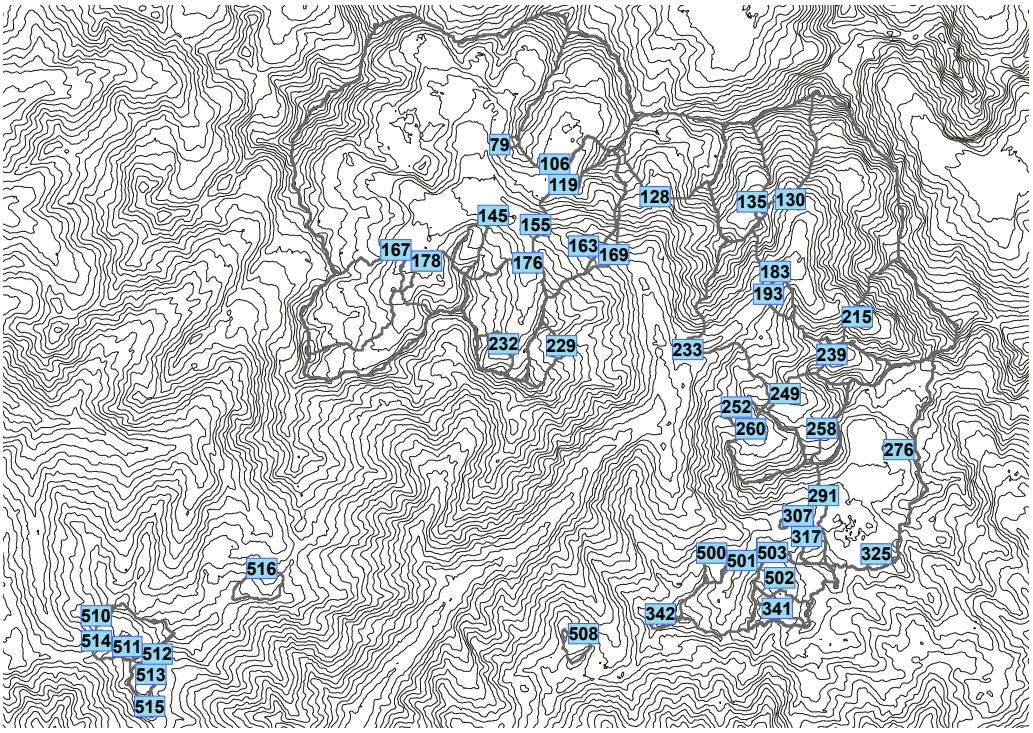

Figure 5.7: Lakes modelled in the study area with their corresponding numbers and the watershed as a gray outline.

Personal declaration

I hereby declare that the submitted thesis is the result of my own, independent work. All external sources are explicitly acknowledged in the thesis.

Place, date

Signature